# Dynamics of Southern Ocean Mixed Layers

Thesis by
Giuliana Augusta Viglione

In Partial Fulfillment of the Requirements for the
Degree of
Doctor of Philosophy


CALIFORNIA INSTITUTE OF TECHNOLOGY
Pasadena, California

2019
Defended 6 June 2019

Giuliana Augusta Viglione
ORCID: 0000-0002-2282-521X

“In the midst of winter, I found there was, within me, an invincible summer.”

- Albert Camus, *Return to Tipasa*

# ACKNOWLEDGEMENTS

This thesis would not have been possible without the love, support, and guidance of innumerable people. I cannot list everyone by name, but know that I am thankful to all the friends, family, and colleagues who have supported me over the years.

First thanks must go, now and always, to my parents, who have always encouraged me to do whatever would make me happy. My mother, who instilled in me a life-long love of reading and writing, and my father, whose resilience and positivity is an inspiration. I love you both more than I can say.

My brother, Niko, has always been there for me. Thank you for giving me all of your Beatles CDs when I was seven and for teaching me to push the boundaries of what I thought possible. I couldn't ask for a better big brother. And to Irie, my big sister — you bring so much joy into my life. Thank you for teaching me to follow my own path.

The rest of my family is too large to list, but they have all helped shape me into the person I am today. To all of the Vigliones and LoPrestis, Brewers and Alexanders, Cusacks and Dorans: thank you. And to the Montes, Windmans, and Noyans, family in all but blood relation: thank you too.

Andy has been the best advisor I could have possibly hoped for. Thank you for all the support, both academic and emotional, through the highs and lows over the years. And thank you for helping shape me into the scientist I am today, and for supporting me as I found a new path to take. I can only hope my next mentor will be as willing to talk with me about soccer as you are.

Thank you to the rest of my committee: Simona Bordoni, Jess Adkins, and Janet Sprintall. Thank you for the invaluable advice and guidance over the years, from TAC meetings to run-ins in the Linde-Robinson kitchen. And thank you to Simona for always cooking proper Italian food for us, Jess for your ridiculous touchdown celebrations, and Janet for teaching me cribbage at sea.

Thank you to the entire Thompson group, as well as the Callies and Klein extended group/family, all of whom have provided stimulating discussion over the years, both research-related and not. I am very fortunate to have entered the group at the same time as Zach Erickson and Xiaozhou Ruan, and it has been a pleasure to grow as a scientist alongside them. I must also give special thanks to Emily Newsom, with whom I shared many laughs and many special trips.

In addition to Zach and Xiaozhou, I would not have gotten through graduate school without Sean Mullin and Cody Finke, fellow members of our first-year cohort. You have been there for the best times and the worst, and I will always be grateful for that.

I have also had some great mentors, both official and unofficial, during my time at Caltech. Thanks to Sarah Slotznick for morning teas, Matt Coggon for afternoon beers, and Toby Bischoff, Andrew Stewart, Taso Dimitriadis, Felicia Hunt, and Trity Pourbahrami for everything in between.

I have had the great privilege of sailing on three research cruises throughout my PhD. This thesis would not have been possible without the help of everyone on the ARSV *Laurence M. Gould* and the R/V *Thomas G. Thompson*, who provided invaluable research support, entertainment, and laughter during my 95 days at sea. Special recognition goes to Jamie Yin, Max Kotz, Isa Rosso, and Zac Anderson, who became life-long friends in the short span of a single cruise.

Thank you to everyone involved with Caltech Letters, for starting me on the path to science journalism. And thank you to everyone involved with the AAAS Mass Media Fellowship, especially my editor, Russ Walker, for his encouragement and snark, Tim Treuer for some top-notch karaoke sessions, and my Dream Team: Ian Haydon, Jon Lambert, and Katie Wu. You inspire me.

My officemates, past and present, have always helped keep the mood light and known when a cup of tea or a crossword puzzle is in order. Thanks for putting up with year-round Christmas decorations, my lunchtime soccer watching habit, and the 2014 World Cup bracket that still occupies far more space than it should on our whiteboard.

I spent two years volunteering with Out for Undergrad. Thanks to everyone involved with the engineering conference for all the ridiculous times and late nights. You are all incredible people, and I'm lucky to have snuck my way into your midst (thanks for pretending I'm an engineer).

Thanks to my fellow residents of Dustin's Place, who always made coming home a joy: Aaron, Arian, Brigitte, Nathaniel, Vinicius, Sandwich, and, of course, Dustin.

I never felt at home in Pasadena until I met the Pasadena Reds and the rest of the Lucky Baldwin's morning soccer crew. 4:30 matches are a slog, but it was always worth it to be there with all of you. Thanks for the pints.

There are countless friends at Caltech I could thank for making my time here as wonderful as it has been, but I have to call out three in particular: my partners in crime, Kelvin Bates, Rachel Galimidi, and Nathan Schoepp. Thank you for all the wine nights, both happy and sad. And Kelvin — thank you for being the bae-st.

It feels a bit silly to thank a cat, but Tarquin has provided me with incredible amounts of both emotional support and cuddles over the past year and a half, and I am incredibly grateful to have her in my life.

To Hanna and Jen — your lives taught me to live my own to the fullest. I love you and I miss you every day.

Lastly, immeasurable thanks go to Ollie, who pushes me every day to be a better scientist, a better journalist, and a better person. You have been a light in my life over the past two and a half years, and I couldn't have asked for a better partner or best friend. Thank you for everything.

# ABSTRACT

While it is often conceptualized in a spatially and/or temporally averaged sense, the mixed layer depth of the global ocean exhibits significant variability in both space and time. The mixed layer plays a key role in controlling the exchange of heat and gases between the atmosphere and the ocean interior; an inaccurate portrayal of mixed layer depths can be a major source of error in global climate models. In particular, the Southern Ocean, or the waters around Antarctica, take up a significant portion of anthropogenically released carbon dioxide and subduct it into the deep ocean, affecting global climate on both relatively short and glacial timescales. Variability in the mixed layer also affects the formation and subduction of mode waters, the partitioning of waters between the upper and lower overturning cells, and biological productivity. The stratification of the mixed layer is significantly modified by submesoscale dynamics, which are not resolved in current state-of-the-art climate models. The parameterization of these dynamics represents a large source of uncertainty, and better observations and a better understanding of the submesoscale can be used to improve climate predictions.

In this work, the variability of Southern Ocean mixed layers is examined using both numerical and observational methods. General circulation model output is combined with a simple advection scheme to examine upwelling pathways, mixed layer residence times, and air-sea equilibrium in the Southern Ocean. Virtual Lagrangian drifters are released around the basin and tracked as they outcrop into the mixed layer, where they can exchange properties with the atmosphere. These studies are combined with high-resolution observations of mesoscale and submesoscale dynamics in the Southern Ocean, which play a leading order role in setting the stratification of the mixed layer. Seaglider data are used to construct potential vorticity fields, which are used to identify possible instances of different submesoscale instabilities in Drake Passage. Seasonal and zonal mixed layer variability are also examined using these observations. A second set of Seaglider observations are used to diagnose changes in ventilation and eddy stirring on sub-seasonal timescales at the Polar Front, one of the major fronts of the Southern Ocean. This thesis aims to expand current knowledge of mixed layer dynamics, especially at the submesoscale, and examine their implications for global circulation and climate.

# PUBLISHED CONTENT AND CONTRIBUTIONS

Viglione, G. A. et al. (In revision). "Controls on wintertime subduction in southern Drake Passage". In: *Geophys. Res. Lett.*
G.A.V. participated in the execution of the field campaign, analyzed the data, and wrote the manuscript.

Viglione, G. A. et al. (2018). "Abrupt transitions in submesoscale structure in Southern Drake Passage: Glider observations and model results". In: *J. Phys. Oceanogr.* 48.9, pp. 2011–2027. DOI: 10.1175/JPO-D-17-0192.1.
G.A.V. participated in the field campaign, analyzed the data, rewrote and ran the simple model, and wrote the manuscript.

Viglione, G. A. and A. F. Thompson (2016). "Lagrangian pathways of upwelling in the Southern Ocean". In: *J. Geophys. Res.-Oceans* 121.8, pp. 6295–6309. DOI: 10.1002/2016JC011773.
G.A.V. participated in the conception of the project, modified and ran the model, analyzed the data, and wrote the manuscript.

# TABLE OF CONTENTS

# LIST OF ILLUSTRATIONS

*Chapter 1*

# INTRODUCTION

The Southern Ocean plays a leading-order role in the world's climate. By connecting the other major ocean basins (Talley, 2013), the Southern Ocean allows for the inter-basin transport of heat, nutrients, and dissolved gases such as carbon dioxide, setting itself apart as a critical component of the global overturning circulation via adiabatic pathways linking the ocean interior to the mixed layer (J. A. Marshall and Speer, 2012). Modeling, remote sensing, and *in situ* observational studies have also shown the Southern Ocean's importance in the formation and subduction of mode waters (Naveira Garabato et al., 2009; Sallée et al., 2010; Close et al., 2013), the subduction and ventilation of anthropogenic carbon (Sallée et al., 2012), the filling of the deep ocean via bottom water formation (Gebbie and Huybers, 2011), and more. On glacial-interglacial timescales, the Southern Ocean is also thought to significantly impact global climate via modulation of deep-sea storage of carbon and the overturning circulation (e.g., Ferrari et al., 2014; Hines et al., 2019).

The main feature of the Southern Ocean is the Antarctic Circumpolar Current (ACC), a fast, eastward-flowing current that surrounds the Antarctic continent. The existence of the ACC is permitted by the absence of major landmasses in the latitude band that spans Drake Passage, approximately 55 °S to 63 °S. The geostrophic component of the current is supported by steeply sloping isopycnals, while meridional transport across the ACC occurs primarily by along-isopycnal eddy stirring. Thus, the ACC is a constant balance between a wind-driven Ekman component that tilts isopycnals and baroclinic instability generating eddies in an attempt to relax these same isopycnals.

Although this paradigm describes the ACC in a general sense, the three-dimensional structure and variation of the ACC have also been suggested to be a tight control on the overturning circulation and air-sea exchange (e.g., C. S. Jones and Cessi, 2016; Tamsitt et al., 2016; Dufour et al., 2015; Thompson and Naveira Garabato, 2014; Talley, 2013; Sallée et al., 2012). This largely zonal structure is typically related to interactions with major topographic features within the ACC, among them, Drake Passage, Kerguelen Plateau, Campbell Plateau, and the East Pacific Rise. Additionally, varying water mass properties and stratifications among the

other ocean basins mean that the ACC encounters changing northern boundary conditions as it flows around the Antarctic continent. It logically follows that the lower cell of the global overturning circulation, which is exposed to the atmosphere via the outcropping of isopycnals into the surface mixed layer, experiences zonal variations which may significantly impact climate by the storage and reventilation of deep-ocean carbon (J. A. Marshall and Speer, 2012; Ferrari et al., 2014).

The ACC comprises five major fronts: the Southern Boundary of the ACC (Bdy), the Southern ACC Front (SACCF), the Polar Front (PF), the Subantarctic Front (SAF), and the Subtropical Front (STF), which marks the northernmost excursion of subantarctic waters (Orsi et al., 1995) (labeled in Figure 1.1). This frontal system is characterized by largely homogeneous water mass properties in the inter-frontal zones bounded by large changes in properties over short latitudinal extents at the fronts themselves. These fronts also appear in satellite altimetry as large jumps in sea surface height (Kim and Orsi, 2014). Drake Passage serves as a choke point for the Southern Ocean, where all of the fronts of the ACC are compressed to less than 10 degrees of latitude.

Fronts typically act as barriers to mixing, giving rise to the aforementioned inter-frontal zones. Weak cross-frontal exchange is found at the majority of ACC fronts (Naveira Garabato et al., 2011; Klocker et al., 2012; Ferrari and Nikurashin, 2010; Thompson and Sallée, 2012). At the mesoscale, fronts generally modify eddy mixing lengths and eddy diffusivities across the ACC in a way that inhibits eddy mixing across fronts in the upper 1 km (Naveira Garabato et al., 2011). However, Naveira Garabato et al. (2011) note that this characteristic barrier-like behavior can break down under certain circumstances and in certain locations. The authors do find all of the fronts in Drake Passage to be strongly eddy-suppressing. Much of this work is based on mixing length theory, which describes a characteristic length scale over which a fluid parcel can move before exchanging properties, such as momentum or temperature, with the background fluid (Prandtl, 1925). Mixing lengths can provide insight into the efficiency and speed at which eddies can transport properties from the surface mixed layer to the interior of the ocean.

This subduction of surface waters and the corresponding ventilation of deep waters is one of the distinguishing features of the Southern Ocean. Gebbie and Huybers (2011) estimated that 15% of the surface area of the ocean is responsible for filling 85% of its interior volume; this occurs only at localized hotspots in the North Atlantic and the Southern Ocean. The location of these subduction zones is critical

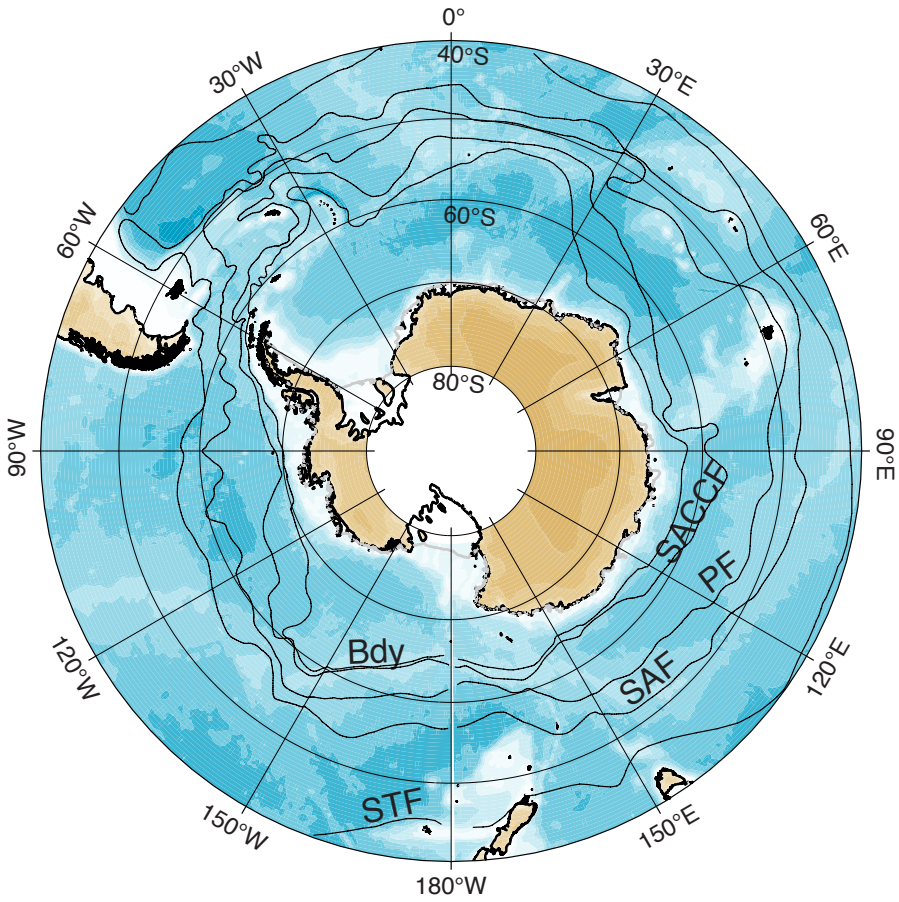


Figure 1.1: Southern Ocean bathymetry from 40 °S to 90 °S (filled blue contours). Thin black lines indicate the canonical fronts of the Antarctic Circumpolar Current (ACC): the Southern Boundary of the ACC (Bdy), the Southern ACC Front (SACCF), the Polar Front (PF), the Subantarctic Front (SAF), and the Subtropical Front (STF), as defined by Orsi et al. (1995).

for understanding the interior property distributions of the ocean, as well as its role in the carbon cycle, but residence times in the surface mixed layer must also be considered, since waters can only equilibrate with the atmosphere while they are in the mixed layer. Once water parcels are subducted into the interior and no longer subject to surface forcings, these properties, such as potential temperature and salinity, are conserved and can be used to track water masses and their mixing.

Locations and rates of subduction have been thoroughly researched (e.g., Broecker et al., 1998; Donners et al., 2005; Smethie Jr. and Fine, 2001), but similar analyses of upwelling are lacking (Sallée et al. (2010) provides a notable exception). A thorough understanding of the mechanisms and associated timescales of both of

these processes is critical to accurately modeling the transport of dissolved gases and nutrients on a global scale. This is of particular importance because the controlling factor of the oceanic sequestration of carbon is the exchange of waters between the surface and interior oceans (Sarmiento et al., 1992; Matear, 2001; Lévy et al., 2013; Bopp et al., 2015).

Air-sea equilibration of carbon dioxide in the Southern Ocean is of particular interest as approximately 40% of anthropogenically released carbon is estimated to enter the ocean south of 40 °S (Sallée et al., 2012). Given that the ocean as a whole takes up about one-third of anthropogenic carbon (Le Quéré et al., 2009), the Southern Ocean absorbs nearly 15% of anthropogenic carbon emissions. Air-sea exchange is also key for tracking watermass motion, either via transit time distributions (as in Waugh et al. (2006) and Peacock and Maltrud (2006)) or by tracing the penetration of such anthropogenically derived gases as chlorofluorocarbons (e.g., Bullister, 1989; Fine, 1993; Warner et al., 1996).

In addition to controlling the uptake of properties from the atmosphere via gas exchange, surface-interior exchange, mode water formation, and even the global overturning circulation are all highly linked to variations in the mixed layer depth. The mixed layer depth provides a control on the overturning circulation in the Southern Ocean by dictating which isopycnals outcrop at the surface, which in turn determines their buoyancy modification and whether they become part of the upper or lower overturning cell (D. Marshall, 1997; Abernathey et al., 2016).

These properties and processes are all closely tied to the mixed layer depth, which has significant seasonal variability in both observations (Dong et al., 2008) and models (Sallée et al., 2013). Indeed, Sallée et al. (2010) found the seasonally varying component of the mixed layer depth to explain up to 88% of the Southern Ocean mixed layer depth variation. However, the simple application of changing surface buoyancy forcing in one-dimensional representations of mixed layer dynamics is insufficient to capture the dynamics of these layers (e.g., Fox-Kemper et al., 2011; Belcher et al., 2012). The inclusion of wind forcing improves these estimates (Davis, Niiler, et al., 1981), but mixed layer dynamics remain too complicated for simple modeling.

In addition to providing a mechanical forcing on the surface layer, wind forcing induces an Ekman transport that can redistribute surface buoyancy. A down-front (up-front) wind causes the destratification (restratification) of the mixed layer (Thomas and Ferrari, 2008). This so-called Ekman buoyancy flux depends on lateral buoyancy

gradients at scales that are not resolved in current GCMs, known as submesoscales. Mixed layer eddies at these scales also actively remix and restratify the mixed layer; these also must be parameterized rather than resolved directly in large-scale models (Fox-Kemper et al., 2008). Submesoscale motions are typically characterized by length scales $O(1 - -10)$ km, time scales on the order of one to several days, and by Rossby numbers approaching $O(1)$. The Rossby number is a non-dimensional parameter defined as

$$Ro = \frac{U}{fL}, \tag{1.1}$$

where $f$ is the Coriolis parameter, given as $f = 2\Omega \sin\theta$, $\Omega$ is the rotation of the earth, $\theta$ is a given latitude, $U$ is the characteristic velocity, and $L$ is the characteristic length scale. The Rossby number compares the effects of rotation to inertial forces, such that low-Rossby number flows are flows that feel the effects of the earth's rotation. Thus, submesoscale motions exist in the realm where inertial terms are nearly equal to rotational forces and the ageostrophic components of flows are becoming important.

Many of the conditions favorable to an energetic submesoscale field are frequently found in the Southern Ocean, making it a critical region for study. The Southern Ocean is characterized by deep mixed layers and low vertical stratification coupled with strong horizontal stratification where isopycnals tilt up to the surface and form strong frontal currents. Additionally, there is strong surface cooling for much of the year, causing convection and even further destratification. The winds over the region primarily blow in a westerly direction, along the ACC, preconditioning the ocean here for submesoscale activity via Ekman buoyancy fluxes. Finally, the ACC is home to a vigorous mesoscale eddy field, a precursor to strong submesoscale activity, largely through the generation of strain by mesoscale stirring.

Thus far, submesoscale motions have predominantly been studied via idealized, process-based models (e.g., Boccaletti et al., 2007; Capet et al., 2008; Thomas and Ferrari, 2008; Mahadevan et al., 2010). These studies have been crucial to the development of parameterizations that use larger-scale variables such as wind stress and mixed layer depth to calculate the effects of various submesoscale processes. The MIT general circulation model (MITgcm; J. A. Marshall et al. (1997) and Hill et al. (2007)) has been run at sufficiently high resolutions (1/48°, Latitude/Longitude/polar-Cap model (Fox-Kemper and Menemenlis, 2008),

hereafter LLC) to observe submesoscale motions, even in the polar regions; however, the LLC output is restricted to a single calendar year. Numerical simulations have shown submesoscales to play an important role in setting vertical velocities and tracers fluxes (e.g., Klein and Lapeyre, 2009; Balwada et al., 2018). Submesoscale motions have also been shown by Lévy et al. (2010) to modify the circulation and properties at larger scales. Drake et al. (2018) found that the timescales of Southern Ocean upwelling decreased as model resolution increased; the authors attribute this change primarily to unresolved eddies and other small-scale features.

Given the potential impacts of submesoscales in the Southern Ocean, several regional, high-resolution modeling studies have been carried out in such varied regions as Kerguelen Plateau (Rosso et al., 2014) and the Scotia Sea (Bachman et al., 2017a). Rosso et al. (2014) showed that resolving submesoscales lead to enhanced vertical velocities and vertical exchange; Bachman et al. (2017a) demonstrated that shoaling mixed layers accompany increased model resolution. However, the difficulty and expense of making observations at these resolutions mean there is still a dearth of observations supporting these numerical studies.

Previous observations of submesoscales have primarily been carried out in Western Boundary Currents (e.g., D'Asaro et al., 2011; Thomas et al., 2013; Todd et al., 2016) and subtropical regions (e.g., Hosegood et al., 2013; Callies et al., 2015; Thompson et al., 2016b). More recently, studies such as those reported in Adams et al. (2017) and du Plessis et al. (2017) have extended the reach of these observations to the Southern Ocean. The majority of these studies have predominantly found submesoscale activity in winter months, when deeper mixed layers and reduced vertical stratification predispose the ocean to enhanced submesoscales (e.g., Callies et al., 2015; Buckingham et al., 2016; Thompson et al., 2016b). However, studies using high-resolution models have suggested that the seasonal cycle of submesoscale activity is smallest in the Southern Ocean, that is, submesoscales may be expected all year round (Rocha et al., 2016; Su et al., 2018).

One key factor that has allowed the proliferation of these submesoscale-resolving observational programs has been the development of ocean gliders and similar autonomous underwater vehicles (Daniel L Rudnick et al., 2004). Gliders typically sample over periods of many months, collecting varied data such as temperature, salinity, dissolved oxygen, and fluorescence. A caveat to the use of gliders to study the submesoscale is that a glider can only cover approximately 20 kilometers per day. This means that rather than submesoscale-resolving, these field programs should

perhaps be thought of as submesoscale-permitting, in that they allow the capture of the length scales characteristic of submesoscales, but on timescales over which coherent submesoscale motions may evolve.

Gliders have been used to study meso- and submesoscale motions in a variety of contexts. A 2008 glider study in the North Atlantic demonstrated a link between the upper ocean restratification by eddies and spring phytoplankton blooms (Mahadevan et al., 2012). The Ocean Surface Mixing, Ocean Submesoscale Interaction Study (OSMOSIS) field campaign occupied a 20 km-by-20 km box in the North Atlantic for an entire year; the glider data were used to diagnose likely submesoscale instabilities from potential vorticity (PV) structures (Thompson et al., 2016b). Similar analyses have been carried out in the Gulf Stream (Todd et al., 2016) and the Subantarctic Zone (du Plessis et al., 2017). The data from the Changes in Stratification at the Antarctic Peninsula (ChinStrAP) field program, some results of which are published in this thesis as Chapter 3, have been used additionally to explore export pathways of carbon from the euphotic zone (Erickson et al., 2016) and turbulent mixing in bottom boundary layers (Ruan et al., 2017).

Gliders have been of particular use, although certainly particularly challenging as well, in studying the Southern Ocean, one of the most difficult places on Earth to conduct field work. The remote location, as well as the harsh storms and seas, often sub-freezing temperatures, and formation and advection of sea ice, make this region inhospitable for most of the year. Indeed, Drake Passage is the only region of the Southern Ocean in which at least one $pCO_2$ measurement has been made in every month of the year (Takahashi et al., 2009). Given the zonal variability in air-sea exchange (Dufour et al., 2015), mode water formation and subduction (Sallée et al., 2010), and export pathways from the Southern Ocean (Tamsitt et al., 2017), the paucity of data may lead to erroneous conclusions about the circumpolar characteristics and behavior of the Southern Ocean. Indeed, a recent study by Gray et al. (2018) shows a vast underestimation of $CO_2$ outgassing from conventional measurements as compared to Argo float data; part of this discrepancy may be explained by the circumpolar extrapolation of data from Drake Passage to other parts of the Southern Ocean.

At slightly larger (i.e., meso-) scales, significant advances in understanding the effects of these motions have been made both with gliders and other methods such as Lagrangian particle tracking in eddy-resolving GCMs. Using gliders, Thompson et al. (2014) implicated mesoscale eddies as one of the primary ways in which warm,

salty Circumpolar Deep Water can be advected into the cavities beneath ice sheets in Antarctica, melting them from below. Lagrangian particle tracking, a technique pioneered in the mid-90s (Davis et al., 1996), has experienced a resurgence lately; as GCM resolutions have improved, mesoscale dynamics can increasingly be studied in this manner. Recent Lagrangian studies have examined the export of waters from Drake Passage (Friocourt et al., 2005), studied transport along the western Antarctic Peninsula (Piñones et al., 2011), and revealed a new, spiraling structure of upwelling in the Southern Ocean (Tamsitt et al., 2017).

Such techniques have been extensively validated by comparison of virtual Lagrangian pathways with drifter and/or float profiles (Sebille et al., 2009; Gary et al., 2012; Kwon et al., 2015). Many of the previous Lagrangian trajectory studies have disregarded particles after they outcrop into the mixed layer, leaving open questions as to the residence times of water in the mixed layer and thus the extent of air-sea equilibration in the Southern Ocean; this is especially important to explore based on the findings of D. C. Jones et al. (2014) that $CO_2$ equilibration timescales can vary spatially by an order of magnitude, primarily based on differing mixed layer depths.

In order to better constrain global climate models, and therefore better predict future global climate, improvements must be made in the way that submesoscale motions are parameterized in these models. However, better parameterizations require better data in order to properly constrain them. In this thesis, I provide unique data and analyses of variability in submesoscale and mesoscale motions in the Southern Ocean and their effects on mixed layer depths — key for the proper representation of bottom water formation, deep-sea carbon storage, and other critical components of the climate system.

This thesis comprises three studies examining the dynamics of and variations in Southern Ocean mixed layers using a variety of techniques. Chapter 2 discusses a virtual Lagrangian drifter experiment in the Southern Ocean. Virtual drifters were seeded at depth in an eddy-permitting ocean-only general circulation model and advected forward in time. The outcropping of the drifters in the mixed layer was used to determine upwelling "hotspots," mixed layer residence times, and density modification. Chapters 3 and 4 discuss results from two glider-based observational programs in Drake Passage. Chapter 3 is based on a summertime deployment across the shelf and slope of southern Drake Passage, in which gliders and reanalysis data were used to investigate differences in submesoscale activity, mixed layer depths, and instability characteristics across a large bathymetric feature, the Shackleton

Fracture Zone. Chapter 4 is based on an autumn/wintertime deployment of two gliders that traversed southern Drake Passage from the Southern Boundary of the ACC to the Polar Front. This study examines differences in meso- and submesoscale characteristics that lead to variations in ventilation on a sub-seasonal timescale. Finally, Chapter 5 provides a brief summary of the work done in this thesis and an outlook for future research directions.

*Chapter 2*

# LAGRANGIAN PATHWAYS OF UPWELLING IN THE SOUTHERN OCEAN

Viglione, G. A. and A. F. Thompson (2016). "Lagrangian pathways of upwelling in the Southern Ocean". In: *J. Geophys. Res.-Oceans* 121.8, pp. 6295–6309. DOI: 10.1002/2016JC011773.

## 2.1 Abstract

The spatial and temporal variability of upwelling into the mixed layer in the Southern Ocean is studied using a 1/10° ocean general circulation model. Virtual drifters are released in a regularly spaced pattern across the Southern Ocean at depths of 250, 500, and 1000 m during both summer and winter months. The drifters are advected along isopycnals for a period of four years, unless they outcrop into the mixed layer, where lateral advection and a parameterization of vertical mixing is applied. The focus of this study is on the discrete exchange between the model mixed layer and the interior. Localization of interior-mixed layer exchange occurs downstream of major topographic features across the Indian and Pacific basins, creating "hotspots" of outcropping. Minimal outcropping occurs in the Atlantic basin, while 59% of drifters outcrop in the Pacific sector and in Drake Passage (the region from 140°W to 40°W), a disproportionately large amount even when considering the relative basin sizes. Due to spatial and temporal variations in mixed layer depth, the Lagrangian trajectories provide a statistical measure of mixed layer residence times. For each exchange into the mixed layer, the residence time has a Rayleigh distribution with a mean of 30 days; the cumulative residence time of the drifters is 261 ± 194 days, over a period of four years. These results suggest that certain oceanic gas concentrations, such as $CO_2$ and $^{14}C$, will likely not reach equilibrium with the atmosphere before being re-subducted.

## 2.2 Introduction

The Southern Ocean is a critical component of the global overturning circulation, especially due to its adiabatic pathways between the ocean interior and the mixed layer (J. A. Marshall and Speer, 2012). The three-dimensional structure of the Southern Ocean, and in particular, the Antarctic Circumpolar Current (ACC), has

also been suggested to have key controls on the overturning circulation and air-sea exchange (C. S. Jones and Cessi, 2016; Tamsitt et al., 2016; Dufour et al., 2015; Thompson and Naveira Garabato, 2014; Talley, 2013; Sallée et al., 2012). In particular, zonal structure is typically related to interactions with topographic features in the ACC. Furthermore, the ACC links the major ocean basins. Due to variations in stratification and water mass properties between the basins, the ACC encounters highly varying conditions along its northern boundary. Thus it is to be expected that the exposure of the lower overturning cell to the atmosphere, occurring through the outcropping of density surfaces into the surface mixed layer, also experiences zonal variations which can significantly impact climate via deep-ocean carbon storage and reventilation (J. A. Marshall and Speer, 2012; Ferrari et al., 2014).

The broad ventilation of deep waters and the subduction of surface and intermediate waters is one of the distinguishing features of the Southern Ocean. It is estimated that 15% of the surface area of the ocean, clustered around the Southern Ocean and the North Atlantic, is responsible for filling 85% of its interior volume (Gebbie and Huybers, 2011). Whereas the location of subduction hot spots is critical for understanding interior property distributions, surface residence times must also be considered. Waters can only equilibrate with the atmosphere during the time they spend in the mixed layer. Once these waters are brought down into the deep ocean, their properties are conserved, since they are no longer subject to direct surface forcing. Although significant work has been done identifying regions and quantifying rates of subduction (e.g., Broecker et al., 1998; Donners et al., 2005; Smethie Jr. and Fine, 2001), there have been fewer such analyses of upwelling regions, with Sallée et al. (2010) providing a notable exception. Given the importance of water exchange in setting global climate, a thorough understanding of the mechanisms and time scales of both subduction and upwelling is critical to modeling the transport of dissolved gases and nutrients on a global scale.

Of particular importance is the uptake of carbon dioxide by the ocean. The ocean is able to mitigate the atmospheric effects of climate change by absorbing 25–30% of anthropogenically released carbon dioxide annually (Le Quéré et al., 2009). Several modeling studies have shown that oceanic sequestration of carbon is limited by the exchange of waters between the surface and interior oceans (Sarmiento et al., 1992; Matear, 2001; Lévy et al., 2013; Bopp et al., 2015), indicating that the Southern Ocean is the critical region where carbon-rich waters can be subducted and stored.

Indeed, it has been found that more than 40% of anthropogenically released carbon enters the ocean south of 40°S (Sallée et al., 2012). Thus, constraining the pathways of upwelling and subduction in the Southern Ocean is key to modeling and predicting future climate change.

The seasonally varying component of the mixed layer depth has been found to explain up to 88% of the variation in mixed layer depth around the Southern Ocean (Sallée et al., 2010). However, this study was based on observations from Argo floats, which lack the resolution to distinguish mesoscale features. These smaller-scale patterns may also have a significant role to play in establishing variability of the mixed layer. In addition, there is a component of the variability that is due to spatial patterns of wind stress, buoyancy flux, and interactions with bottom topography. There are large zonal variations in mixed layer depths across the Southern Ocean, which have been thought to correspond in part to bathymetric features, as discussed by Hägeli et al. (2000) and shown in both our modeled mixed layer and observationally derived mixed layer fields (Figure 2.1). This influence is an indirect effect — the topography steers the circulation, which affects the slope of the outcropping isopycnals and thus, the mixed layer depth (Sallée et al., 2010). Bathymetric features also significantly affect diapycnal and isopycnal diffusivities (LaCasce et al., 2014) and therefore, upward mixing. The spatially variable upward mixing affects the sites and rates of ventilation. The spatial pattern is also dictated by the variance in wind stress, heat and freshwater fluxes, and northward Ekman transports of cold water. All of these processes, in addition to determining the mixed layer depth, are critical for setting the formation of mode waters in these regions (Dong et al., 2008).

Since the mixed layer depth, which is highly variable, is responsible for setting ventilation in the Southern Ocean, it follows that ventilation would also exhibit significant spatial patterns. Sallée et al. (2010) used a combination of satellite and *in situ* data alongside climatologies and parameterizations to estimate rates of ventilation around the Antarctic Circumpolar Current (ACC). They found highly localized regions of subduction and upwelling, and linked these to density classes corresponding to specific water masses such as Antarctic Intermediate Water (AAIW) and Subantarctic Mode Water (SAMW) at certain latitudes. Their conclusions are supported by data collected by Argo float profiles and analyzed for mixed layer depths around the Southern Ocean (Dong et al., 2008). These authors find that the deepest mixed layers around the ocean occur in areas where the surface density (and thus, the density of the mixed layer) corresponds to that of SAMW, suggesting that

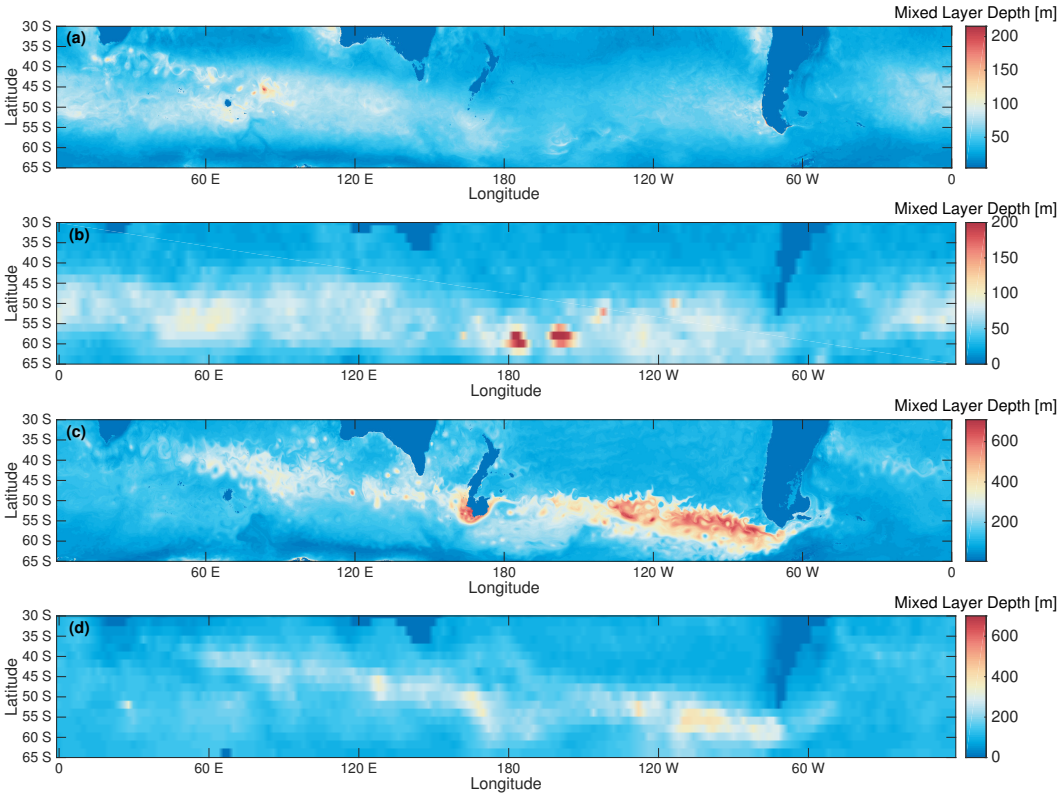


Figure 2.1: Seasonally averaged mixed layer depth for austral summer (DJF) from (a) OFES model output and (b) Argo float data and for austral winter (JJA) from (c) OFES output and (d) Argo data; note the change in color scale between panels. Notable features include mixed layer variability at mesoscales in both seasons and topographically localized mixed layer deepening in the JJA months.

these are regions where this mode water is formed. Mode waters also have a significant influence on global climate, as they can "store" climate anomalies from one year to the next by acting as an upper-ocean reservoir for anomalous heat, nutrients, and carbon dioxide (Kwon et al., 2015). Our focus here allows us to examine the interior sources of what will eventually be subducted as mode waters.

In this study, high-resolution ocean model output is paired with an isopycnal advection scheme and used to identify Lagrangian pathways of Southern Ocean transport and localized regions of significant upwelling activity. Similar approaches have been used to study oceanic currents since the mid-1990s (Davis et al., 1996), but increased computational power over the past two decades has meant that results from this type of study have resolved more structure. Similar analyses to the study performed here have been used to examine water export from Drake Passage (Friocourt et al., 2005), abyssal export of Antarctic Bottom Water (Sebille et al., 2013),

and transport pathways along the western Antarctic Peninsula (Piñones et al., 2011), among other phenomena. Several studies also compare simulated drifter trajectories to pathways mapped via drifters and/or floats (e.g., Kwon et al., 2015; Gary et al., 2012; Sebille et al., 2009). The advantages of a Lagrangian study are that it allows an examination of the pathways connecting intermediate waters to the surface ocean and an exploration of the interconnectivity of the ocean basins in a three-dimensional sense.

The following section, section 2.3, describes the model output and the Lagrangian trajectory algorithm. Section 2.4 discusses the results of the simulations. Section 2.5 provides an interpretation of the findings of the study and examines its limitations, while Section 2.6 summarizes the paper.

## 2.3 Methods

### Description of the OFES Model

We examine the Lagrangian pathways of interior-mixed layer exchange and surface residence times through the use of an eddy-resolving numerical simulation, which allows us to capture temporal/spatial scales and durations that are challenging for most observing systems, e.g., ships or Argo floats. Our approach is to use an eddy-resolving model of the Southern Ocean in order to accurately portray these mesoscale motions. Ocean Global Climate Model for the Earth Simulator (OFES) is a 1/10° model with 54 variably spaced levels and realistic bathymetry (Masumoto et al., 2004). OFES is based on GFDL/NOAA's Modular Ocean Model version 3 (MOM3), with bathymetry based on the OCCAM project at Southampton Oceanography Centre. Although the OFES model goes to 75°S, output was only loaded to 65°S for computational efficiency; since less than 7% of outcropping occurred south of 60°S, this choice is unlikely to have skewed the results of this study in any meaningful way.

OFES provides daily snapshots of temperature, salinity, and three-dimensional velocity fields for a period of 8 years (1990–1997) following a 50-year spin-up using monthly climatological forcing. There is no difference in surface forcing across the different years, but internal variability exists. Thus, the climatological forcing better allows an estimate of the influence of internal eddy variability on outcropping and was therefore chosen over the interannual forcing used by Sebille et al. (2012). This study loaded model output every third day and interpolated between the snapshots using a spline interpolation scheme to provide the fields at each timestep. Previous

work with this model had confirmed that high-frequency dynamics of the region were not aliased by sub-sampling in this manner (Thompson and Richards, 2011).

**Description of Deployments and the Advection Scheme**

Virtual drifters were released in the OFES model at 23 different sites in the ACC; at each of these sites, 1000 drifters were released at each of three different depths and on two different starting dates. Deployments were evenly spaced at 30° longitude increments at both 50°S and 55°S, with no deployments at 50°S, 60°W due to the shallow bathymetry at this location (shown in Figure 2.2). For each deployment site, initial drifter positions were randomly distributed within a 2°-by-2° box centered at the given coordinates. At each location, deployments were performed on each of three isopycnal surfaces. The chosen potential density surfaces were not necessarily the same at each deployment site, but rather were selected to coincide with approximate initial depths of 250, 500, and 1000 m.

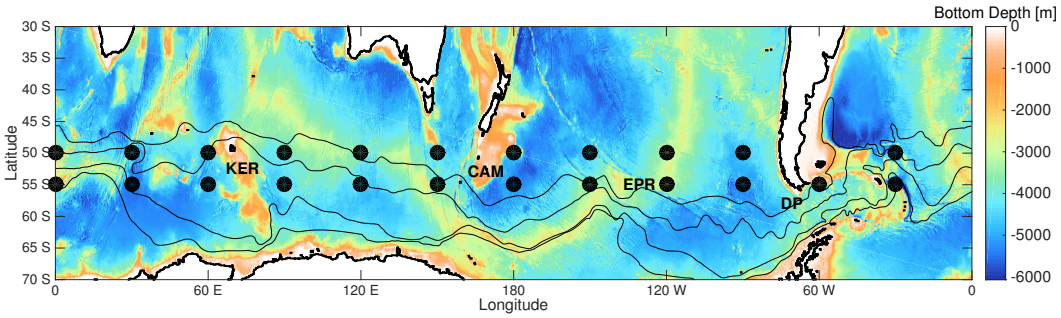


Figure 2.2: Bathymetry of the Southern Ocean in the OFES model; black circles represent the deployment zones of the virtual drifters. Each deployment occurred in a 2° by 2° box. For each point shown, a total of 6 deployments were performed: at depths of approximately 250, 500, and 1000m, and at starting dates of both January 1 and July 1. See details in section 2.3. Black lines denote the climatological mean fronts of the Southern Ocean as given by Orsi et al. (1995). From top to bottom: the Subantarctic Front, the Polar Front, the Southern ACC Front, and the Southern Boundary of the ACC. Labels denote the major bathymetric features discussed in this work: Kerguelen Plateau, KER; Campbell Plateau, CAM; East Pacific Rise, EPR; and Drake Passage, DP.

The drifters were initialized on either January 1 or July 1 and advected forward for a period of 4 years using a time step of 2 hours. The drifter trajectories are constrained by design to be adiabatic in the interior; no sub-grid scale diffusion was added. Thus, at each time step, the two-dimensional horizontal velocity field is interpolated on to the density surface of each drifter position and used to update the

horizontal position, while maintaining the trajectory on a density surface determines the vertical displacement. While diapycnal mixing is small throughout most of the Southern Ocean, larger diapycnal velocities can occur near topographic features (Sheen et al., 2013). However, as shown below, mixed layer outcropping events are qualitatively similar at all deployment depths, e.g., outcropping sites are not strongly dependent on particular isopycnals. Thus, our assumption of an adiabatic interior is unlikely to change the spatial characteristics of the outcropping events. A sample set of trajectories and a depth-time plot for a single deployment are shown in Figure 2.3. Over the four-year advection period, drifters, deployed at 250 m, occupy roughly half the zonal extent of the ACC. For this particular deployment, the vertical dispersion of the drifters increases abruptly after day 423, which coincides with the passage of the drifters' mean position over and around Kerguelen Plateau.

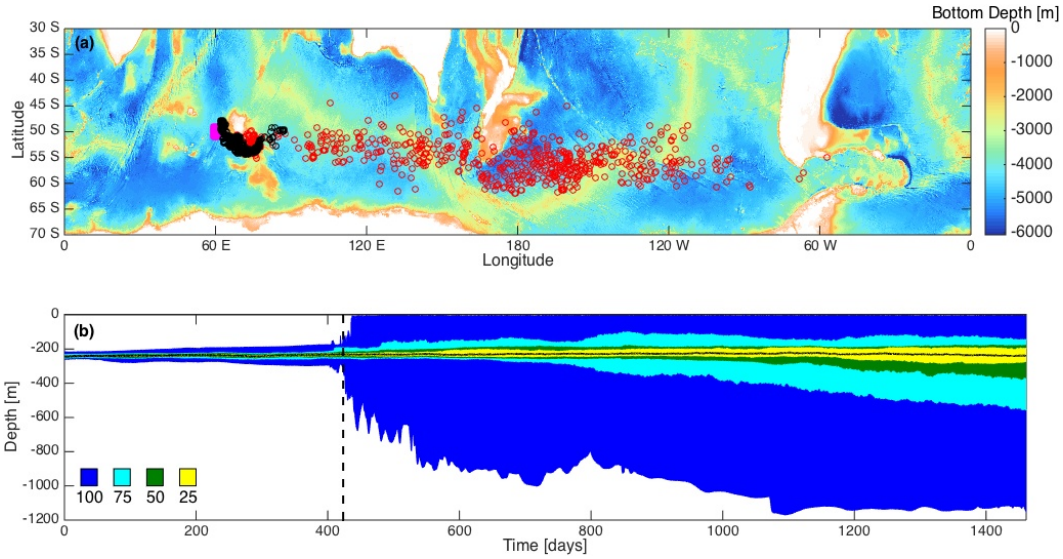


Figure 2.3: Sample diagnostics from a single deployment, centered at 50°S, 60°E and a depth of 250 m; the deployment date was July 1. (a) Trajectories of individual drifters over a 4 year period indicating deployment locations (magenta circles) and ending locations (red circles). (b) Vertical distribution of the drifters, as given by the envelope containing 25% (yellow), 50% (green), 75% (cyan), and 100% (blue) of the drifters. The thick black curve gives the mean depth of all drifters. The dashed line at day 423 corresponds to most drifters reaching the Kerguelen Plateau and corresponds to the black circles in panel (a).

The assumption of isopycnal motion was relaxed when drifters cross into the mixed layer. The mixed layer was defined by a density difference criterion of $\rho = 0.03$ kg/m$^3$ from the density at 10 m depth, following Boyer Montégut et al. (2004). Once drifters crossed into the mixed layer, it is assumed that the turbulent mixing

dominates the vertical displacement of the drifter. Thus we applied a random walk in the vertical with a maximum displacement of 20 m per time step, similar to the method employed by Sebille et al. (2013) and consistent with an average diapycnal diffusivity of $139 \times 10^{-4}$ m$^2$ s$^{-1}$ acting over the 2 hour time step. This mixed layer diffusivity is consistent with values previously determined by McPhee and Martinson, 1994 and Large et al., 1994. In the mixed layer, the horizontal displacements were determined by advection by the local horizontal velocities. The drifter advection algorithm avoided vertical advection out of the mixed layer. If the random walk placed a drifter above the ocean surface, it was restored to a depth of 5.5 m. If the drifter was displaced out of the bottom of the mixed layer, it was placed 0.5 m above the base of the mixed layer. A sensitivity study was performed on this parameter; there was no change in outcropping frequency or pattern for placement between 0.1 and 5 m above the base of the mixed layer. This meant that the drifters could only leave the mixed layer by horizontal advection across lateral mixed layer gradients, or by a shoaling of the mixed layer above their position. This minimizes rapid, high-frequency exchange across the base of the mixed layer, but physically represents reduced mixing turbulence and a stronger stratification at the base of the mixed layer.

When drifters exited the mixed layer, they were not required to return to the density surface they occupied prior to entering the mixed layer. The new density surface at which they crossed the base of the mixed layer back into the interior was recorded and subsequent advection in the interior followed this new surface. Thus, changes in density between upwelling and subduction provides an indication of the sense of water mass modification in the mixed layer. Throughout each deployment, time series were recorded of latitude, longitude, depth, and density of each drifter, as well as the mixed layer depth at the drifter position and a bianary diagnostic labelling whether the virtual drifter was in or out of the mixed layer.

## 2.4 Results

An instance of outcropping was defined as a time at which a drifter was in the mixed layer and had not been in the mixed layer at the time step immediately prior. Thus for each drifter, we can obtain the latitudes and longitudes of each instance of outcropping throughout the simulation. This approach is similar to the Lagrangian analysis of front-crossing events in Thompson and Sallée (2012). These instances of outcropping are binned into 1°-by-1° boxes (Figure 2.4). Each instance of outcropping is counted, regardless of prior instances of outcrop. In

order to highlight the contrast between regions of high outcropping and those of low outcropping, the number of drifters per box is displayed on a logarithmic color scale. The spatial patterns and indeed, the intensity (defined by the number of outcropping drifters), of outcropping events are qualitatively similar between the set of drifters deployed in austral summer and those deployed in austral winter, with the root mean squared difference between the boxes only 13 instances of outcropping over the course of the simulation. This similarity can be attributed to the tendency of drifters to primarily outcrop in winter regardless of season of deployment, which will be discussed in detail later on. Relatively little outcropping occurs in the Atlantic and Indian basins, with upwelling predominately happening in the Pacific sector. 59% of outcropping events occur in the ACC between 140°W and 40°W. Furthermore, outcropping appears to be concentrated in distinct regions within the sector, rather than occurring uniformly throughout the ocean; 23% of outcropping events occur over the 4% of longitudes encompassing Drake Passage (Figure 2.4).

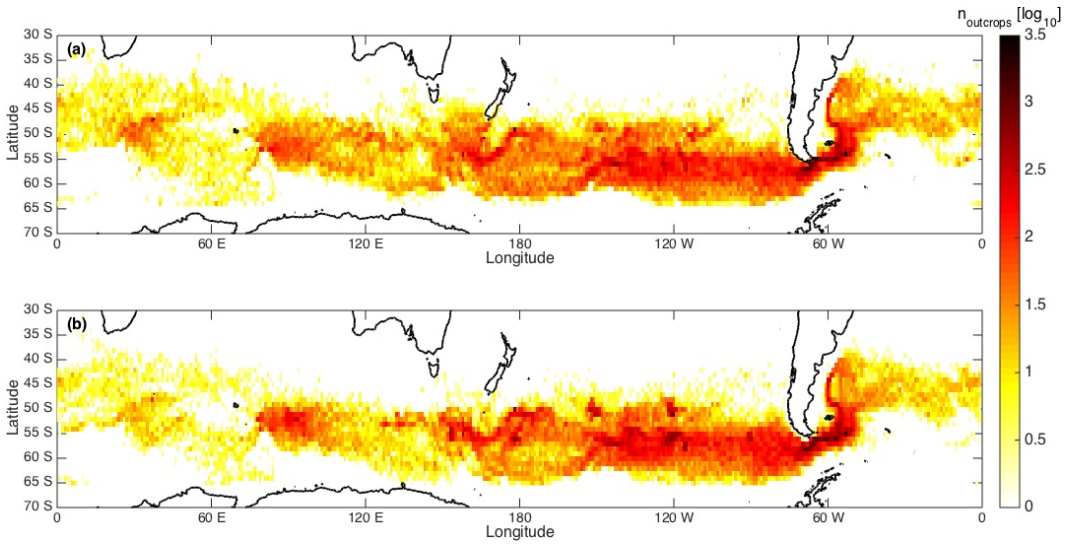


Figure 2.4: Heat map showing all outcropping locations (logarithmic scale) across the 138 deployments (138,000 trajectories) for the (a) January 1 deployments and (b) July 1 deployments. Outcropping events were binned into 1°-by-1°boxes and summed over the entire duration of the simulations. Increased upwelling occurs downstream of significant bathymetric features: Kerguelen Plateau, Campbell Plateau, the East Pacific Rise, and within and downstream of Drake Passage.

The spatial patterns of upwelling are similar between the drifters deployed at 250 m and 500 m, as both show strong signals of upwelling in Drake Passage and throughout the Pacific (Figure 2.5). However, there is notably less upwelling from the 500 m depth in the Indian basin; in addition, although the enhanced outcropping

zones still exist, the strength of these hotspots in comparison to the rest of the basins is reduced when examining the set of drifters deployed at 500 m. Outcropping events are an order of magnitude or more smaller for those drifters deployed at 1000 m due mainly to the limited length of integration; the majority of these outcropping events is in the eastern Pacific sector of the ACC and within Drake Passage. From top to bottom, these panels show outcropping for drifters deployed at (a) 250 m, (b) 500 m, and (c) 1000 m. The colorbars for panels (a) and (b) are the same logarithmic scale, while the colorbar shifts for panel (c) due to the greatly reduced instances of outcropping.

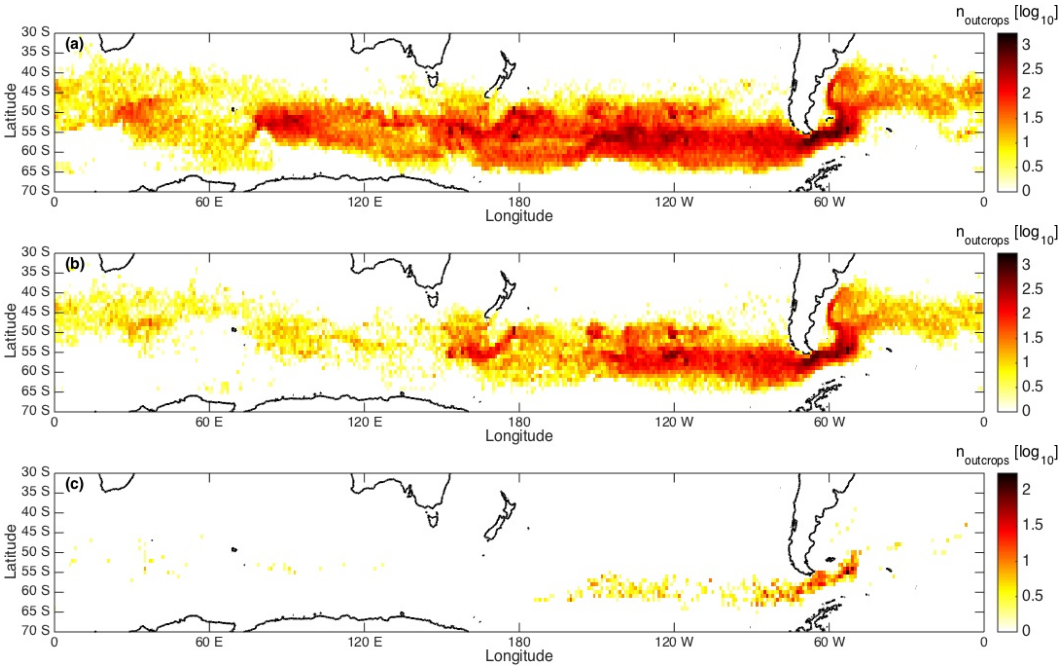


Figure 2.5: As in Figure 2.4: a heat map of outcropping zones for drifters deployed at (a) 250 m, (b) 500 m, and (c) 1000 m depths.

Distinct regions of the ocean are seen to contain most instances of outcropping (Figures 2.4 and 2.5). In order to determine what set these locations apart from other sites in the ocean, outcropping "hotspots" were defined as those 1°-by-1° grid boxes in which there had been 600 or more instances of outcropping across all simulations. 73 grid boxes were found to meet this criterion, with 17% of outcropping events occurring in only 0.6% of grid boxes. Several further methods of analysis were aimed at determining the differences between these regions and the remainder of the ocean. For all depths studied, the distribution of densities outcropping in the hotspot regions was narrower than the density distribution of all outcropping events

(Figure 2.6), even though outcropping hotspots are found in the Pacific and Indian sectors as well as Drake Passage. Panels (a–c) in this figure show the frequencies of density at outcrop by starting depth—250 m, 500 m, and 1000 m, respectively. The histograms show the frequency of all outcropping, the frequency of outcropping in hotspots and the initial deployment density distributions. Note that drifters may outcrop in density classes lighter than the deployment density range (as long as it is not the first outcropping event in the trajectory) due to modification in the mixed layer. The spatial pattern of the outcropping of these density classes is qualitatively similar to those shown in Figure 10 of Sallée et al. (2010).

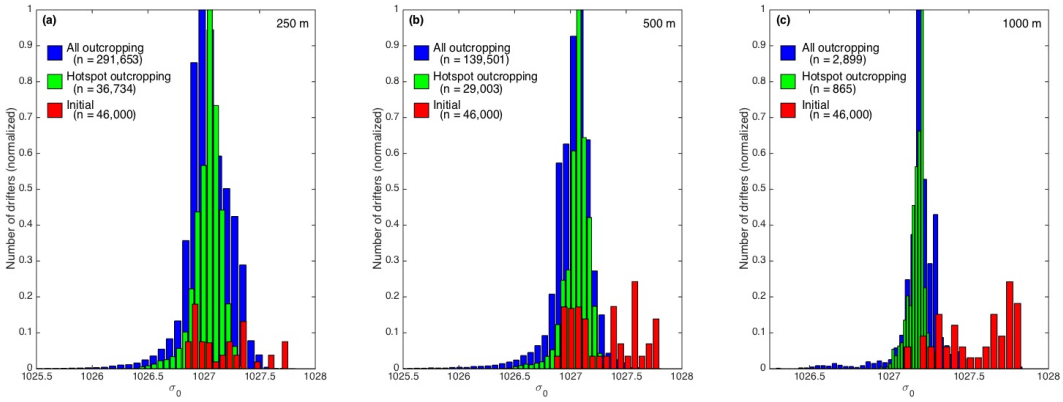


Figure 2.6: Frequency of outcropping as a function of density classes for (a) 250 m, (b) 500 m and (c) 1000 m deployments. The density class gives the drifter's isopycnal at the time of outcrop; this is calculated for all drifters (blue) and those drifters that outcrop at hotspot locations (green). The red values show initial deployment densities. For easier comparison, the blue and red histograms are normalized to the maximum of the blue; the green was normalized to its maximum. The total number of drifters in each category is listed on each panel. In panel (c), the initial density distribution (red) was reduced by a factor of 40.

Only drifters originating from certain regions outcrop during this four year period. Less than 5% of outcropping drifters were sourced from each longitude between 30°E and 60°W, a feature that is even more striking when considering only drifters that first outcropped in a hotspot region. In this case, each of these longitudes contributes < 1% of outcropping drifters (Figure 2.7). Across all outcropping drifters, the percentages outcropping starting at the remaining latitudes were roughly equal, with only the deployments at 150°E and 180° showing significantly higher instances than the other longitudes. However, in the case where only outcrops in hotspot zones were considered, significantly more drifters outcrop at 180°, 120°W, and 90°W, with these three longitudes alone responsible for nearly 2/3 of the outcropping drifters.

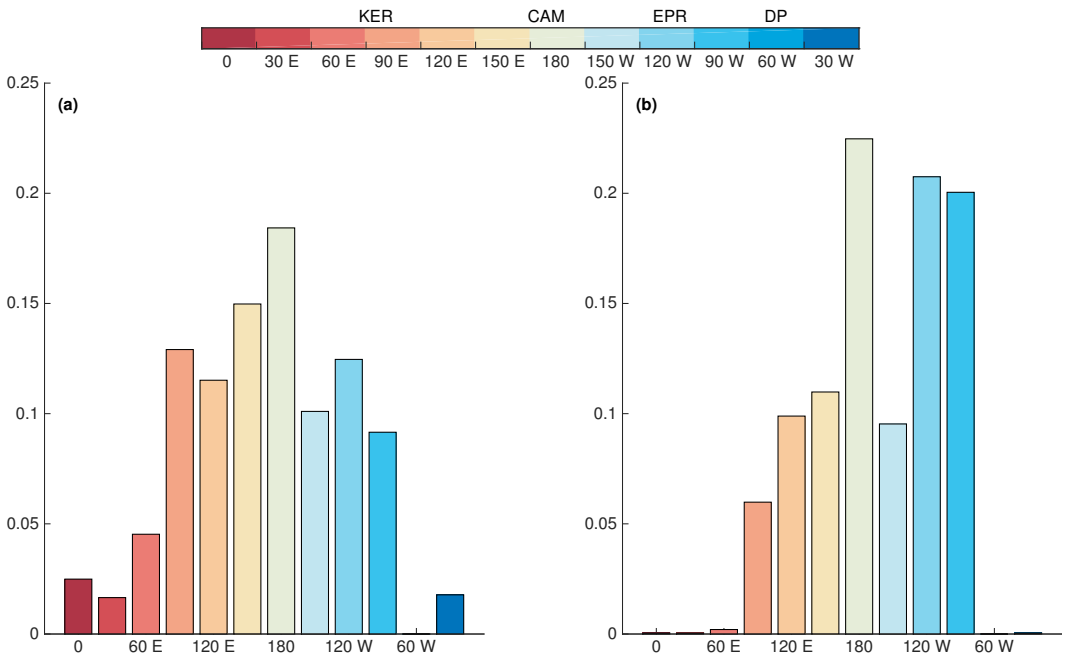


Figure 2.7: Summary of initiation longitude for (a) all outcropping drifters for (b) drifters outcropping in hotspot zones. Labels above the colorbar indicate approximate positions of major bathymetric features: Kerguelen Plateau, KER, Campbell Plateau, CAM, East Pacific Rise, EPR, and Drake Passage, DP.

There is also a spatial pattern to the average age at which drifters outcrop, with young drifters upwelling in the West Indian and Pacific sectors and older drifters outcropping in Drake Passage and the Atlantic. Drifters upwelling on the southern flank of the ACC also tended to be significantly older than the drifters upwelling further north; note that the southernmost outcropping positions are located further away from the deployment latitudes. On average, it takes less time for drifters deployed in July to outcrop, as compared to the January deployments. This feature is especially distinct in the Indo-Pacific sector (Figure 2.8), emphasizing the importance of the seasonal cycle of mixed layer depths in setting outcropping locations. This figure displays the average time, measured from the deployment date, for a drifter to outcrop for each 1° by 1° grid box. This represents the mean time to outcrop averaged over all drifters outcropping in a particular box. Only boxes in which at least 5 drifters outcropped were included in the map. The two panels show drifters deployed on (a) January 1 and (b) July 1. The patterns in Figure 2.8 are consistent with the data in Figure 2.7, which shows the source region being spatially localized; thus the difference in time to outcropping sites reflects the advection period.

The majority of drifters outcrop within the first year. Roughly 2/3 of the drifters

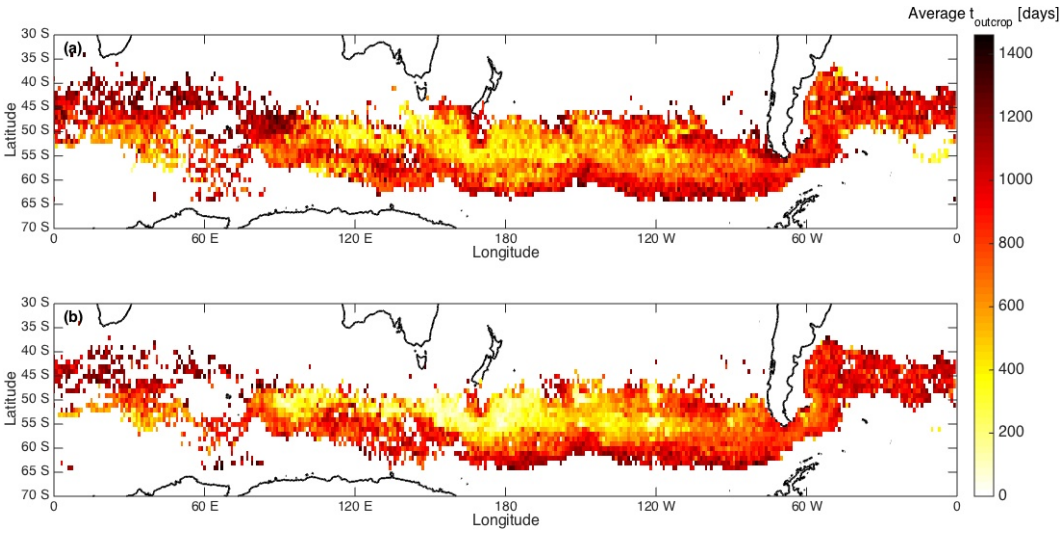


Figure 2.8: Average time (days) to first outcrop since deployment dates of (a) January 1 and (b) July 1 across the Southern Ocean. Drifters from all depths are included.

deployed on a given date outcrop within 0.4 years of the corresponding austral winter season, with the remaining drifters outcropping at a slower and slower rate throughout the remainder of the simulation. This timing is dominated by the seasonal variations of the mixed layer depth with most outcropping events occurring in winter. Thus July deployments are rapidly entrained into the mixed layer, while January deployments experience a ~6 month advection period before outcropping becomes intense (Figure 2.9). This seasonality of outcropping persists throughout the four year deployment and can be seen through the distinct step-like shape of the curves in Figure 2.9.

The season in which drifters are deployed also has little effect on the patterns of outcropping as a function of mixed layer depth, with the majority of drifters doing so in regions where the mixed layer is between 50 and 200 m deep. However, when outcropping hotspots are considered, this peak occurs over a narrower range, between 100 and 200 m depth (Figure 2.10). Here, all outcropping instances are shown in panel (a), while in panel (b), only drifters outcropping in hotspot regions are taken into account. Each panel shows three lines: one which represents January 1 deployments (red), one which represents July 1 deployments (green), and one which represents mixed layer depths over an annual cycle (black dashed). By comparing the two panels, it is apparent that there is a sharper peak in the mixed layer depths at outcropping hotspot regions and that this peak occurs at shallower depths than the corresponding peak when the full domain is considered. This suggests that

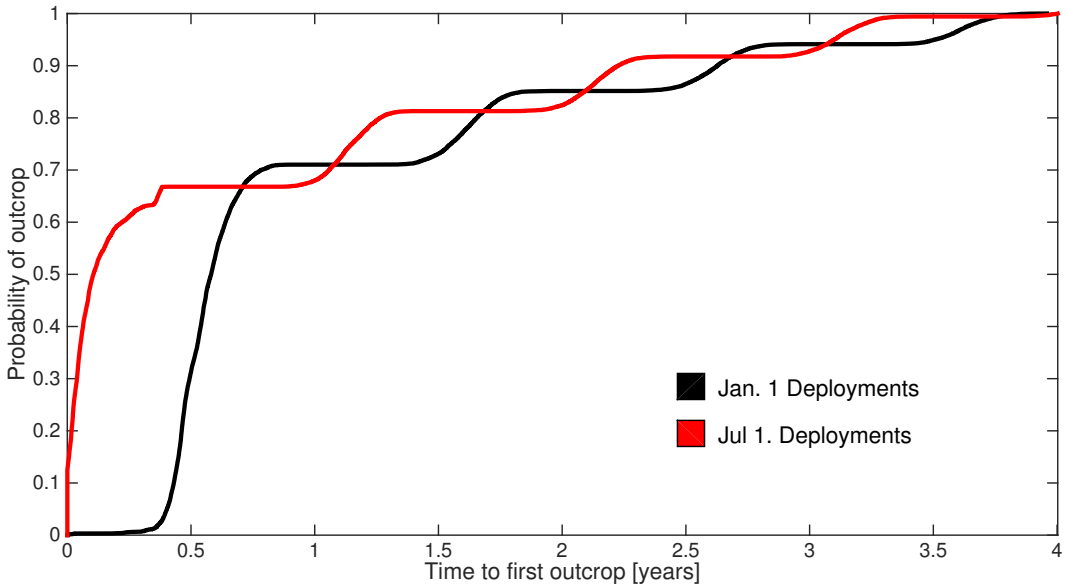


Figure 2.9: Cumulative distribution functions (CDF) depicting the time to first outcrop for each drifter that outcropped at least once during the simulation. The black curve shows the CDF for drifters that were deployed in January; the red curve shows the CDF for drifters deployed in July.

mixed layer depth alone is not able to explain the phenomenon of these outcropping hotspots.

After four years of forward advection, only a small subset of drifters spend more than two cumulative years in the mixed layer, and virtually no drifters persist longer than three years of deployment. On average, if a drifter crosses into the mixed layer at least once during its deployment, it will spend a period of 261 days in the mixed layer (Figure 2.11). The four lines in Figure 2.11 correspond to snapshots taken at the end of each year of deployment, such that the blue curve contains data from the first year, the red curve contains data from the first two years, and so on. The mean cumulative residence time increases as each year passes, as signified by the circles on the x-axis of Figure 2.11, which show the mean residence time at the end of each year of the simulation. The inset figure shows the mean time spent in the mixed layer by an outcropping drifter as a function of simulation time, with the magenta line providing a reference scenario in which all drifters spend all their time in the mixed layer. A fit to this curve shows that outcropping drifters spend, on average, 20% of their time in the mixed layer, a result that is robust regardless of season of deployment. Initial depth of deployment also has a small effect on this result, with drifters deployed at 250 m spending 22% and those deployed at 500 m spending

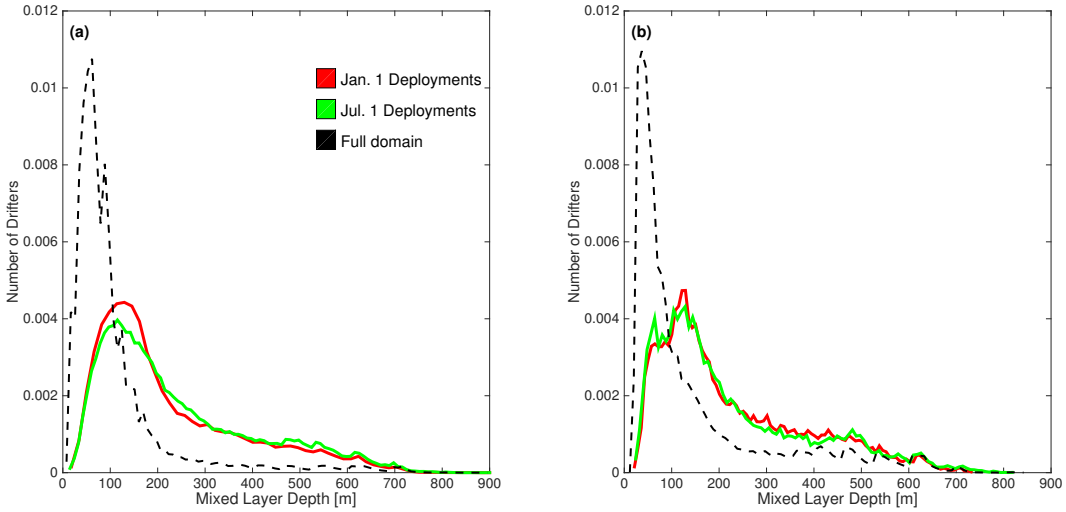


Figure 2.10: Probability distribution functions showing the mixed layer depth at a drifter's point of outcrop for (a) all outcropping drifters and (b) for drifters outcropping in hotspots. The outcropping events are normalized such that the area under the curve sums to 1 and the x-axis gives the mixed layer depth in meters. The histograms are split by deployment date, with January 1 deployments in red and July 1 deployments in green. Mixed layer depths over one year across the domain (from 45°S to 65°S) are given by the dashed line in panel (a), while mixed layer depths over the same one-year period at the hotspots are given by the dashed line in panel (b).

17% of their time in the mixed layer.

Throughout the four year deployment, a greater number of drifters are gaining density during their residence in the mixed layer, but the amount of density modification for drifters losing density is much higher than it is for drifters that gain density. In fact, the average amount of density gain in the mixed layer is +0.22 kg/m$^3$, while the average amount of density loss is –0.47 kg/m$^3$. This result suggests that there is a net densification of water in the mixed layer in the study region. This is corroborated by the results of Iudicone et al. (2008), who showed net downwelling over the bulk of the density classes examined in this study. Additionally, the amount of time spent in the mixed layer seems to have a fairly small effect on the amount of density modification that occurs (Figure 2.12), likely reflecting both the non-linearities produced by the mixed layer and buoyancy flux variability and the way in which the mixed layer has been parameterized in this study. In this figure, each instance of outcropping was counted separately, even if a drifter outcropped multiple times.

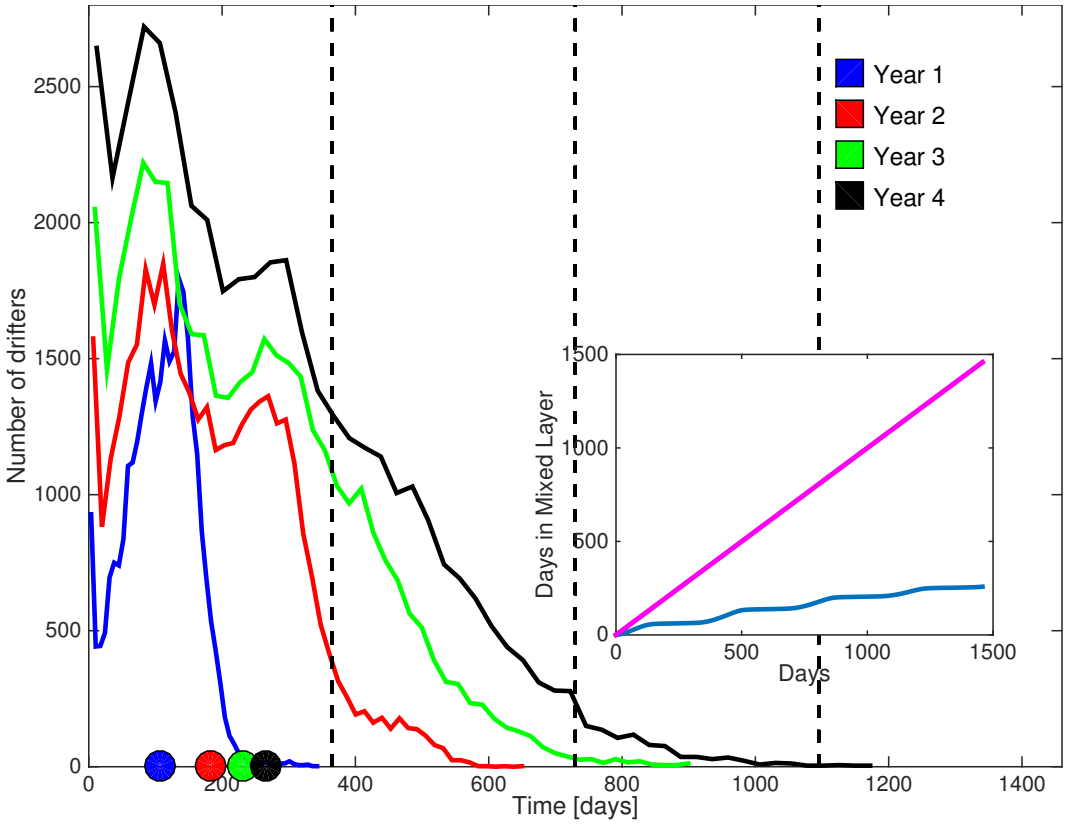


Figure 2.11: Cumulative mixed layer residence time for all drifters that outcrop at least once. The blue, red, green, and black lines respectively represent the first, second, third, and fourth years of deployment (inclusive). The dashed vertical lines delineate the years since deployment. The circles along the x-axis denote the mean residence times for each year of the simulation. Inset: Days of simulation vs. the mean time spent in the mixed layer. The magenta line represents the scenario that all outcropping drifters stay in the mixed layer for the duration of the simulation. The blue curve is the mean over the July deployments.

## 2.5 Discussion

### Localization of Outcropping

As noted in Section 2.4, there is significant spatial variability in outcropping sites across the Southern Ocean, a trend that persists regardless of the season in which drifters were deployed or their initial depths. While few drifters outcrop in the Atlantic and Indian basins, significant outcropping occurs in the Pacific, a result that is evident even when considering the relative sizes of the ocean basins. Examining smaller scales, the outcropping is predominantly constrained to specific, highly localized regions of the ocean, which appear to be correlated with major bathymetric features of the ocean. "Hotspots" of upwelling can be seen near Kerguelen and

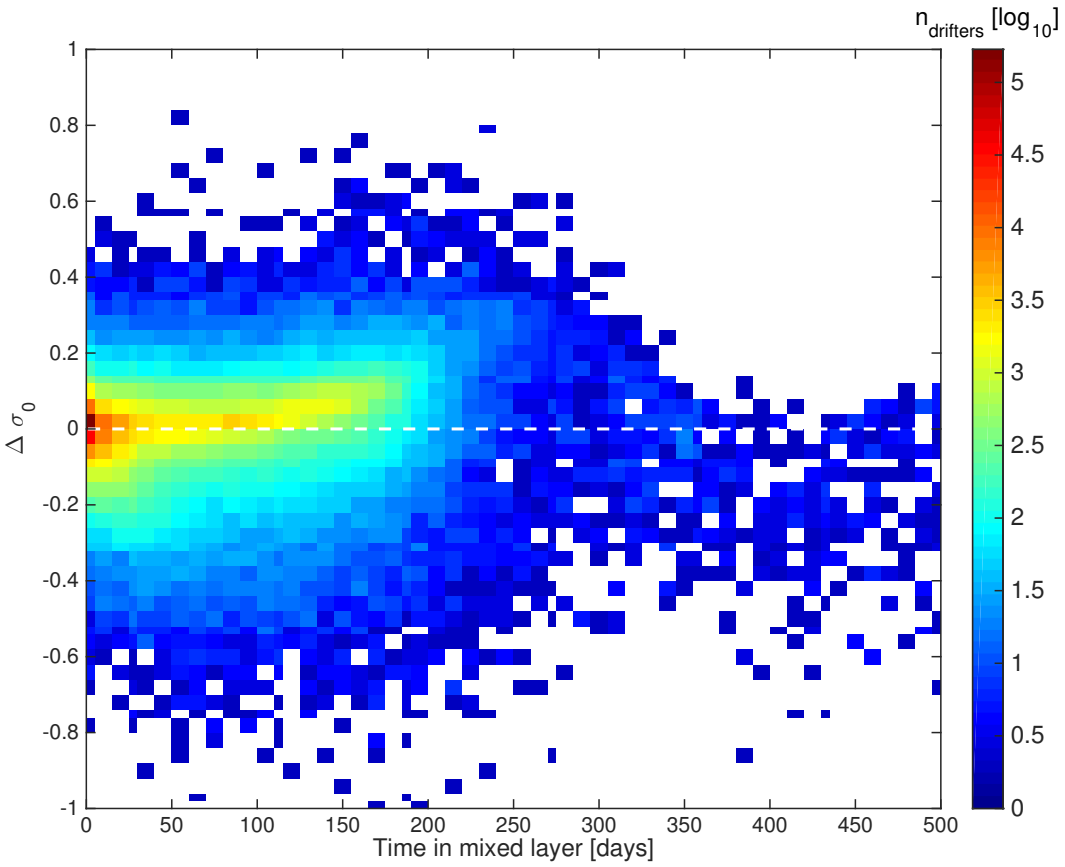


Figure 2.12: Two-dimensional histogram depicting change in density between drifters entering and exiting the mixed layer. On the x-axis is the number of consecutive days spent in the mixed layer. The y-axis shows the change in potential density, $\sigma_0$ (kg m$^{-3}$). The colorbar is on a logarithmic scale. White line indicates zero density modification.

Campbell Plateaus, in the lee of the East Pacific Rise, and throughout Drake Passage, all regions in which there are abrupt changes in topography over relatively short horizontal distances.

As shown by Figure 2.1, deep mixed layers (> 500 m) are seasonally found in the lee of major bathymetric features of the Southern Ocean. This may lead to the conclusion that topographic deepening of mixed layers is responsible for enhanced entrainment of waters and thus, increased outcropping frequency in the lee of these major plateaus and ridges. It is important to note that the modeled mixed layer depths show significant (> 50 m) deviation from the observed mixed layer depths over much of the Southern Ocean, especially when attempting to resolve the deep wintertime mixed layers of the Indian basin. However, as shown in Figure 2.10, the majority of outcropping is occurring into shallower mixed layers on the order

of 100–200m. This suggests that there may be another mechanism responsible for setting the locations of the hotspot outcropping zones, such as deflection of isopycnals upwards over significant bathymetry, causing water masses to rise in the water column and then advect across lateral mixed layer depth gradients downstream of these features, as discussed by Sallée et al. (2010).

**Buoyancy Forcing and Variability**

As water masses are exposed to the surface mixed layer, surface buoyancy forcing may modify the surface layer such that subsequent subduction need not occur on the same isopycnal on which the water upwelled. This diabatic transport in the mixed layer is a major component of the water mass modifications in the Southern Ocean. It has been proposed that both limbs of the overturning circulation, e.g., waters becoming both more and less buoyant at the surface, outcrop in the ACC (J. A. Marshall and Speer, 2012), although we note that the largest sources of densification are likely to occur very close to the Antarctic coast (Rintoul, 2013; Naveira Garabato et al., 2016). Previous work has shown the importance of buoyancy fluxes within the ACC on the global overturning circulation (Weijer et al., 2002; J. A. Marshall and Speer, 2012). A direct diagnosis of the of the water mass transformation, as completed in Bishop et al., 2016 and Newsom et al., 2016, is beyond the scope of this study, but would be reflected in the mixed-layer drifter tendencies if the model is in a statistically steady state.

The zonal structure of buoyancy forcing in the Southern Ocean has been the focus of recent work emphasizing its impact on the global OC (Cerovečki et al., 2011; Tamsitt et al., 2016; Thompson et al., 2016a). As seen in Figures 2.4 and 2.5 and discussed in Section 2.5, strong spatial patterns of upwelling exist across the Southern Ocean; this will lead to similarly variable patterns of buoyancy fluxes, since the Southern Ocean is responsible for the spatial variability of air-sea buoyancy exchange, as shown in Tamsitt et al. (2016). Indeed, the zonal structure in surface buoyancy flux shown by that work reflects the locations of the outcropping hotspots identified in this study. However, attempts at calculating the intensity of the overturning circulation, as mediated by surface buoyancy forcing, typically rely on climatological estimates of the surface buoyancy distribution, surface flux, and mixed layer depth, e.g., J. A. Marshall and Radko (2003). These terms combine in a non-linear expression for the overturning streamfunction. However, since all three of these terms are time-dependent, it is not clear that time-averaged or climatological values of these properties will provide accurate estimates of the overturning streamfunction. Our

results show all of these properties exhibit intermittency in both space and time. The temporal correlation of these different properties and their impact on overturning rates remain relatively unexplored.

**Mixed Layer Residence Times**

One of the notable results of this study, as seen in Figure 2.11, is the relatively short residence time experienced by waters in the mixed layer in the Southern Ocean. During the July deployment, roughly two-thirds of the drifters outcrop in the first three months following deployment. Yet, on average, the drifter spend less than half a year in the mixed layer. The combination of the spatial heterogeneity and the seasonal cycle of the mixed layer causes a long-term residence time, e.g., over a seasonal cycle, to be rare. The implications of this short residence time is that the ability of a Lagrangian water mass to equilibrate gases concentrations via air-sea exchange will undergo a seasonal cycle with reduced opportunities to exchange properties in the biologically productive summer months. Previous studies have quantified the air-sea equilibration timescale for carbon dioxide as ranging from 6–24 months; the high end of this range is typically associated with the Southern Ocean south of Australia and New Zealand (D. C. Jones et al., 2014). Combined with the inset of Figure 2.11, this suggests that over large swaths of the Southern Ocean, complete equilibration of carbon dioxide with the atmosphere may take 5–10 years. If this is shorter than the timescale of subduction of a given parcel into the ocean interior, full equilibration may be highly limited around the Southern Ocean.

Another implication of the seasonality drifters experience in the mixed layer is that the cumulative residence time is also lowered. Again referring to Figure 2.11, the cumulative residence times approximate a Rayleigh distribution. A Rayleigh distribution is found in cases where two non-correlated, normally distributed variables combine to produce a third quantity. In this case, the mixed layer depth and the vertical position/trajectory of the drifters influence the residence time of the drifters in the mixed layer. The vertical positions are close to a normal distribution given the treatment of particles in the mixed layer; the mixed layer depths can be crudely approximated by a normal distribution. Thus, as a rudimentary fit, the Rayleigh distribution is appropriate, although this could certainly be the subject of further examination in future work. This figure also demonstrates that over the course of the 4-year simulation, no drifters are able to remain in the mixed layer for close to the entire length of the simulation. In fact, few drifters even spend three cumulative years in the mixed layer. This, too, affects the extent to which waters can equilibrate

carbon dioxide and other properties with the atmosphere. From Figure 2.12, there is no apparent correlation between mixed layer residence time and the magnitude of density modification, as measured by the difference in isopycnal upon entering and exiting the mixed layer. This implies that parcels of water that retain a disequilibrium between ocean and atmosphere gas concentrations, can still experience large density changes due to surface buoyancy forcing. This allows these water masses to participate in the overturning circulation and potentially be subducted to depth, limiting the parcel from future interaction with the atmosphere. This is of particular importance for analyses that use transit time distributions (TTDs) to infer water mass pathways throughout the ocean, e.g., Waugh et al., 2006; Peacock and Maltrud, 2006. These studies typically assume that water parcels instantaneously equilibrate with the atmospheric gas concentrations in determining surface initial conditions. This study suggests that additional information about surface residence times could influence these surface boundary conditions.

**Limitations of the Study**

This study provides new insight into the three-dimensional pathways of upwelling water masses, localized regions of outcropping, and mixed layer residence times in the Southern Ocean. However, the scope of the study is necessarily limited by a number of factors that may affect the robustness of the result. Firstly, the horizontal resolution of the OFES model is 1/10°, meaning that it does not resolve submesoscale features. Submesoscale features have been shown to be significant in enhancing vertical velocities as well as exchange across the base of the mixed layer (Klein and Lapeyre, 2009; Thomas et al., 2013). These features are not represented in this model, nor are they parameterized. Observational evidence of the prevalence of submesoscale dynamics in the Southern Ocean has been limited; however, the region is pre-conditioned to be favorable to these types of flows due to the presence of eddying currents and filamentation, frequent storms and a long-term, down-front orientation of the wind stress with geostrophic fronts. One of the benefits of this study was the ability to use offline GCM data with a temporal resolution of three days. If a submesoscale-resolving model were to be used in place of OFES, the model output may need to be loaded with greater frequency, making the study significantly more computationally expensive.

As detailed in Section 2.3, drifter motion in the mixed layer is represented by a random walk with a maximum velocity of 0.28 cm $s^{-1}$, consistent with estimates of vertical diffusivities within the mixed layer. The additional constraint is placed upon

the drifters that they cannot vertically advect out of the mixed layer, in order to prevent the case where drifters continually oscillate across the base of the mixed layer. However, this may be a crude approximation to true mixed layer-interior exchange dynamics. For instance, active mixing layers may be decoupled from the total depth of the mixed layer for a number of reasons, including surface restratification by buoyancy or wind forcing, (Taylor and Ferrari, 2010) By forcing drifters to remain in the mixed layer until the boundary shoals or they horizontally advect across a strong gradient in mixed layer depth, we may be artificially enhancing the residence time of the mixed layer. We note that both localized convective events and advection by enhanced vertical velocities at the ocean submesoscale are not resolved by the OFES model. These have the potential to make a significant contribution to the total mixed layer-interior exchange, but observations of these processes in the Southern Ocean are limited. For this reason we have decided not to try and represent their effects by parameterizations, as in Omand et al., 2015.

We have also neglected interior diapycnal mixing in our advective scheme, constraining the drifters to move along isopycnals outside of the mixed layer. Previous observations of the Southern Ocean have shown diapycnal mixing to be large in localized regions of the ACC, especially near shallow/rough topography (Naveira Garabato et al., 2004; LaCasce et al., 2014), such as the outcropping regions identified here. However, throughout the bulk of the Southern Ocean, the approximation of isopycnal movement is a sound one, and the deep mixed layers near significant topographic features in the model may imitate the diapycnal mixing in these regions.

Lastly, this study was intentionally broad in its scope, attempting to sample the entire Southern Ocean and identify specific outcropping hotspots. Now that such regions have been identified, further work can be done targeting the source regions of specific water masses from each ocean basin. Site- or basin-specific sampling could be probed with numerical models that have a higher resolution than was employed in this study.

## 2.6 Conclusions

This study employs an eddy-resolving OFES GCM to explore the Lagrangian pathways of upwelling in the Southern Ocean. Virtual drifters were deployed across the Southern Ocean in two seasons, allowing us to examine both spatial and temporal variability of outcropping.

Specific sites stand out as “hotspots” where the majority of waters upwell into the

mixed layer. The locations of these hotspots, in the lee of Kerguelen and Campbell Plateaus, around the East Pacific Rise, and through Drake Passage, suggest not only geographic localization but topographic control of upwelling. The use of virtual drifters allows for analysis at finer scales than previous methods that have studied outcropping and subduction in the region, e.g., Sallée et al. (2010) and Gebbie and Huybers (2011). This allows for the identification of smaller-scale features and variability, although the broad patterns are consistent with these previous result. The confirmation of strong topographic control on mixed layer ventilation is an important result with respect to longer-scale climate variability, in that this feature is likely less susceptible to temporal changes and might focus future observational efforts or paleoceanographic studies.

Several scales of variability are highlighted in the patterns of outcropping in the Southern Ocean. The intra-basin contrast reflects a wavenumber 1 pattern, with very little outcropping occurring in the Atlantic and most drifters upwelling in the Pacific basin. However, there are many smaller-scale variations as well. Large bathymetric features show strong and abrupt changes in outcropping frequency moving from the upstream to downstream sides. There is also potentially mesoscale variability due to the generation of deeper mixed layers in the lee of strong topography. As discussed in Section 2.5, one of the limitations of the study is the resolution of the chosen GCM, limiting our ability to assess the impact of submesoscale processes on outcropping frequency and surface residence times.

We have also demonstrated that the mixed layer residence time is short, as compared to the duration of the trajectories. Drifters may outcrop into the mixed layer multiple times during their life span, however, each outcropping event is associated with a residence time on the order of one month; residence times greater than a year are observed infrequently. The cumulative residence times experienced by the drifters are similarly short, although a small subset of drifters spent between 1 and 3 years in the mixed layer over the 4-year simulation. When examined in conjunction with studies of air-sea equilibration timescales, e.g., D. C. Jones et al. (2014), this suggests that mixed layer residence time is a significant hindrance to achieving air-sea equilibrium of certain gases, such as $CO_2$ (typical residence time of 6–12 months) and $^{14}CO_2$ (typical residence time of order 10 years), in the Southern Ocean.

This study suggests that the Lagrangian time history of water parcels in the Southern Ocean may impact interior tracer distributions. We have not assessed the impact

of these outcropping frequencies on the overturning circulation, as modulated by surface buoyancy forcing, but we note that assessments of the strength of this modification typically apply time-averaged or climatological distributions of mixed layer depths as well as heat and freshwater forcing. This study points to the need, in future work, to assess the temporal correlation of these properties and their impact on global water mass transformation rates.

*Chapter 3*

# ABRUPT TRANSITIONS IN SUBMESOSCALE STRUCTURE IN SOUTHERN DRAKE PASSAGE: GLIDER OBSERVATIONS AND MODEL RESULTS

Viglione, G. A. et al. (2018). "Abrupt transitions in submesoscale structure in Southern Drake Passage: Glider observations and model results". In: *J. Phys. Oceanogr.* 48.9, pp. 2011–2027. DOI: 10.1175/JPO-D-17-0192.1.

## 3.1 Abstract

Enhanced vertical velocities associated with submesoscale motions may rapidly modify mixed layer depths and increase exchange between the mixed layer and the ocean interior. These dynamics are of particular importance in the Southern Ocean, where the ventilation of many density classes occurs. Here we present results from an observational field program in southern Drake Passage, a region preconditioned for submesoscale instability due to its strong mesoscale eddy field, persistent fronts, strong down-front winds, and weak vertical stratification. Two gliders sampled from December 2014 through March 2015 upstream and downstream of Shackleton Fracture Zone (SFZ). The acquired time series of mixed layer depths and buoyancy gradients enabled calculations of potential vorticity and classifications of submesoscale instabilities. The regions flanking the SFZ displayed remarkably different characteristics despite similar surface forcing. Mixed layer depths were nearly twice as deep and horizontal buoyancy gradients were larger downstream of the SFZ. Upstream of the SFZ submesoscale variability was confined to the edges of topographically steered fronts, whereas downstream these motions were more broadly distributed. Comparisons to a 1-D mixing model demonstrate the role of submesoscale instabilities in generating mixed layer variance. Numerical output from a submesoscale-resolving simulation indicates that submesoscale instabilities are crucial for correctly reproducing upper ocean stratification. These results show that bathymetry can play a key role in generating dynamically distinct submesoscale characteristics over short spatial scales and that submesoscale motions can be locally active during summer months.

## 3.2 Introduction

The Southern Ocean plays a key role in Earth's climate due to the ventilation of deep waters and the subduction of newly formed intermediate and bottom waters. Upwelling and subduction rates depend on surface forcing, mixed layer depths, and the spatial and temporal distribution of surface outcrop positions of density classes (D. Marshall, 1997; Abernathey et al., 2016). Oceanic submesocale motions are known to significantly impact upper ocean stratification and exchange between the mixed layer and thermocline (Klein and Lapeyre, 2009; McWilliams, 2016). The submesoscale is distinguished by Richardson and Rossby numbers approaching $O(1)$. Unlike low-Ro, large-scale flows, which drive horizontal stirring of large-scale buoyancy and tracer gradients, submesoscale motions lead to large vertical velocities and fluxes (Mahadevan and Tandon, 2006).

The Southern Ocean and the Antarctic Circumpolar Current (ACC) are associated with many of the characteristics that are conducive to generating submesoscale motions: (i) persistent frontal currents with strong lateral buoyancy gradients, (ii) strong surface forcing, (iii) vigorous stirring by an energetic mesoscale eddy field, and (iv) weak vertical stratification. While much of our understanding about submesoscales has been achieved through idealized modeling approaches, (e.g., Boccaletti et al., 2007; Capet et al., 2008; Thomas and Ferrari, 2008; Mahadevan et al., 2010), regional, submesoscale-resolving simulations in the Southern Ocean, such as around Kerguelen Plateau (Rosso et al., 2014) and Drake Passage (Bachman et al., 2017a), have demonstrated the impact of these scales on upper ocean stratification and vertical exchange with the ocean interior. In particular, Rosso et al. (2014) reports enhanced vertical exchange and velocities when submesoscales are resolved, while Bachman et al. (2017a) shows that mixed layers shoal with increased model resolution.

Observations of the submesoscale in the Southern Ocean are sparse due to the difficulty and expense of field campaigns in this region. Even in Drake Passage, which is the most intensively studied region of the Southern Ocean (Meredith et al., 2011), observations are typically carried out on large temporal and spatial scales, such as the repeat expendable bathythermograph sections of Drake Passage (Sprintall, 2003) and the UK-led SR1b line. Little observational work is available at the submesoscale to corroborate the modeling work that has been done in the region. Adams et al. (2017) provides a notable exception; this field program surveyed an active submesoscale field surrounding a large coherent mesoscale eddy pinched off

from the Polar Front. New analysis of high-resolution model output by Su et al. (2018) suggests that the Southern Ocean also has the smallest seasonal cycle of submesoscale activity. In contrast to *in situ* studies in subtropical regions which predominantly found submesoscale activity in wintertime (e.g., Callies et al., 2015; Thompson et al., 2016b; Hosegood et al., 2013), we present evidence for intermittent episodes of a highly active submesoscale field during summer months in Southern Drake Passage.

In recent years, autonomous underwater vehicles, such as Seagliders, have been increasingly used as a method of observing submesoscale dynamics over longer time periods than is allowed by ship-based field campaigns. A 2008 observational study in the North Atlantic used gliders to provide evidence for an eddy-driven restratification of the upper ocean that spurred spring phytoplankton blooms in the North Atlantic (Mahadevan et al., 2012). More recently, the 2012–13 Ocean Surface Mixing, Ocean Submesoscale Interaction Study (OSMOSIS) campaign studied a small patch of the open ocean for an entire year, documenting a range of submesoscale instabilities (Thompson et al., 2016b). Todd et al. (2016) used gliders to study the potential vorticity (PV) structure of the North American Western Boundary Currents, and du Plessis et al. (2017) carried out similar analyses in the ACC's Subantarctic Zone.

The goals of the field program presented here, Changes in Stratification at the Antarctic Peninsula (ChinStrAP), were to observe mixed layer depth variability and its impact on the ventilation and subduction of near-surface water masses at submesoscale temporal and spatial resolution. ChinStrAP provides the first submesoscale-resolving seasonal-scale observational experiment in Drake Passage, collected by Seagliders over a period of 4 months in the austral summer of 2014–15. The gliders sampled on either side of the Shackleton Fracture Zone (SFZ), providing insight into two distinct dynamical regimes. Upstream of the SFZ, the Southern Boundary of the ACC (SBACC) and the Southern ACC Front (SACCF) are strongly constrained by topography close to the shelf, but deflect northward as they pass over the SFZ (Orsi et al., 1995). The injection of Weddell Sea Waters by the Antarctic Slope Front (ASF) (Gill, 1973; Jacobs, 1991) and Weddell Front downstream of the SFZ (Heywood et al., 2004; Thompson et al., 2009) lead to further differences in properties between the regions (Patterson and Sievers, 1980; Whitworth et al., 1994). Although we cover a relatively small region of the Southern Ocean, these observations show abrupt changes in the characteristics of the submesocale motions and their impact on the upper ocean hydrography; lessons from this region may be

extended to other parts of the Southern Ocean.

Following earlier observational studies, we analyze the glider data for instances where the ocean is preconditioned towards gravitational and/or symmetric instability in the mixed layer. Symmetric instability is a shear instability that extracts kinetic energy from geostrophic flows via slantwise convection. The resulting rearrangement of water parcels leads to low PV in the mixed layer, conditioning it to further submesoscale instabilities (Haine and J. A. Marshall, 1998). We also investigate the relative impacts of mixed layer baroclinic instability (BCI), which shoals the mixed layer by the slumping of isopycnals (Haine and J. A. Marshall, 1998), and Ekman buoyancy flux, or wind-driven re- and de-stratification (Thomas, 2005). When a wind stress is applied in a down-front orientation, the resulting Ekman transport carries denser water over lighter waters, causing vertical convection and a destruction of stratification and PV. When the wind has an up-front orientation, the Ekman transport moves lighter water over denser water, causing an increase in stratification throughout the Ekman layer depth, which can lead to a restratification of the mixed layer. Parameterizations are used to compare the potential effects of Ekman buoyancy flux and BCI on the mixed layer buoyancy budget. As in du Plessis et al. (2017), we use a 1-D mixed layer model to discern the role of surface forcing on setting upper ocean stratification. The model is then modified to incorporate the effects of Ekman buoyancy flux and BCI. Our results suggest that these processes are at least as important as the surface wind and buoyancy forcing in setting mixed layer variability in the Southern Ocean. Finally, a high-resolution global circulation model is used to validate our mixed layer observations and to confirm the feasibility of calculating PV from gliders.

The paper is organized as follows. Section 3.3 contains a description of the ChinStrAP field program, a description of the supplementary datasets used, the theoretical framework used to quantify the effects of submesoscale processes on the stratification of the upper ocean, and a brief description of the bulk mixed layer model used to replicate the observed mixed layers. Section 3.4 provides a characterization of the study site using previously derived parameterizations to examine the spatial and temporal variability of submesoscale instabilities, and evaluates the efficacy of the mixed layer model. Section 3.5 further analyzes the variability across Shackleton Fracture Zone (SFZ), a prominent bathymetric feature off the tip of the Antarctic Peninsula and proposes the cause of the dynamical differences between the regions just upstream and downstream of the SFZ. Here we also discuss the limitations of

the study. Our conclusions are presented in Section 3.6.

## 3.3 Methods

### Field program description

Two key foci of the ChinStrAP field campaign were (i) identifying regions of southern Drake Passage that may be conditioned for submesoscale instabilities and (ii) determining the relative importance of submesoscale motions and atmospheric forcing on the upper ocean stratification. Two Seagliders were deployed north of the Antarctic Peninsula and piloted in cross-shelf sections over a period of four months (December 2014 to April 2015) (Figure 3.1a–b). Shipboard Rosette CTD casts conducted during the glider deployment cruise were used for glider sensor calibration and initialization of the PWP model (Section 3.43.4, Figure 3.8a).

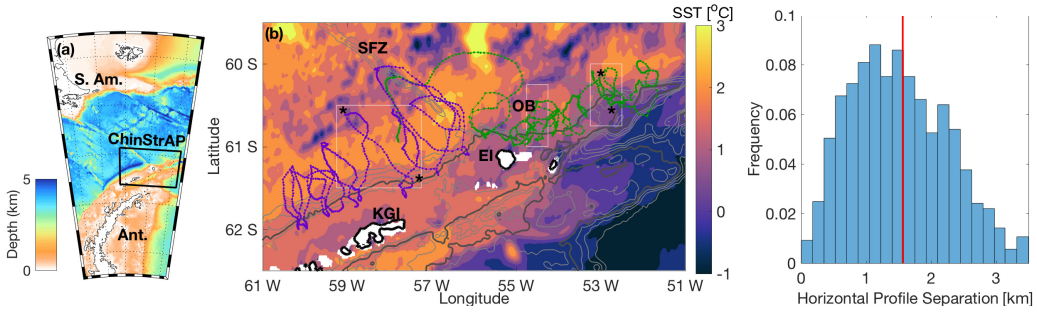


Figure 3.1: Overview of the ChinStrAP field program. (a) Bathymetry of Drake Passage region (from ETOPO1) including the ChinStrAP study area (black box). (b) ChinStrAP glider lines from SG-W (purple) and SG-E (green) are overlaid on 1-km resolution GHRSST from 3 February 2015 (Chao et al., 2009). Bathymetric contours are shown in 500-m intervals (gray) with the 0 m contour in black and 1000 m contour bolded. Major bathymetry features are labeled: Shackleton Fracture Zone (SFZ), Ona Basin (OB), Elephant Island (EI), and King George Island (KGI). Black asterisks indicate sections used in Figure 3, white boxes indicate subdomains of LLC model. (c) Histogram of horizontal separation of glider profiles for both vehicles shows a mean of 1.6 km (red).

The gliders profile in a V-shaped pattern, sampling continuous, inclined profiles to either 1000 m or the ocean floor, whichever depth was shallower. A full-depth dive took approximately 5 hours to complete, and spanned a horizontal displacement of between 0.1–7 km, depending on the strength of the background flow (Figure 3.1c). A full transect across the shelf was completed over a period of roughly one week. During each dive, measurements of temperature, pressure, and salinity data were collected from a Seabird SBE3 temperature sensor and a SBE4 conductivity sen-

sor (CTSail). The unpumped CTD sampled every 5 seconds throughout the dive, approximately every 1 m. The initial accuracy of the temperature and salinity is approximately 0.002°C and 0.002 psu, respectively, with expected drifts over the deployment of less than 0.001°C and 0.001 psu. Both gliders were additionally equipped with an Aanderaa 4330F oxygen optode, and a WET Laboratories Environmental Characterization Optics (ECO) Puck measuring fluorescence and optical backscatter; an analysis of subduction pathways based on the optical data is given in Erickson et al. (2016).

The raw glider data were processed using the University of East Anglia's Seaglider Toolbox, which corrects for lag and inertial effects, then were manually despiked. These data were objectively mapped onto a regular grid in depth and time, with a vertical resolution of 5 meters and a horizontal temporal resolution of approximately 1 hour (using a Gaussian weighting function with a vertical scale of 15 m and a temporal scale of 4 hours). A comparison of the raw data to the objectively mapped dataset revealed no significant aliasing due to this choice of resolution; a sensitivity study on the horizontal grid showed this resolution to introduce minimal spurious features while retaining the most information about submesoscale processes. The horizontal glider position was interpolated to this grid to give a monotonically increasing along-track distance, from which horizontal spatial gradients could be calculated. This dataset necessarily conflates spatial and temporal variability, and it remains a significant challenge to separate out these effects in our analysis; we appeal to a high-resolution numerical model to provide additional confidence in our analysis.

Glider SG-W was deployed north of King George Island at 58.82°W, 61.73°S, and completed 771 dives over a four-month period. The second glider, SG-E, was deployed northeast of Elephant Island at 52.48°W, 60.48°S, and completed 642 dives over three months. The two locations are separated by the SFZ, a large bathymetric ridge that runs northwest-southeast perpendicular to the mean flow of the ACC through Drake Passage (Figure 3.1). Throughout the deployment, SG-W predominantly sampled the region upstream of the SFZ, while SG-E remained mainly downstream of the SFZ. Both regions, occupying the same latitudes, experience roughly the same surface heat and surface wind stress. The winds are predominantly westerly and do not vary significantly over the area the gliders sampled. This work considers the influence of submesoscale instabilities on the mixed layer depth and surface buoyancy budget. The mixed layer depth was calculated using a density

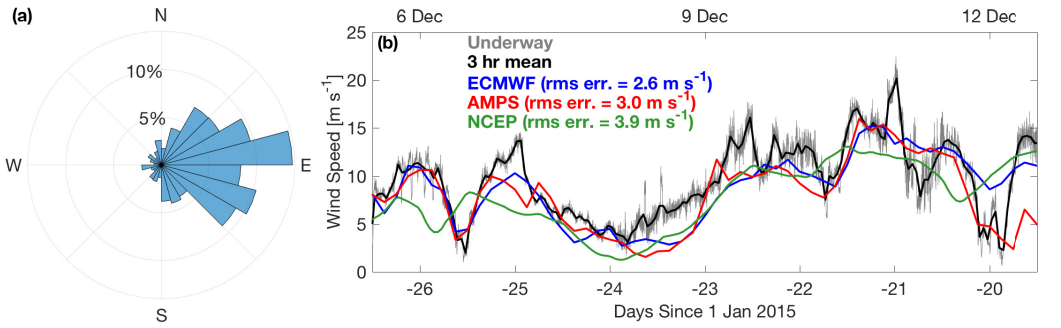


Figure 3.2: (a) A histogram of wind directions from ECMWF over the study region from December 2014–April 2015 shows predominantly westerly winds. (b) A comparison of three tested reanalysis products, ECMWF (blue), AMPS (red), and NCEP (green) and shipboard wind speed data (instantaneous wind speed in gray, 3-hour running mean in black).

threshold criterion using $\Delta\sigma = 0.125$ kg m$^{-3}$ (Monterey and Levitus, 1997); this value was chosen because it gave the best visual agreement with the surface mixed layer in individual profiles.

### Additional data sets

Wind speed and wind direction data were available four times daily from ECMWF ERA-Interim reanalysis (Dee et al., 2011), which has a horizontal resolution of ~80 km. ECMWF was selected because it most accurately reproduced both wind speed and direction as measured by the shipboard instruments over a one-week period during the deployment cruise (Figure 3.2b). Freshwater and surface heat fluxes were also taken from ECMWF to be consistent with the wind stress data.

### Mixed layer model description

In the following data set we explore the impact of lateral (or three-dimensional) submesoscale dynamics on setting the upper ocean stratification. This was achieved by first using the one-dimensional Price-Weller-Pinkel bulk mixed layer model (PWP) proposed by Price et al. (1986); a similar analysis was carried out by du Plessis et al. (2017) for a different region of the Southern Ocean. Precipitation, longwave radiation, and sensible and latent heat are applied at the surface, while shortwave radiation is absorbed at depth with two wavelength-dependent exponentially decaying terms, with these attenuation distances defined by Paulson and Simpson (1977). Turbulent mixing is parameterized based on the strength of the local wind stress. The surface fluxes and wind stress were interpolated to the glider position at each time step.

Using a time step of 1 hour, surface buoyancy and momentum fluxes are applied and mixed down through the water column, and bulk and gradient Richardson numbers are calculated. If these are below critical values ($Ri_b < 0.65$; $Ri_g < 0.25$ as in Price et al. (1986)), water is entrained from below and the process is repeated.

The PWP model was initialized with the shipboard CTD calibration cast, as the higher vertical resolution acquired by the CTD (1 m as opposed to 5 m from the glider) was found to improve the performance of the model; there was little difference between glider and CTD profiles at this location. In order to distinguish the effects of atmospheric forcing from those of submesoscales, advection, and other three-dimensional processes, a modified PWP model (hereafter, mPWP) was also run, which included parameterizations of an equivalent heat flux from baroclinic instability and Ekman buoyancy flux, detailed in Section 3.3. The implementation of the mPWP will be discussed further in Section 3.4.

**Potential vorticity calculations**

We follow the framework of earlier studies (Thomas et al., 2013; Thompson et al., 2016b; du Plessis et al., 2017) that have used the Ertel potential vorticity (PV) as a diagnostic tool to determine times when portions of the mixed layer may be preconditioned towards instabilities that will act to restore PV to neutral stability conditions. A brief summary of this technique is provided here. The full Ertel PV is given by

$$q_{Ertel} = \omega_a \cdot \nabla b = (f + \zeta) N^2 + \left(w_y - v_z\right) b_x + (u_z - w_x) b_y, \tag{3.1}$$

where $\omega_a = 2\Omega + \nabla \times \mathbf{u}$ is the absolute vorticity, $b$ is the buoyancy, defined as $b = g(1 - \rho/\rho_0)$ with $\rho_0$ as a reference density 1027.15 (the mean density over the deployment), $\Omega$ is the angular velocity of the Earth, $\mathbf{u}$ is the three-dimensional fluid velocity, $N^2 = b_z$ the vertical stratification, and $\zeta = v_x - u_y$, the vertical relative vorticity. Subscripts above indicate partial differentiation.

A limitation of the PV approach is that observations are restricted to the vertical and a single horizontal dimension (Shcherbina et al., 2013; Thompson et al., 2016b). During this particular mission, the gliders were piloted perpendicular to the fronts to the degree possible based on the current speeds; this limits the error in the two-dimensional PV calculation (see Section 3.5). A comprehensive explanation behind the simplifying assumptions made can be found in Thompson et al. (2016b), among

others. The resulting observational PV is given as

$$q_{Obs} = (-v_z, 0, f + v_x) \cdot (b_x, 0, b_z) = (f + \zeta)N^2 - \frac{b_x^2}{f}, \tag{3.2}$$

and the validity of these assumptions will be discussed in Section 3.5.

From the PV calculations, conditions favorable for submesoscale instabilities can be identified using the balanced Richardson number, as in Thomas et al. (2013):

$$\phi_{Ri_b} = \tan^{-1}\left(-\mathrm{Ri}_b^{-1}\right), \tag{3.3}$$

with a critical balanced Richardson angle, $\phi_c = \tan^{-1}\left(-\frac{\zeta}{f}\right)$, separating regimes of symmetric, gravitational, and mixed symmetric/gravitational instability from the stable regime.

**Submesoscale instability calculations**

In addition to the instability criteria described above, which require PV > 0 (opposite sign of $f$), the release of available potential energy stored in the mixed layer through BCI, which does not require PV > 0, may also impact the upper ocean stratification (Boccaletti et al., 2007). Fox-Kemper et al. (2008) provided a parameterization for the effective streamfunction caused by this baroclinic instability dependent on the mixed layer depth $H$ and horizontal buoyancy gradient, $|\nabla b|$. As the gliders can only resolve one horizontal direction, we can write the parameterization as

$$\psi_{BCI} = C_0 \frac{b_x H^2}{f} \mu(z), \tag{3.4}$$

with $b_x$ being the horizontal buoyancy gradient in the direction along the glider track. The empirical constant $C_0$ may vary throughout the ocean, but in the absence of any direct measurements of this value, we take $C_0 = 0.06$ as in Fox-Kemper et al. (2008) and previous glider studies. The function $\mu(z)$ describes the vertical structure of $\psi_{BCI}$; here we set this term equal to unity for simplicity. Using $\psi_{BCI}$ and the lateral buoyancy gradient, the re-stratifying buoyancy flux can be determined, and for ease of comparison to the surface fluxes, as in Mahadevan et al. (2012), this can be expressed as an equivalent heat flux (W m$^{-2}$):

$$Q_{BCI} = 0.06 \frac{b_x^2 H^2}{f} \frac{C_p \rho_0}{\alpha g}, \tag{3.5}$$

where $C_p$ is the specific heat of seawater and $\alpha$ is the thermal expansion coefficient, a function of temperature and pressure.

Another key factor in setting the stratification of the upper ocean is the the interaction between surface wind forcing and upper ocean fronts, a process known as the Ekman buoyancy flux (Thomas, 2005). This effect can also be written as an overturning streamfunction, again with the simplification that we only consider the wind stress component perpendicular to the glider path:

$$\psi_{EBF} = \frac{\tau^y}{\rho_0 f}. \tag{3.6}$$

If we again consider the buoyancy gradient in the along-track direction, $b_x$, we can write an equivalent heat flux expression analogous to (3.5),

$$Q_{EBF} = -\frac{b_x \tau^y}{f} \frac{C_p}{\alpha g}. \tag{3.7}$$

We acknowledge that our analysis disregards much of the intricacy of the vertical structure of the upper ocean, in particular, by eliminating the depth-dependence of the $Q_{BCI}$ parameterization (3.5) and by assuming the equivalence of the Ekman layer and mixed layer depths. Nonetheless, observational evidence from Lenn and Chereskin (2009) supports the notion that in Drake Passage, Ekman layer depths approach the annual-mean mixed layer depths of 120 m. Disentanglement of the vertical structure is beyond the scope of the paper, and we will focus on the parameterizations in terms of relative, rather than absolute, changes.

**Global circulation model description**

Output from a global high-resolution general circulation model based on a Latitude/Longitude/polar-Cap (hereafter LLC) configuration of the MIT general circulation model (MITgcm; J. A. Marshall et al. (1997); Hill et al. 2007) is used to assess the validity of our glider PV analysis. The LLC simulation is a 1/48° MITgcm model with 90 vertical levels, with a horizontal resolution of approximately 0.75 km in the polar regions and a vertical resolution of 1 m near the surface to better resolve the diurnal cycle.

The model configuration includes a flux-limited, seventh-order, monotonicity-preserving advection scheme (Daru and Tenaud, 2004) and the modified Leith scheme of Fox-Kemper and Menemenlis (2008) for horizontal viscosity. Vertical viscosity and diffusivity are parameterized according to the K-profile parameterization (KPP) (Large et al., 1994). Bottom drag is quadratic (drag coefficient, $C_D = 2.1 \cdot 10^{-3}$) and side drag is free slip. Partial cells (Adcroft et al., 1997) are used to represent the sloping sea floor in our z-level vertical discretization. Bathymetry is from Global Topography v14.1, updated from Smith and Sandwell (1997).

The simulation is initialized from a data-constrained global ocean and sea ice solution provided by the Estimating the Circulation and Climate of the Ocean, Phase II (ECCO2) project (Menemenlis et al., 2005; Menemenlis et al., 2008; Losch et al., 2010) and includes tidal forcing. The inclusion of tides allows to successfully reproduce shelf-slope dynamics and water mass modification (Flexas et al., 2015). Surface boundary conditions are 6-hourly output from the ECMWF atmospheric operational model analysis, starting in 2011, with spatial resolution of about 79 km. One year of hourly model output of full 3-dimensional model prognostic variables is available (from September 2011–August 2012).

We used three subdomains: one located upstream of the SFZ, one located between the SFZ and the Ona Basin, and one located downstream of both the SFZ and the Ona Basin, plotted on Figure 3.1b. Comparisons between the observations and the LLC model were made in order to validate the assumptions made in our calculations of potential vorticity (PV) and MLD. Temperature, salinity, and horizontal velocities from the model were used to calculate both the Ertel PV (3.1) and an observational PV (3.2).

## 3.4 Results

### Site characterization

The observations collected in the ChinStrAP field program allow for the examination of both temporal (summer and into early fall) and spatial variability of mixed layer depths and dynamics. Following Whitworth et al. (1998), we define Circumpolar Deep Water (CDW) as the subsurface temperature maximum ($\theta_{max}$). In our region, $\theta_{max}$ corresponds to a neutral density ($\gamma^n$) of 28.00 kg m$^{-3}$. Water above CDW is Antarctic Surface Water (AASW), and subsurface $\theta_{min}$ indicate presence of Winter Water (WW) formed during the cold season.

Upstream of the SFZ, the mixed layer depth does not vary significantly, and it is clearly defined by the shallow, warm/fresh AASW that sits above WW (Figure 3.3a). Downstream of the SFZ, the mixed layers are much more variable and there are sharp lateral gradients in the density field that are not associated with the main fronts of the ACC. This is indicative of enhanced stirring by an active mesoscale eddy field (Figure 3.3b). In both representative sections, warmer surface waters are found offshore than on the shelf; this pattern is also reflected in the high-resolution SST data shown in Figure 3.1b.

The predominant watermass upstream of the SFZ is CDW, which is found all the way

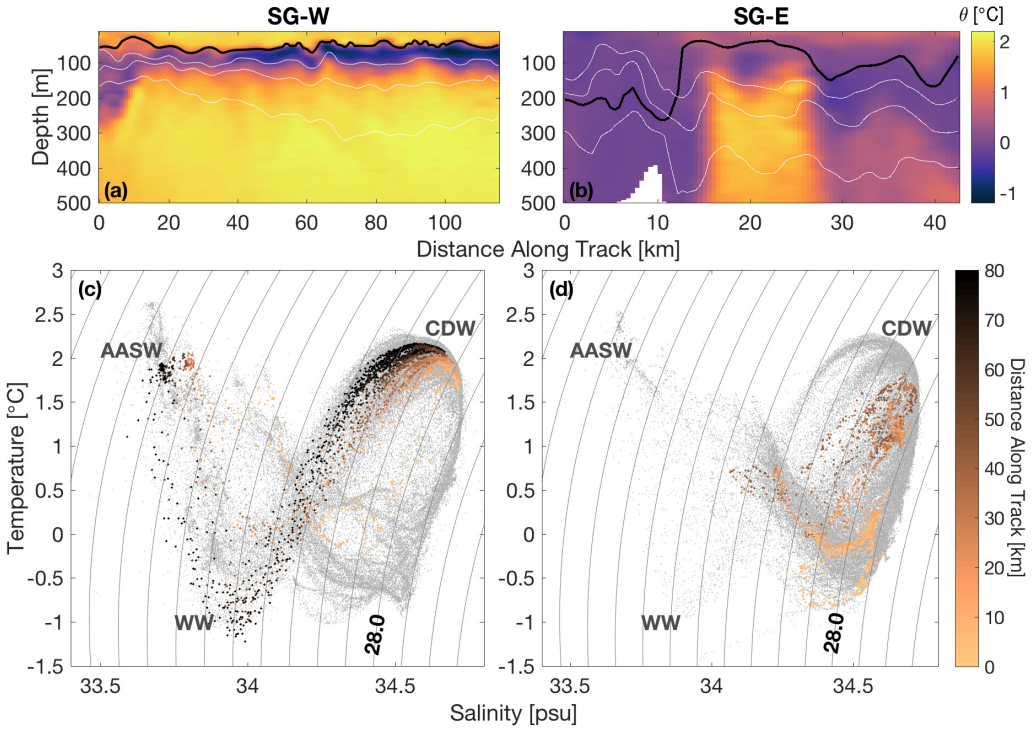


Figure 3.3: Temperature-depth sections of glider data (a) upstream and (b) downstream of the SFZ. Sections denoted by stars on the map in Figure 3.1b. The black line is mixed layer depth using $\Delta\sigma_0 = 0.125$ kg m$^{-3}$, white contours are potential density surfaces: (a) 27.4, 27.5, 27.6; (b) 27.65, 27.7, 27.75. (c,d) Temperature-Salinity diagrams of glider data collected during the deployment for (c) SG-W and (d) SG-E. Labels denote Antarctic Surface Water (AASW), Winter Water (WW), and Circumpolar Deep Water (CDW). Contours give neutral density surfaces in increments of 0.1, with the 28.0 neutral density contour labeled. The gray dots indicate measurements over the entire deployment; the colored dots (enlarged for contrast) give the measurements from the sections in (a,b).

up to the shelf break. It is capped by a layer of AASW on top of WW, which leads to the stability in the mixed layer described above. Downstream of the SFZ, there is weak vertical stratification, but there are sharp distinctions between the subsurface watermasses in the horizontal as evidenced by the gaps in the T/S structure that are not evident upstream (Figure 3.3c–d).

One of the strongest distinctions between the two regions is the depth and variability of the mixed layers upstream and downstream of the SFZ. The mixed layer depths upstream of the SFZ are 65±19 m, while downstream the average depth is 119±92 m. Furthermore, upstream of the SFZ, mixed layer depth has an inverse correlation

with bathymetry, with deeper mixed layers being found on the continental shelf/slope and shallower mixed layers as the glider moves into deeper waters (Figure 3.4a). In contrast, mixed layers downstream of the SFZ show more spatial variability, with a general trend of increasing mixed layer depth from west to east downstream of the SFZ. SG-E occupied these stations further downstream from the SFZ at the beginning of the deployment. Since mixed layers would be expected to be deeper in autumn, towards the end of the deployment (Figure 3.4b), we attribute this pattern to spatial, rather than temporal variability. While the peak in the histogram of the mixed layer depths is similar in both regions, there is a much longer tail in the mixed layer depth distribution in the region downstream of the SFZ as compared to the upstream region (Figure 3.5a). The glider sampled very deep mixed layers on the shelf downstream of the SFZ, where stratification is low. Previous works (e.g., Patterson and Sievers (1980)) have shown that deep mixed layers in this region are not restricted to wintertime, as lateral mixing processes may lead to homogeneity through the entire water column. However, even discarding the data collected over the shelf, the mixed layers downstream of the SFZ are significantly deeper than those upstream.

**Mesoscale context**

The deflection of the SACCF over the SFZ leads to a more unstable front downstream of the SFZ than upstream, where the front follows bathymetry, essentially being steered by contours of $f/h$. Similarly, the SBACC, which is also topographically steered upstream of the SFZ, is deflected around the Ona Basin just downstream of the SFZ (Orsi et al., 1995), which may impart additional variability (Barré et al., 2008). The area to the east of the SFZ and surrounding Elephant Island, known as the Weddell-Scotia Confluence, is also prone to increased variability due to the interaction of a number of distinct boundary currents. In addition to the SBACC, the ASF sheds eddies and filaments off Ona Ridge (Flexas et al., 2015), and the Antarctic Coastal Current circulates between the Antarctic Peninsula and the northern islands before meeting up with the ASF (Palmer et al., 2012). The injection of Weddell Sea waters and the shedding of Weddell eddies downstream of the SFZ also results in a region that, while close in distance to the upstream region, is much more energetic (Palmer et al., 2012; Thompson and Youngs, 2013).

The horizontal buoyancy gradients exhibit significant variability upstream and downstream of the SFZ. The horizontal buoyancy gradient was calculated as the average over the mixed layer depth, discarding the top 5 meters. Upstream of the SFZ, the

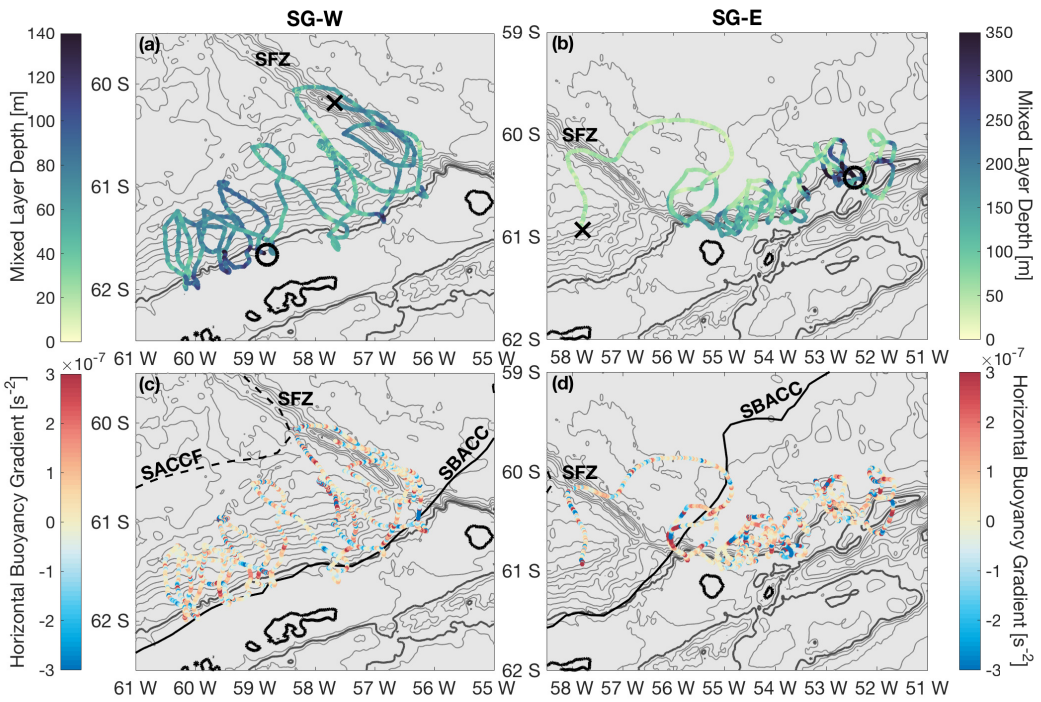


Figure 3.4: Maps of mixed layer depths (a,b) and horizontal buoyancy gradients, $b_x$, (c,d) for gliders SG-W (left) and SG-E (right). 1000 m isobath is bolded; note the difference in mixed layer depth range in panels (a) and (b). Circle indicates deployment location, X indicates recovery location. (c,d) The solid black line denotes the mean position of the SBACC over the study period, and the dashed line indicates the mean position of the SACCF.

largest values of $b_x$ are located near the positions of the SBACC. Downstream, the high values of $b_x$ are not constrained to the mean frontal positions, and are indicative of a more energetic meso- and submesoscale field (Figure 3.4c–d, fronts located using AVISO and the contours specified in Kim and Orsi (2014)). A comparison of the histograms of the horizontal buoyancy gradients in both regions reveals a significant offset between the two curves, with the downstream region more likely to exhibit larger gradients (Figure 3.5c). This result is robust to the choice of mixed layer depth criterion. The zonal wind stress is virtually identical between the two regions (Figure 3.5b) and therefore this surface forcing alone can not explain the spatial variability in submesoscale activity.

**Upper-ocean restratification processes**

Glider data and ECMWF reanalysis winds are used to determine the effects of surface forcing and submesoscale processes on the stratification of the upper ocean,

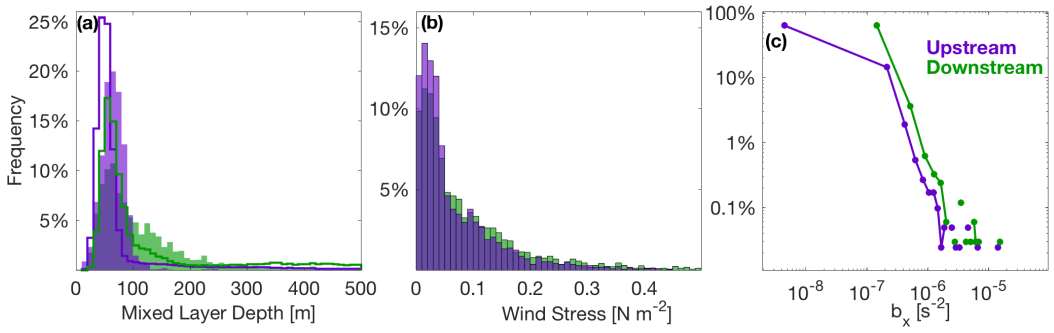


Figure 3.5: Comparisons of histograms of key properties upstream (purple) and downstream (green) of the SFZ: (a) Mixed layer depth [m], (b) down-front wind stress, $\tau^y$ [N m$^{-2}$], (c) absolute value of horizontal buoyancy gradient, $b_x$ [s$^{-2}$]. In (a), outlines denote MLD from LLC model, boxes from glider observations.

as detailed in Section 3.3. The parameterizations of Fox-Kemper et al. (2008) and Thomas (2005) are used to calculate equivalent heat fluxes caused by BCI and Ekman buoyancy forcing, respectively (Figure 3.6), which are then compared to the surface heat flux $Q_{surf}$. Since the two gliders are at roughly the same latitude and the cloud cover across the SFZ is similar throughout the deployment, $Q_{surf}$ is approximately the same across the two regions. There is a strong diurnal cycle but the forcing over the study period warms the surface ocean with a mean value of $Q_{surf}$ = 188 W m$^{-2}$. The surface heat flux decreases from summer into early fall during the deployment, with the mean over the first third of the deployment $Q_{surf}$ = 197 W m$^{-2}$ and the mean over the last third of the deployment $Q_{surf}$ = 63 W m$^{-2}$. The magnitudes of $Q_{BCI}$ and $Q_{EBF}$ are larger, with mean values of 580 W m$^{-2}$ and 273 W m$^{-2}$, respectively (Figure 3.7). Upstream of the SFZ, the equivalent heat flux extrema are intermittent, happening roughly once per week, associated with the deeper mixed layers and strong horizontal buoyancy gradients near the shelf break (Figure 3.4a,c). Downstream of the SFZ, large values of $Q_{BCI}$ are more frequent. The large contribution of BCI to the total heat flux (Figure 3.7c) suggests that baroclinic instability should have a leading order impact on setting the mixed layer depth. The contributions of these submesoscale heat fluxes to upper ocean stratification are explored in the following section.

**Modeling the observed mixed layers**

The PWP model was previously shown to accurately reproduce mixed layer depths in regions such as the North Pacific (Price et al., 1986) and the tropical Indo-Pacific

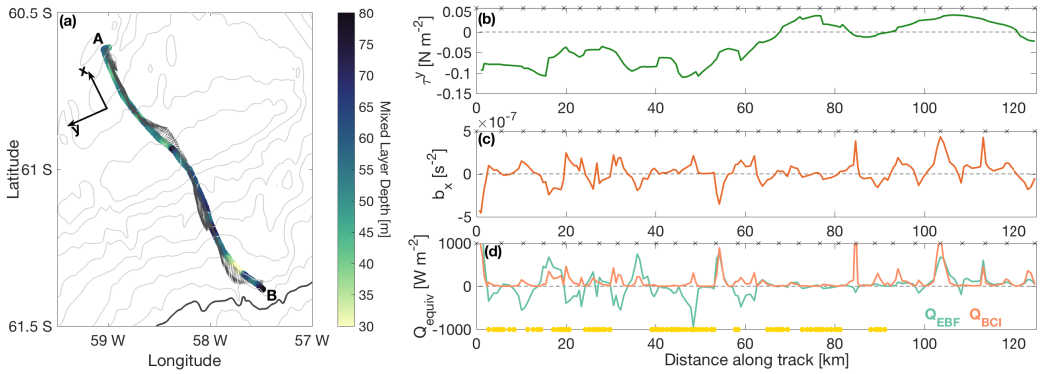


Figure 3.6: Sample transect showing calculations of $Q_{EBF}$ and $Q_{BCI}$. (a) Mixed layer depth as measured by SG-W over a single cross-shelf transect from A to B. Denoting the winds and light contours give the bathymetry (1000 m isobath bolded). x-y axis orients the reader for the calculations performed. (b) Along-front (i.e., perpendicular to glider track) wind stress component. (c) Horizontal buoyancy gradient, $b_x$, as measured by the Seaglider. (d) Following (6) and (8), $Q_{BCI}$ (light orange) and $Q_{EBF}$ (blue-green) over the sample transect. For panels (b–d), the x marks on the top axis show the positions of the individual Seaglider dives; yellow circles on bottom axis of (d) show periods of more than 25% gravitational instability in the mixed layer.

(Shinoda and Hendon, 1998). However, the ChinStrAP region was characterized by an abundance of lateral processes, which are not captured by the traditional PWP model. We hypothesize that by incorporating the effect of these 2-dimensional processes into a modified PWP model, the model will perform better in capturing mixed layer depth variability. Indeed, the unmodified PWP model results in mixed layer depths that are significantly deeper than those observed by the glider. For SG-E, the PWP model outputs a mean mixed layer depth and standard deviation of 229±33 m, compared to 119±86 m as observed by the glider (a 92% error in mean and a 62% error in standard deviation of the mixed layer). Not only is the modeled mean mixed layer depth significantly deeper than the actual mixed layer, the mixed layer variance is not well-captured by the PWP model.

To improve the performance of the PWP model, we accounted for the effects of submesoscale motions via the parameterizations for $Q_{EBF}$ and $Q_{BCI}$ (described in Section 3.3). These two terms were combined into a forcing term that is applied equally over the mixed layer depth at each time step in the model, $Q_{sub}$, given as

$$Q_{sub} = Q_{EBF} + Q_{BCI}. \tag{3.8}$$

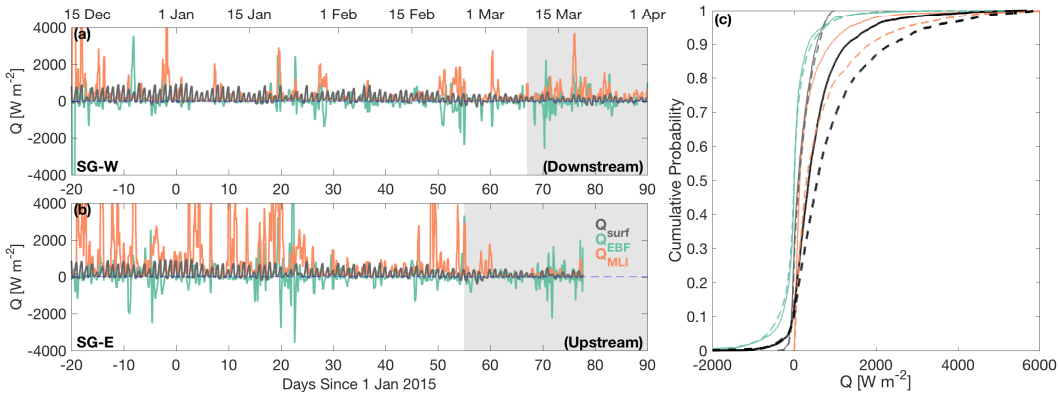


Figure 3.7: Time series of heat forcing and equivalent buoyancy fluxes for (a) SG-W and (b) SG-E: $Q_{surf}$ (gray), $Q_{MLI}$ (orange), and $Q_{EBF}$ (green). Positive (negative) values are heat into (out of) the ocean. Gray boxes indicate times when SG-W (SG-E) is downstream (upstream) of the SFZ. (c) Cumulative distribution of $Q_{surf}$ (gray), $Q_{MLI}$ (orange), $Q_{EBF}$ (green), and total heat flux (black) for SG-W (solid) and SG-E (dashed).

The result of this mPWP model is closer to the observations in terms of both mean mixed layer depth and variance, providing mixed layers of 177±81 m (a 6% difference from the standard deviation of the glider observations, although still a 48% difference from the mean of the observations). Although the individual mixed layer shoaling/deepening events do not match up between the observations and the mPWP model, the modified model does capture much of the character of the observed mixed layer, with large variations of mixed layer depth over relatively short timescales (Figure 3.8). The model output is also consistent with our findings that the submesoscales are dominantly restratifying over the period of deployment, and indicates that accounting for the submesoscale motions is critical to correctly model mixed layer depths and variability.

Shoaling of the mean mixed layer throughout the sample period can be observed in both the PWP and mPWP models, although the effect is much more pronounced for the mPWP configuration. Large et al. (1994) discuss the need for advection of cold water and salt into mixed layer models to offset the long-term drifts caused by net surface heating/freshwater flux. mPWP exhibits a larger shoaling over the model run as there is a greater (equivalent) heat flux being applied to the surface. The mPWP model captures the transition from deep to shallow mixed layers observed by the glider moving from December/January into the end of the summer, while the standard PWP model does not. Remaining differences between the observations

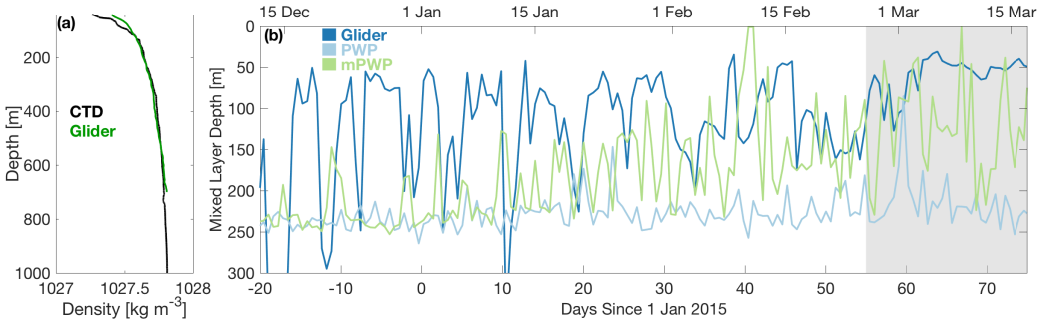


Figure 3.8: (a) Density profile from CTD (black) and glider SG-E (green). (b) Comparison of mixed layer depth from observations from SG-E (dark blue), PWP model (light blue), and mPWP model.

and the mPWP model can be attributed to other processes, such as Langmuir circulations, or wave-forced turbulence, which have been shown by Belcher et al. (2012) to play a significant role in setting mixed layer depths in the Southern Ocean. Similarly, lateral advection and large-scale gradients in the background stratification are not captured in the model, and may also help to explain some of the remaining discrepancies.

**Variation of instabilities**

There is also significant variation between the two regions with regards to the types of instabilities the mixed layer is conditioned to undergo, as described in Section 3.3 (Figure 3.9). A comparison of the two time series of submesoscale instabilities shows that the region upstream of the SFZ is more susceptible to gravitational instability. In contrast, the area downstream of the SFZ experiences frequent, but intermittent, episodes that would indicate symmetric instability, sometimes extending through the whole mixed layer (Figure 3.9b). The spatial pattern of instabilities (Figure 3.9c) shows that symmetric instability is favored both on- and off-shelf downstream. Upstream of the SFZ, periods of conditioning of 25% or more of the mixed layer towards gravitational instability occur 28% of the time. This is especially common far from the shelf break. These classifications are consistent with Adams et al. (2017), who observed conditions suitable for gravitational and symmetric instabilities during early fall in the Scotia Sea. We propose that the enhancement of gravitational instability upstream of the SFZ can in part be attributed to the persistent forcing of the ACC's topographically steered fronts by down-front winds. On a dive-by-dive basis, it may not be possible to identify forcing factors

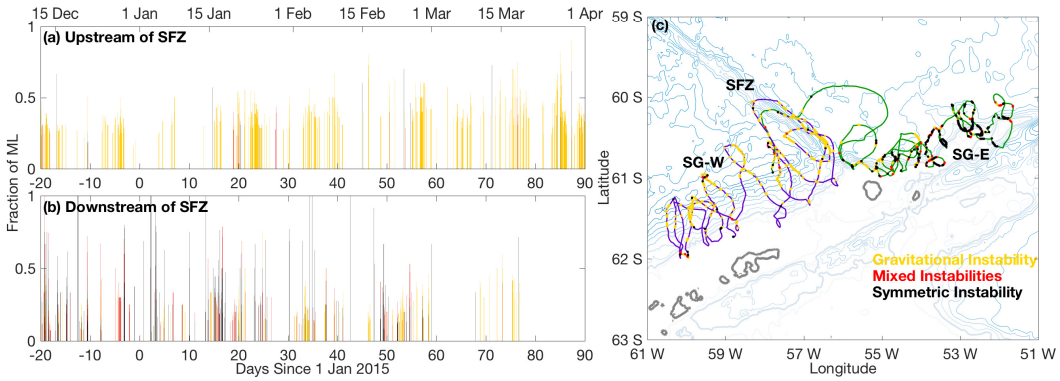


Figure 3.9: Time series of submesoscale instability preconditioning (a) upstream and (b) downstream of the SFZ for gravitational (yellow), mixed gravitational/symmetric (red) and symmetric (black) instabilities. (c) Map of the study area (1000 m isobath bolded) with glider tracks for SG-W (purple) and SG-E (green). The series has been filtered such that more than 20% of the mixed layer is conditioned for a given instability at a given time step.

contributing to a certain type of instability conditioning, however, there is a larger-scale pattern aligning periods of gravitational instability with higher EBF off the shelf (as compared to on-shelf), as seen in Figure 3.6. We leave a more in-depth investigation of the mechanisms behind the specific instabilities to a future work.

**Validation of glider-based PV calculations**

The calculation of PV from the Seagliders requires the gliders to be piloted perpendicular to the orientation of the front. This requires the following assumptions: (a) variation in the along-front direction is negligible and (b) velocities across the front are negligible. With the additional assumption that vertical velocities are small, we obtain an expression for observational PV (3.2). In order to verify the validity of these simplifications, the LLC 1/48° GCM was utilized. Three subdomains over the deployment area were extracted from the model output, comprising over 150 sections. The full Ertel PV and the observational PV calculated from these transects show many of the same structures; the amplitude of the observational PV estimates tend to be smaller than the full PV, especially in the mixed layer (Figure 3.10a–b). These calculations were performed within the top 200 meters depth using snapshots every two hours over a period of 5 days for each subdomain. Comparing the signs of the respective PV calculations reveals the same sign at 92.3% of all these points in space and time. False positives, or times when the observational PV indicates instability but the full PV does not, occur only 2.1% of the time. As the three subdo-

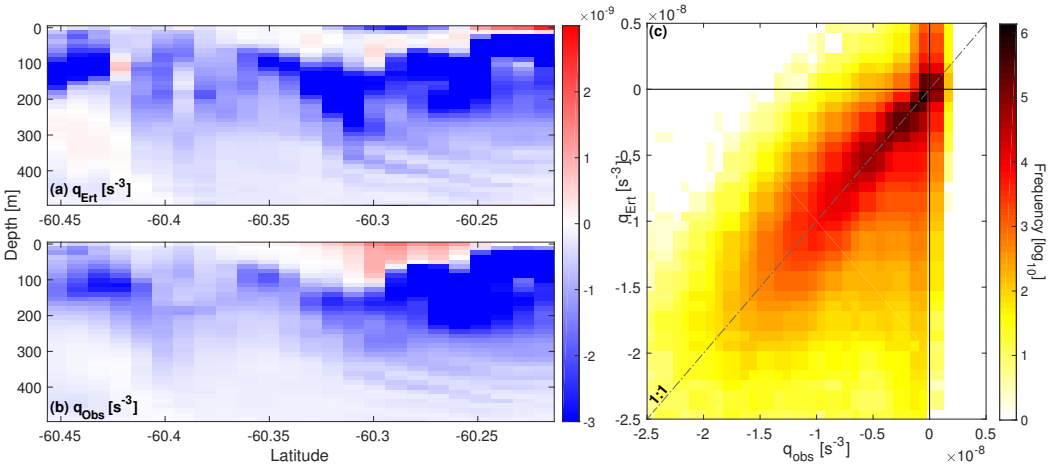


Figure 3.10: Representative potential vorticity section as calculated from the 1/48° LLC model configuration. (a) $q_{Ert}$, the full Ertel PV as given by (1); (b) $q_{Obs}$, the observational PV as given by (2). This transect coincides with the downstream section highlighted in figure 3.1b. (c) Histogram heat map (log scale) of $q_{Ert}$ and $q_{Obs}$ from the top 200 m of 150 modeled transects.

mains were chosen from multiple regions with different dynamics, and calculations were performed for a range of days and times, this provides additional confidence in the assumptions and thus, the PV and instability calculations.

## 3.5 Discussion

### Summer submesoscale activity

Previous studies have shown that the intensity of submesoscale activity can undergo a strong seasonal cycle, linked to changes in the mixed layer depth and in some cases to mesoscale stirring (Sasaki et al., 2014; Callies et al., 2015; Buckingham et al., 2016). Instances of symmetric instability have been observed in western boundary currents (D'Asaro et al., 2011; Thomas et al., 2016) and conditions suitable for symmetric instability have been documented in the subtropical open ocean in both the Atlantic (Thompson et al., 2016b) and Pacific (Hosegood et al., 2013) basins. However, these previous studies have either focused explicitly on the winter season or have found a particularly vigorous submesoscale field during the winter months. This study, in contrast, took place during the summer months and into the early fall, when shallower mixed layers and increased stratification have previously been found to suppress submesoscale activity in other ocean basins. Our findings of an active submesoscale in the Southern Ocean corroborate the results of du Plessis et al. (2017), who conducted a similar survey in the Subantarctic Zone in spring–summer

time.

In the ChinStrAP study, we found evidence supporting the existence of symmetric instability in Southern Drake Passage during the austral summer (Dec.–Mar.). Favorable conditions for symmetric instability were found downstream of the SFZ for the duration of the study. The likely presence and prevalence of submesoscale instabilities, even in the summertime, requires a reevaluation of the way that dynamics of this scale are considered in climate and circulation models, e.g., via new parameterizations for SI put forth by Bachman et al. (2017b). As seen in Klein and Lapeyre (2009), density gradients at the submesoscale can be responsible for up to 50% of the vertical exchange between the mixed layer and the thermocline below. Combined with the active summertime submesoscale presented here, this suggests that current models may be underestimating the strength of the dynamical component of the Southern Ocean biological pump.

**Spatial variations: Upstream vs. downstream of Shackleton Fracture Zone**

Three key components contribute to the parameterizations of $Q_{EBF}$ and $Q_{BCI}$: mixed layer depth; horizontal buoyancy gradient, $b_x$, indicative of mesoscale and submesoscale stirring; and wind stress-front orientation, $\tau^y$. While the mode of the mixed layer depth (histogram peak in Figure 3.5a) is similar across our study region, the distribution of mixed layer depths upstream of the SFZ is much tighter, while downstream of the SFZ, there is a long tail on the distribution (Figure 3.5a). The other main difference between the regions is in the horizontal (along-track) buoyancy gradient, $b_x$, where there is an offset between the histograms, with stronger buoyancy gradients downstream of the SFZ (Figure 3.5b).

The differences in horizontal buoyancy gradients upstream and downstream of the SFZ suggest different dynamical regimes, which imply differing magnitudes, types, and frequency of submesoscale instabilities. Upstream of the SFZ, there are strong events of EBF and/or BCI with a significant impact on the equivalent heat budget of the upper ocean (Figure 3.7a,c), but these events are localized to a narrow region associated with the SBACC. The topographically constrained fronts and the persistence of the westerly (down-front) winds generate the gravitational instabilities classified in Figure 3.9. In contrast, these same events downstream of the SFZ are much more frequent and occur over a broader spatial extent, due to both the larger buoyancy gradients and deeper mixed layers, both of which precondition the upper ocean for symmetric instability. Critically, these differences occur despite

experiencing the same surface forcing fields.

We propose that the increased submesoscale activity downstream of the SFZ is due to two main factors: spatial variations in eddy kinetic energy and upper ocean stratification. Differences in the surface eddy kinetic energy (EKE) are captured clearly in both satellite altimetry data as well as output from the LLC (Figure 3.11). These patterns in EKE are strongly influenced by the bathymetry, both due to the deflection of the SBACC over the SFZ and the retroflection of the ASF exiting the Weddell Sea. Both of these processes tend to generate mesoscale eddies that will increase lateral stirring and induce variability at submesoscales. The LLC shows how the ACC becomes unstable as it passes through the SFZ, leading to an increase in EKE downstream. This signal is weaker in the observed sea surface height variability due to the much lower resolution of AVISO compared to the LLC, but the observations still show that the average summertime EKE is enhanced downstream of the SFZ (Figure 3.11a). In addition to EKE, the large-scale circulation supports weaker vertical stratification of the upper ocean downstream of the SFZ. The main cause of this is the shoreward penetration of AASW upstream of the SFZ, whereas the northward deflection of the SBACC limits its southward extension downstream. Thus, downstream of the SFZ, relatively homogeneous upper-ocean density contributes to lower PV and deeper mixed layers that store more potential energy and may thus be more prone to submesoscale instabilities.

**Impact and limitations of the study**

Separating spatial and temporal variability in the glider data is a significant challenge. The experimental design of the field program acted to counteract this in several ways. First, the simultaneous piloting of the gliders upstream and downstream of the SFZ allows the direct comparison of dynamics and watermass properties between the two regions. Each glider also occupied transects in approximately the same location over multiple weeks; these multiply occupied sections support that variability is predominantly spatial, rather than temporal. The glider capabilities, e.g., speed through the water, also influence our interpretation of these time series. First, the time to complete a full transect is long compared to the timescales of submesoscale dynamics. Thus, we emphasize that this study provides a statistical survey of the region and not a perfect snapshot of the dynamical regime; we stress the inter-comparison of patterns, rather than the absolute magnitudes. The second is a practical matter; the glider often flew at a speed comparable to or less than that of the depth-averaged current, making it difficult to fly the glider perpendicular to

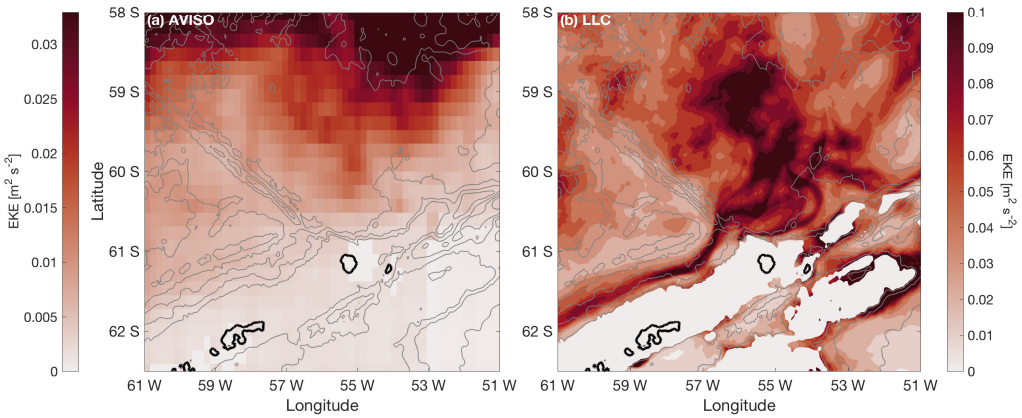


Figure 3.11: Surface eddy kinetic energy [m$^2$ s$^{-2}$] over the ChinStrAP study region (Dec–Mar). Gray contours underneath show the bathymetry of the study region: (a) calculated from AVISO 1/6° altimetry data from 2006–2016 and (b) calculated from the 1/48° LLC MITgcm for December 2011–March 2012. Values have been blanked out for bathymetry shallower than 750 m. EKE in panel (a) has a maximum value that is 1/3 the maximum of EKE in panel (b) due to the differing resolutions of the two datasets.

the front.

The key assumption in our calculations of equivalent heat fluxes and Richardson numbers was that the gliders were flown perpendicular to the frontal structure of the ACC, which allowed us to simplify PV into a two-dimensional expression. This was more successful upstream of the SFZ than downstream, with SG-W maintaining relatively straight trajectories across the continental shelf for the majority of the deployment (Fig. 3.1). Downstream of the SFZ, the frontal structure is less well-defined. Because the glider tracks are less perpendicular to the shelf, it is more difficult to know the glider's orientation with respect to the fronts. Critically, though, the LLC model does reproduce intermittent regions in the surface mixed layer where $PV > 0$ in the summertime, consistent with our observations. Furthermore, analysis of the LLC also demonstrates higher propensities for conditioning towards gravitational instability upstream of the SFZ and towards symmetric instability downstream of the SFZ.

Despite the limitations of this study, the results provide valuable insight into submesoscale variability in one region of the Southern Ocean. Most notably, although previous work has shown the importance of submesoscale activity (e.g., Klein and Lapeyre, 2009; Rosso et al., 2014), this is among the first studies to show such

ubiquitous submesoscale dynamics during the summertime, a period when shallow mixed layers and increased stratification should act to prohibit the instabilities explored in this study (see also du Plessis et al. (2017)). The comparison of observed mixed layers and those calculated by the PWP bulk mixed layer model demonstrate the importance of these dynamics in setting the mixed layer depth and stratification of the upper ocean. We have also shown the existence of two very different submesoscale dynamical regimes separated by a relatively small distance; conditioning by the background flow is largely influenced by the underlying bathymetry. We stress the need to characterize regional variability in the ACC. The abrupt change in submesoscale character due to topography is another example of localized "hot spots" that have a dynamical influence on the Southern Ocean (Abernathey and Cessi, 2014; Thompson and Naveira Garabato, 2014; Dufour et al., 2015; Viglione and Thompson, 2016; Tamsitt et al., 2016). We propose that similar dynamical shifts may occur in other regions of the Southern Ocean with large topographic features, e.g., Kerguelen Plateau and the Pacific-Antarctic Ridge (Rosso et al., 2014), which has implications for the localization of $CO_2$ uptake in the Southern Ocean. In particular, because of the fine spatial structure of these upper ocean processes, long time series of $pCO_2$ concentrations in specific locations, such as Drake Passage (Takahashi et al., 2009), may provide misleading information about the Southern Ocean carbon cycle if simply extrapolated circumpolarly.

### 3.6 Conclusions

Two Seagliders were deployed north of the Antarctic Peninsula from December 2014–April 2015, sampling both up- and downstream of the Shackleton Fracture Zone (SFZ). Sampling at a mean horizontal resolution of 1.6 km, this study resolves the upper ocean submesoscale density structure of a key region of the ocean for water mass ventilation and modification (Sallée et al., 2010; Abernathey et al., 2016), as well as shelf-slope exchange and water mass modification (Ruan et al., 2017). Although the mesoscale eddy stirring, strong wind forcing, deep mixed layers, and persistent fronts would suggest the Southern Ocean to be a hotbed for submesoscale activity, little observational work has been undertaken here to validate numerical simulations (Rocha et al., 2016; Adams et al., 2017). In this work, we present evidence for an active submesoscale field, even in summer months, but distinct geographical differences in the characteristics of these submesoscale motions. The conditions for symmetric instability are found almost exclusively downstream of the SFZ, suggesting fundamental differences in the dynamics of the regions on either

side of the SFZ. The primary differences between the two regions are deeper mixed layers and stronger lateral buoyancy gradients downstream of the SFZ. Together, these contribute to the preconditioning of the downstream region for increased submesoscale activity.

Finally, comparisons were made between the glider observations and two different models. First, the 1-D PWP bulk mixed layer model was used in an attempt to replicate the time-evolving mixed layer depth. This model was seen to diverge from the observations due to its exclusion of submesoscale and other 3-dimensional processes. When parameterized fluxes, $Q_{EBF}$ and $Q_{BCI}$, were added into the surface forcing, the modified PWP model was more accurate in representing the variability in the mixed layer depth time series, although the mean values were still 50% larger than the observations. PV calculated from the glider observations was compared to the full Ertel PV as diagnosed from the 1/48° LLC model. The LLC was also subsampled and used to calculate the PV using the same simplifications as when calculating the observed PV from the glider. These results showed that while some caution must be used in calculating PV from gliders, the sign of the observed PV is predominantly the same as the sign of the full PV (in 92.3% of instances, both PV calculations had the same sign).

This work provides evidence that the submesoscale is highly active in the Southern Ocean even during the summertime, significantly altering the stratification of the upper ocean with implications for carbon capture and the biological pump. The intermittency of these events as well as the size of the variations over short spatial scales suggest that this is a complex phenomenon that will remain challenging to represent in numerical models not focused on localized regions; this is particularly true for the role of submesoscale on air-sea coupling. The comparison of these observations to a high-resolution model validates the use of gliders to study instabilities at this scale.

*Chapter 4*

# CONTROLS ON WINTERTIME SUBDUCTION IN SOUTHERN DRAKE PASSAGE

Viglione, G. A. et al. (In revision). "Controls on wintertime subduction in southern Drake Passage". In: *Geophys. Res. Lett.*

## 4.1 Abstract

Drake Passage is a key region for exchange between the surface and the interior, yet the impact of submesoscale dynamics on ventilation remains largely unexplored. Here we present submesoscale-resolving hydrographic transects from Drake Passage that span the southern boundary of the Antarctic Circumpolar Current and the Polar Front, collected from two ocean gliders in winter 2016. Despite strong surface wind and buoyancy forcing, a meltwater lens south of the Polar Front suppresses upper-ocean small-scale variability and subduction. Surface-interior exchange is instead localized to the Polar Front. The intensity of ventilation and lateral mixing at the Polar Front increases following a deepening of the mixed layer and a weakening of the PF during mid-winter. This enhances along-isopycnal subduction of surface waters into the interior. These results suggest that ventilation at the Polar Front may vary on sub-seasonal timescales and may be sensitive to non-local processes, e.g., sea ice melt, that impact surface properties.

## 4.2 Introduction

Submesoscale motions in the ocean surface boundary layer can significantly alter upper-ocean stratification and exchange between the mixed layer and the thermocline (Klein and Lapeyre, 2009) with important implications for ocean biogeochemical cycling (Mahadevan, 2016) and ocean ecosystems (Lévy et al., 2018). These motions are characterized by length scales of $O$(1–10 km) and Rossby numbers of $O$(1), and are typically enhanced in regions characterized by high eddy kinetic energy, strong lateral buoyancy gradients, and weak vertical stratification—all features typical of the Southern Ocean. Process-based modeling studies of the Southern Ocean have suggested that submesoscale motions play a critical role in determining vertical fluxes of heat and other tracers (Rosso et al., 2014), mixed layer depths (Bachman et al., 2017a), and exchange across the base of the mixed layer (Balwada et al., 2018),

which underlines the need to accurately represent these dynamics in global climate models. These studies also found an inhomogenous distribution of submesoscale characteristics. While observational studies that directly resolve these scales in the Southern Ocean are limited, recent studies by Adams et al. (2017), du Plessis et al. (2017), and Viglione et al. (2018) all highlight abrupt and intermittent transitions in submesoscale dynamics in the Southern Ocean. Observations of submesoscale spatial and temporal variability are also important to dynamically constrain model parameterizations under different regimes.

The surface outcrop locations of isopycnals also have larger-scale climate implications as this property constrains the strength and structure of the overturning circulation, which influences ventilation and subduction rates along different density classes (e.g., (Speer et al., 2000; Ferrari et al., 2014; Abernathey et al., 2016; Pellichero et al., 2018)). Drake Passage, in particular, is a key region for the formation of mode waters (Naveira Garabato et al., 2009; Sallée et al., 2010; Close et al., 2013) and the subduction of carbon (Sallée et al., 2012). Processes that govern the exchange of carbon with the atmosphere in Drake Passage have had an outsized influence on interpretation of the Southern Ocean's contribution to the carbon cycle, primarily because wintertime $pCO_2$ measurements are uniquely collected in Drake Passage (Takahashi et al., 2009; Takahashi et al., 2012). Such a bias in wintertime $pCO_2$ sampling in the Southern Ocean might help to explain why large differences exist between climatology and recent float-based estimates of carbon fluxes (Gray et al., 2018).

Studies of spatial variations in Southern Ocean turbulent transport have traditionally focused on mesoscale processes and their impact on, for example, subduction (D. Marshall, 1995; Naveira Garabato et al., 2001), or cross-front exchange (Naveira Garabato et al., 2011; Klocker et al., 2012; Ferrari and Nikurashin, 2010; Thompson and Sallée, 2012). Naveira Garabato et al. (2011) concluded that the Antarctic Circumpolar Current (ACC) jets typically suppress mixing, although their focus was on transport below the mixed layer and they were unable to resolve submesoscale motions. Here we address smaller-scale variability and its influence on exchange between the surface boundary layer and the ocean interior; these submesoscale motions have been shown to modify larger-scale circulation and properties (Lévy et al., 2010).

We present a unique, high-resolution hydrographic data set in Drake Passage acquired from autonomous ocean gliders during austral fall and winter 2016. The high

spatial resolution allows us to consider the impact of submesoscale variability on subduction. We focus our exploration on mixed layer variability and the fine-scale frontal structure not resolved by coarser sampling. We find a surprising lack of submesoscale variability in the surface boundary layer south of the Polar Front (PF) in Drake Passage. This abruptly transitions to a more variable regime at the PF. This study contributes to growing evidence that submesoscale dynamics are spatially and temporally heterogeneous in the Southern Ocean, responding to not only to local, mesoscale variability (Viglione and Thompson, 2016; Viglione et al., 2018; Balwada et al., 2018, e.g.,), but also to non-local processes.

## 4.3 Data and Methods

### Ocean glider data

Gliders have been shown to be an effective tool for exploring near-surface variability and submesoscale dynamics (Itoh and D. L. Rudnick, 2017; Todd et al., 2016; Thompson et al., 2016b; Viglione et al., 2018; du Plessis et al., 2017). Here, two Seagliders carried out meridional transects across Southern Drake Passage between May and August 2016 as part of the ChinStrAP2 (Changes in Stratification at the Antarctic Peninsula) field program. The gliders profiled in a v-shaped vertical pattern to a maximum depth of 1000 m, collecting temperature, salinity, and dissolved oxygen concentration data using a SeaBird unpumped CT-Sail and an Aandera optode. Although two gliders were deployed in the field study, analysis from only one glider is shown here; characteristics are similar between the gliders, as seen by comparing the temperature/salinity diagrams in Figure 4.2 and Figure 4.6. The mean separation between glider dives was 4.6 km.

The raw glider data were processed using the University of East Anglia Seaglider toolbox[1] to remove spikes and to correct the lag between temperature and conductivity measurements. The data were then objectively mapped onto a regular grid with 5 m vertical spacing and 2.4 h temporal spacing, which corresponds to a spatial scale of approximately 2.8 km. The interpolation uses a Gaussian weighting function with vertical and temporal scales of 10 m and 4 h, respectively. From sensitivity studies, the results described in Section 4.4 were not significantly affected by the choice of grid spacing. Spatial gradients were calculated using a monotonically increasing along-track distance variable mapped from the glider position onto the temporal grid. All data were processed using the Gibbs Seawater Toolbox (McDougall and

[1]The glider toolbox and documentation can be found here: bitbucket.org/bastienqueste/ueaseaglider-toolbox

Barker, 2011), and we use the quantities conservative temperature ($\Theta$), absolute salinity ($S_A$), and neutral density ($\gamma^n$), unless otherwise noted. Mixed layer depths (MLDs) were calculated with a density difference criterion of $\Delta\sigma_0 = 0.125$ kg m$^{-3}$ from the surface (Monterey and Levitus, 1997), which was found by Viglione et al. (2018) to be most representative of MLDs in Drake Passage. Apparent oxygen utilization (AOU) is used to correct for the temperature dependence of oxygen saturation according to the equation $AOU = [O_2^{sat}] - [O_2]$.

**Other datasets**

Wind speed, wind orientation and surface heat fluxes were obtained from ECMWF ERA-Interim at a temporal resolution of six hours (Dee et al., 2011). The spatial resolution of ERA-Interim in this region is approximately 80 km. Daily absolute dynamic topography data at a resolution of 1/4° obtained from the E.U. Copernicus Marine Environment Monitoring Service were used to determine the PF position.

**Characterization of the study site**

We consider two northward meridional transects; one that crosses the PF in June and one in July. Each glider transect traversed the Southern ACC Front (SACCF) and the PF (defined here and on Figure 4.1a using the absolute dynamic topography contours of -98.5 and -61 cm, respectively, as reported in Kim and Orsi (2014)). Velocity sections were constructed by calculating the geostrophic shear from the glider density field and then referencing this velocity to the depth-averaged current (DAC) observed by the glider. Figures 4.1b,c show the orientation and magnitude of the DAC; for each crossing of the PF we find a local maximum in the DAC, which gives us confidence that the glider crossed the core of the front, although it does not exactly match the PF location from the Kim and Orsi (2014) criteria. The maximum observed velocity of the PF was stronger during the June crossing (0.51 m s$^{-1}$) as compared to the July crossing (0.36 m s$^{-1}$). The geostrophic component of the velocity field can only be resolved in the direction perpendicular to the glider path and therefore the inferred intensity of the PF is dependent on the angle at which the glider crosses the front. However, the angles at which the glider crossed the altimetry-derived PF contour differed by only $\sim 10\%$ between the crossings.

During the glider deployment, Drake Passage experienced a strong, persistent cooling; the mean surface heat flux in Drake Passage from ECMWF during this period was $-168$ W m$^{-2}$, (over the box bounded by 62 °S, 68 °S and 62 °W, 66 °W). The average wind speed over this time period was $10.1 \pm 4.0$ m s$^{-1}$, with maximum

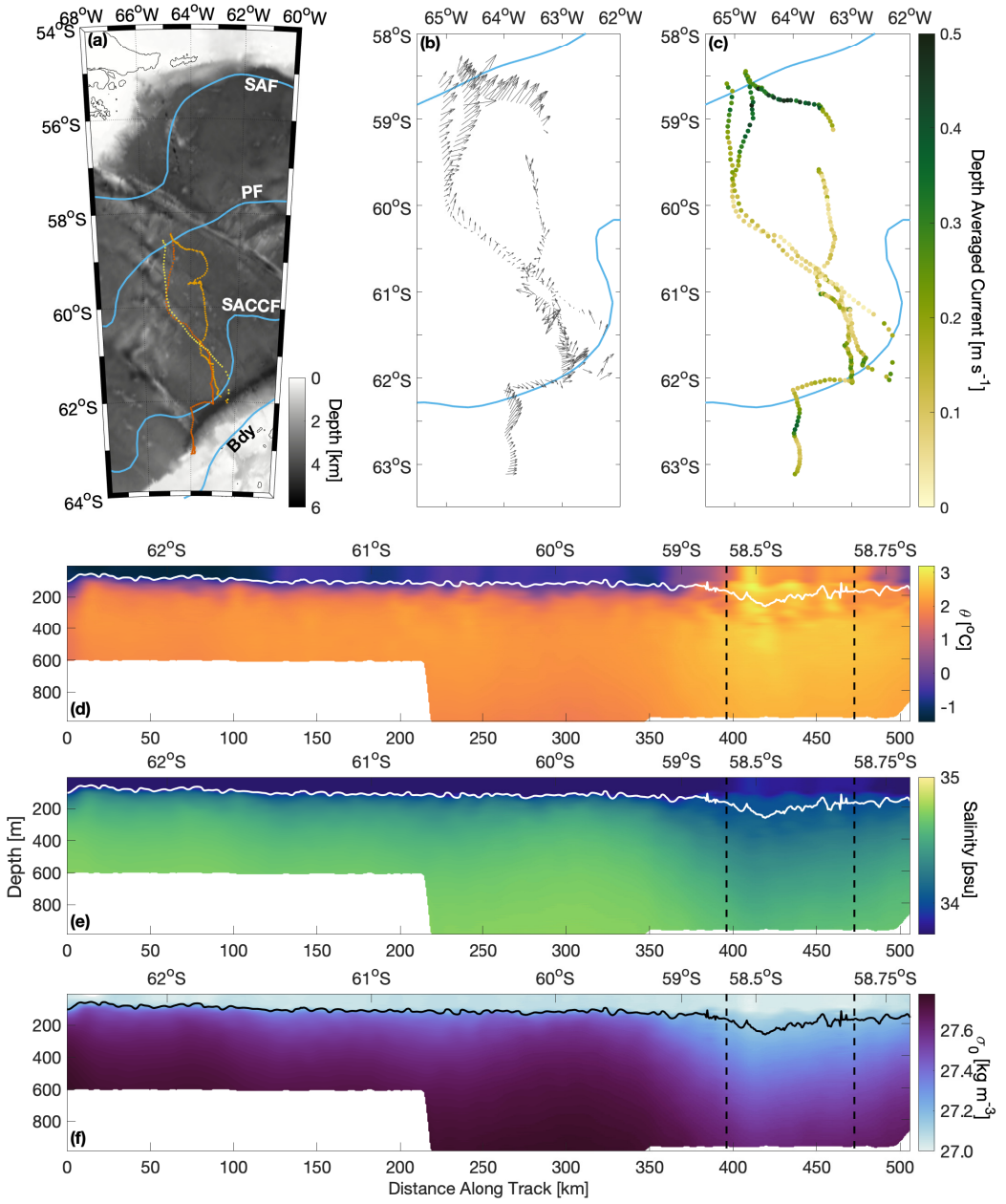


Figure 4.1: (a) Map of the ChinStrAP2 study region. Individual glider surfacing locations are plotted as dots over ETOPO bathymetry, with red, orange, and yellow distinguishing separate transects. Fronts derived from AVISO altimetry and using the definitions of Kim and Orsi (2014) are plotted in blue and labeled: Subantarctic Front (SAF), Polar Front (PF), Southern ACC Front (SACCF), Southern Boundary (Bdy). (b) Quiver plot of depth-averaged current (to 1000 m) derived from the glider path. (c) Depth-averaged current speed. Glider data from the first northward transect, objectively mapped in pressure-distance space, showing (d) potential temperature, (e) salinity, and (f) potential density. White (black) line in d,e (f) denotes the mixed layer depth; dashed lines indicate crossings of the PF.

winds reaching 21.4 m $s^{-2}$. The winds are predominantly westerly, with a mean westerly wind stress of 0.06 N $m^{-2}$. The mean eddy kinetic energy calculated from satellite-derived surface ocean velocity over Drake Passage is 0.01 $m^2$ $s^{-2}$, with no significant change over the study period.

## 4.4 Results

### Mixed layer variability

The PF marks a transition between salinity-stratified (south of the PF) and temperature-stratified (north of the PF) regions of the Southern Ocean. The PF also marks a transition in upper ocean mixed layer variability. South of the PF, the mixed layer was defined by a freshwater layer overlying a strong pycnocline at the base of the mixed layer. This freshwater lens largely suppressed variations in the MLD: the mean and standard deviation of the MLD was 105.4 ± 13.0 m, which did not vary over the deployment period. On approaching the southern boundary of the PF, the mixed layer deepened and the stratification at the base of the mixed layer weakened. During the June crossing of the PF, the maximum MLD was 259 m. The maximum MLD deepened to 422 m during the July crossing (Figure 4.5). This weakening of the stratification at the base of the mixed layer only occurred near the PF; elsewhere in southern Drake Passage the pycnocline remained strong.

The freshwater lens south of the PF that defines the MLD had an average temperature of −0.79°C and an average salinity of 33.67 psu, indicative of cold freshwater influenced by sea ice melt. This is notable because sea ice does not occupy this region of Drake Passage; this freshwater layer must have been sourced remotely. Considering the circulation in this region, the fresher water has likely been advected from the West Antarctic Peninsula and the Bellingshausen Sea.

### Fine-scale structure of the Polar Front

A striking feature of the glider-derived high resolution hydrographic transect is the water mass structure reflected in temperature and salinity properties (Figure 4.2). The major fronts of the ACC support abrupt changes in hydrographic properties (Orsi et al., 1995), which can be diagnosed as gaps or low concentrations of observations in tracer, e.g., $\Theta/S_A$, space. Naveira Garabato et al. (2011) highlighted this distinctive "clumping" of $\Theta/S_A$ data in the Southern Ocean at mesoscale resolution. Fronts appear as gaps in $\Theta/S_A$ space, while profiles within each inter-frontal zone fall into the same space as each other.

In $\Theta/S_A$ space, there are two clear regimes along the transects. South of the PF, the

$\Theta/S_A$ profiles largely fall onto a single curve that remains unchanged throughout the deployment (Figure 4.2a,b). All of the profiles converge to the same temperature and salinity (1.6 °C and 34.9 g kg$^{-1}$) at the base of the thermocline, which represents the subsurface reservoir of Upper Circumpolar Deep Water (UCDW).

In contrast, surface waters at the PF span a larger range of $\Theta$, $S_A$, and density values. Yet, here, a similar "clumping" phenomenon, typically observed at the mesoscale, is found over a narrow meridional band of only $\sim 1^\circ$ of latitude (Figure 4.2c). This suggests submesoscale variability in this region and the establishment of small-scale fronts or eddies in the surface boundary layer. This small-scale tracer variability is similar to that observed at the periphery of a coherent mesoscale eddy in northern Drake Passage by Adams et al. (2017), but has not previously been resolved across the core of the PF. During the second northward crossing of the PF, the $\Theta/S_A$ distribution changes such that the profiles roughly collapse on to two distinct curves in $\Theta/S_A$ space (Figure 4.2c,d), potentially indicating a shift in variability to larger scales. In the following section we argue that the transition to larger-scale variability is related to enhanced stirring near the PF supported by a deeper mixed layer and weaker frontal structure.

**Temporal variations in mean-flow suppression**

Ferrari and Nikurashin (2010) argued that mean flows can suppress lateral mixing by advecting tracers away from eddy-rich regions before strong stirring can occur. This effect was later quantified from observations (Naveira Garabato et al., 2011) using mixing length theory, which describes a characteristic length scale over which a fluid parcel can move before exchanging properties with the background fluid. Their analysis was focused on hydrographic sections across major fronts of the ACC at mesoscale resolution (~50 km station separation). Here, we re-visit this calculation with the ability to assess whether smaller-scale frontal structure can impact mixing. Mixing lengths are calculated using conservative temperature, $\Theta$, according to the following:

$$L_{mix} = \frac{\Theta_{rms}}{\nabla_n \Theta_m}, \tag{4.1}$$

Where $\Theta_m$ is a mean temperature field, $\nabla_n$ is the gradient along isoneutral surfaces, and $\Theta_{rms}$ is a measure of temperature fluctuations. We first objectively map temperature in neutral density space, using an interval of $\Delta\gamma_n = 0.02$ kg m$^{-3}$, and

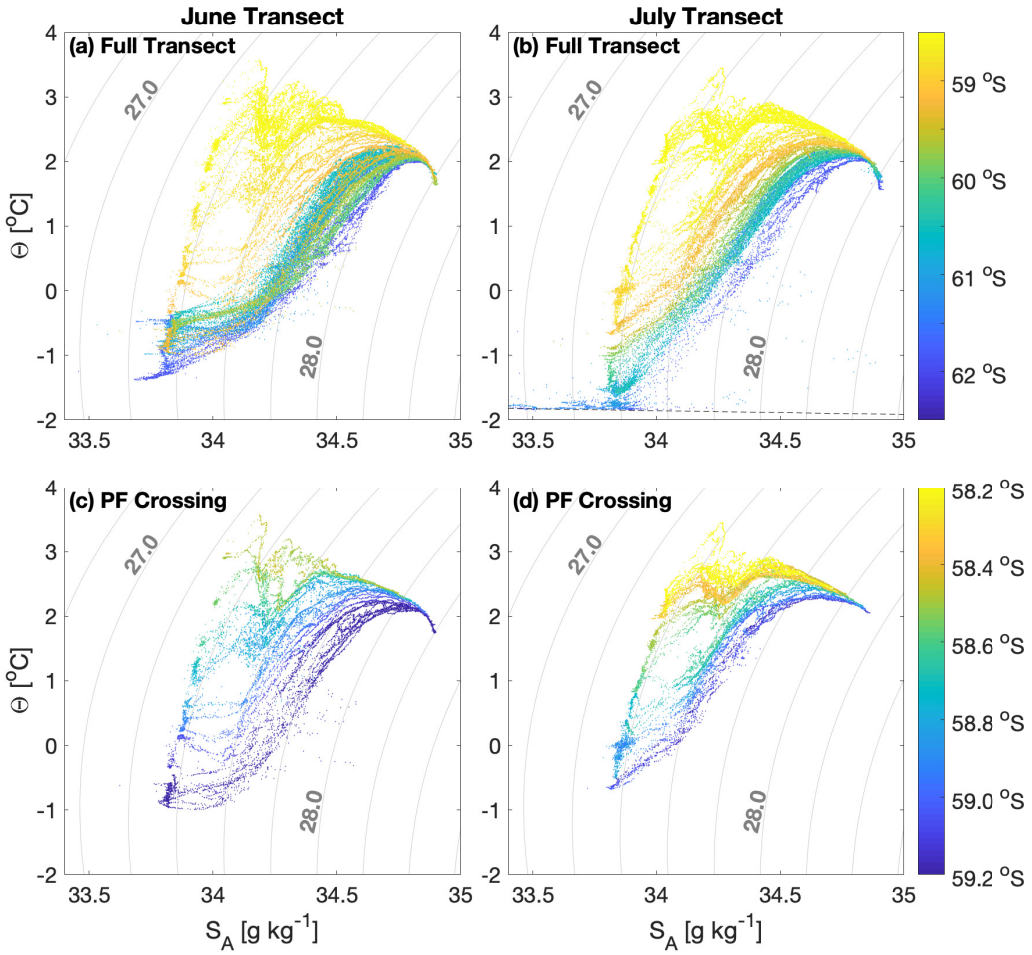


Figure 4.2: Temperature-Salinity diagrams for (left) June northward transect and (right) July northward transect. Points are colored by the latitude at which they were collected. (a,b) show data for the entire transect; (c,d) show data only in the region immediately surrounding the PF (approximately 1 degree of latitude). Dashed line on (b) indicates the freezing point of seawater. For each crossing, the core of the PF was located at approximately 58.5°S.

then smooth over 25 km using a running mean to produce a spatial-mean temperature field, $\Theta_m$, and a large-scale temperature gradient along neutral surfaces, $\nabla_n \Theta_m$ (Figure 4.3a–d). $\Theta_{rms}$ was calculated as the standard deviation of temperature fluctuations, $\Theta'$, away from the background temperature field (Figure 4.3e,f). The geostrophic velocity, $U_{geos}$, was calculated from the glider-derived density data and referenced to the DAC (Figure 4.3i,j). Although Naveira Garabato et al. (2011) used the resulting mixing lengths to calculate an eddy diffusivity, $\kappa$, according to $\kappa = U_e L_{mix} c_e$, where $U_e$ is an eddy velocity and $c_e$ is a constant eddy mixing efficiency. However, we had no reasonable way of calculating an eddy velocity, $U_e$,

and thus did not carry out this analysis. To the extent to which this velocity can be assumed to be invariant, the eddy diffusivity will simply be linearly proportional to the mixing length. This assumption is supported by the comparable eddy kinetic energies in the region during the two transects.

These mixing diagnostics produce different results between the two transects. The magnitude of $\nabla_n \Theta_m$ is large at the PF during the the June transect (Figure 4.3c), but is considerably weaker during the July transect. In fact, $\nabla_n \Theta_m$ is enhanced further south where there is a second, weaker velocity core. The temperature variance, on the other hand, is largest at the PF across both transects. Together these produced nearly an order of magnitude difference in $L_{mix}$. In the June crossing, the vertically-integrated mixing length $L_{mix}$ = 11 km at the PF, which we classify as eddy-suppressing (Figure 4.3g). This is consistent with the findings of Naveira Garabato et al. (2011) in their analysis of ship-based temperature and salinity transects of Drake Passage that were also conducted in non-winter months. In contrast, the late July transect, collected during the ChinStrAP2 campaign, exhibited a mixing length of 105 km (Figure 4.3h), which implies an enhancement of eddy stirring activity. These transects, separated by roughly six weeks, imply the potential for sub-seasonal changes in mixing properties at the PF.

This change in $L_{mix}$ between the first and second transects can be linked to differences in PF characteristics between the transects. Between June and July the PF weakens, becomes broader and shoals. The velocity in the core of the front falls from 0.51 m $s^{-1}$ to 0.36 m $s^{-1}$ (Figure 4.3i,j). Furthermore, in July, the glider observed two velocity cores, which may arise from a meander of the PF or a small eddy. The weakening of the mean flow leads to enhanced stirring across the front by meso- and submesoscale features, in agreement with a broader region of large $\Theta_{rms}$. This shift away from a mean-flow suppression regime has a positive feedback, as increased stirring will serve to broaden the front even more.

## 4.5 Discussion

The Southern Ocean is typically identified as a region that is strongly pre-conditioned for submesoscale variability (Su et al., 2018). However, the glider hydrographic sections presented in this study show minimal evidence for submesoscale variability in southern Drake Passage in fall 2016. Despite strong winds and surface cooling (Figure 4.7), each transect was characterized by shallow mixed layers and strong stratification south of the PF. As a result, both ventilation and subduction are sup-

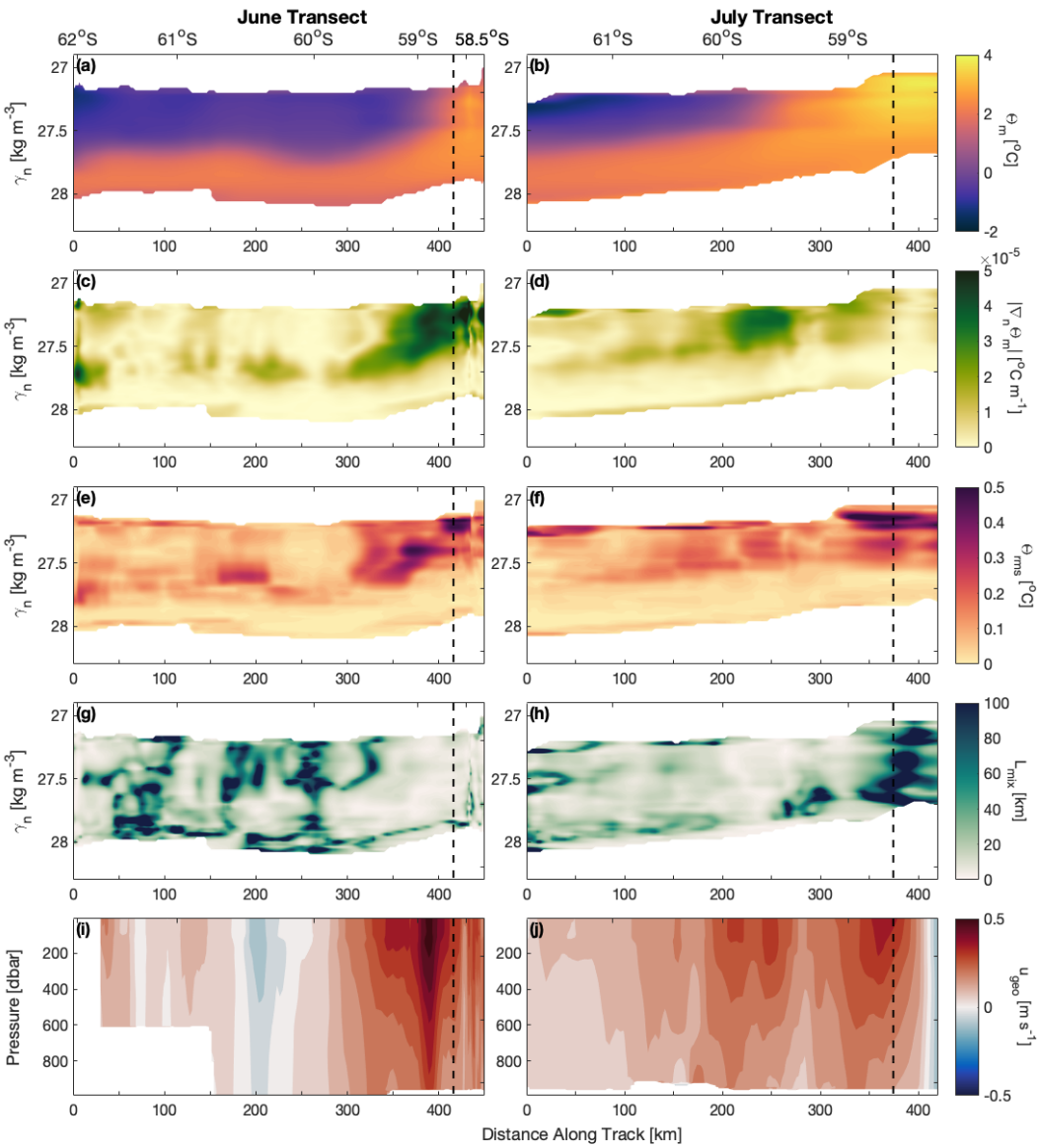


Figure 4.3: Mixing characteristics along two northbound glider transects spanning southern Drake Passage. Panels (a–h) are plotted in distance-neutral density space, panels (i,j) are plotted in distance-pressure space. Left-hand panels (a,c,e,g,i) show observations from the early June transect; right-hand panels (b,d,f,h,j) show observations from the late July transect. (a,b) Smoothed temperature, $\Theta_m$. (c,d) Large-scale temperature gradient along isoneutral surfaces, $\nabla_n \Theta_m$. (e,f) Standard deviation of temperature fluctuations, $\Theta_{rms}$. (g,h) Eddy mixing length, $L_{mix}$. (i,j) Geostrophic velocity, $U_{geo}$. Black dashed lines indicate crossings of the PF.

pressed south of the PF, where the strong freshwater lens prevents exchange between the surface and the deep ocean. The presence of this lens suggests that non-local

processes, e.g., the advection of meltwater from the West Antarctic Peninsula, may influence regions far from melting sites. Sallée et al. (2010), using a combination of *in situ* and remote sensing data at much coarser resolution, highlighted Drake Passage as a key site of mode water formation and subduction. Instead, subduction is strongly localized at the PF where the stratification at the base of the mixed layer erodes and the mixed layer deepens. Furthermore, the multiple transects captured by this study suggest that the subduction may be temporally intermittent; the required conditions will be discussed in the following paragraphs.

Examining only the degree of latitude spanning the PF, significantly different characteristics are prevalent between the early June and late July transects. The collapse of the temperature/salinity properties onto a smaller number of distinct curves is indicative of an increase in the spatial scale of variability. The structure of the T/S profiles south of the PF does not change between the two transects. This implies that ventilation in Drake Passage is both spatially localized and temporally varying. Balwada et al. (2018) used a semi-realistic channel model to investigate the role of small scales on tracer fluxes. They find that despite the increased stratification found in models that resolve submesoscales, tracer fluxes also increase on the order of 50%. Importantly, there is also a spatial dependence to their results—upstream of a bathymetric ridge, the surface vorticity is relatively quiescent, while downstream, there is enhancement of submesoscale activity and coherent vortices. This result is also consistent with the observational study of Viglione et al. (2018), and corroborates our findings of spatial localization of ventilation in Drake Passage.

The Naveira Garabato et al. (2011) study in Drake Passage differs from ours in two major ways: first, our analysis was carried out using higher-resolution data (glider- vs. ship-based), and second, their analysis was carried out during the summer/fall months. Based on the differences in mixing lengths calculated from the late fall vs. the early winter transect in our study, we can ascribe the discrepancy between the two studies to temporal changes on a sub-seasonal timescale. The ERA-Interim reanalysis data (Dee et al., 2011) shows that over the time period of the study, there is no significant change in the strength or frequency of down-front winds, but there is a large change in surface cooling, with average values at the PF increasing from $-126$ W m$^{-2}$ over the first transect to $-245$ W m$^{-2}$ over the second transect. This enhanced cooling leads to the observed destruction of the stratification at the PF moving into the winter season, and may be responsible for the enhancement of along-isopycnal stirring and ventilation that we observe at the PF. The changes in ventilation can

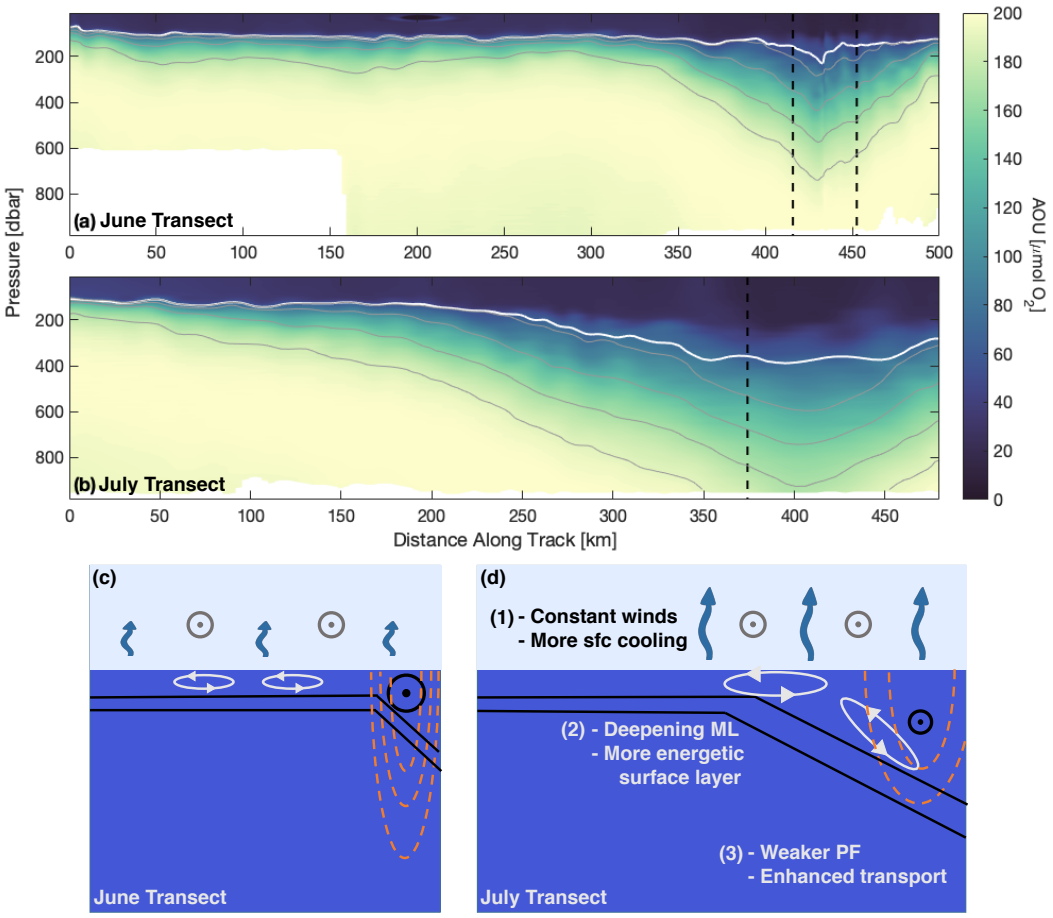


Figure 4.4: Temperature-depth sections of apparent oxygen utilization (AOU) for (a) June and (b) July northward transects. White line indicates the mixed layer depth; gray lines are contours of potential density $\sigma_0$ with 0.1 kg m$^{-3}$ intervals. Low AOU signifies that water has recently been in contact with the atmosphere. Schematics depicting the PF in (c) June and (d) July. As winter progresses, increased surface cooling (blue arrows) deepens the mixed layer, which generates a more energetic surface boundary layer and allows for enhanced stirring (white arrows). This then leads to a broadening and reduction in strength of the PF (red dashed lines indicate isotachs). Together this acts to reduce mean-flow suppression and enhance cross-front along-isopycnal transport.

most clearly be seen in the AOU data of the two transects, where low values of AOU indicate that water has recently been in contact with the atmosphere. While the two transects both show low-AOU waters confined to the mixed layer south of the PF, there is a large change at the PF between the two transects, with low-AOU waters penetrating to nearly 800 m in the second transect (Figure 4.4a,b). Combined

with the earlier results, this suggests a regime shift during winter that occurs over sub-seasonal timescales and allows for enhanced ventilation (Figure 4.4c,d).

Drake Passage has historically been the most frequently occupied region of the Southern Ocean; this is particularly true for winter months (Takahashi et al., 2012). Observations in Drake Passage are largely obtained using underway techniques or as part of the long-term hydrography monitoring program that uses expendable instruments (XBTs and XCTDs) (Sprintall et al., 2012; Gille et al., 2009, e.g.,). These observational methods have their limitations. The spatial resolution of the XCTD measurements, many tens of km or more, is coarse; XCTDs are required to understand lateral buoyancy gradients in the mixed layer due to the salinity stratification in southern Drake Passage. Shipboard underway data, on the other hand, is unable to provide information on the upper ocean's vertical structure. Recently, Gray et al. (2018) reported a significant disagreement in the Southern Ocean's contribution to the global carbon cycle suggesting that previous estimates, largely constrained by underway $pCO_2$ data, were missing a substantial outgassing of $CO_2$ from the Polar Frontal Zone. The observations collected by the gliders and presented here highlight some of the complications linked to extrapolating measurements from one region of the Southern Ocean to other longitudes (and latitudes). Despite intense cooling and strong winds, southern Drake Passage remains strongly stratified and is likely to experience weak exchange with the overlying atmosphere. Drake Passage is the principle location from which the Surface Ocean $CO_2$ Atlas (SOCAT) underway $pCO_2$ data is collected in winter (Bakker et al., 2016). If this capping of surface waters by sea ice melt is unique to Drake Passage, at these latitudes, it may help to explain why outgassing of $CO_2$ was significantly larger in regions south of the Polar Front when estimated from more broadly distributed floats Gray et al. (2018). While the Southern Ocean Carbon and Climate Observations and Modeling (SOCCOM) program will begin to identify some of these regional variations, the abrupt transitions in Southern Ocean dynamics highlighted in this study suggests that global estimates will remain challenging. Accurately capturing small-scale physical processes that impact air-sea exchange and subduction in coupled climate models remains an important research direction.

## 4.6 Conclusions

The ChinStrAP2 field campaign provided a unique dataset comprising several high-resolution transects of Drake Passage collected by ocean gliders during winter months. These observations have offered new insight into the fine-scale structures

of the PF. We find that while the PF acts to suppress eddy mixing during the early transect (consistent with previous autumn studies), this trend reverses in the later transect as the PF weakens. We also reveal that submesoscale activity is suppressed south of the PF, even with strong wintertime surface forcing, due to a highly stable mixed layer that appears to be meltwater advected into the region from upstream. Because of this, ventilation over the study region is restricted to the degree of latitude surrounding the PF, where the stratification weakens and the mixed layers deepen. This effect is enhanced from fall into winter, with high-AOU waters penetrating to depths of approximately 800 m during late July, indicative of a very strong dependence of ventilation on both location and time of year. Recent climatologies will help to identify finer-scale patterns of subduction, e.g., (Pellichero et al., 2017), but additional field work is needed to test temporal variability of frontal regions in the Southern Ocean.

## 4.7 Supplemental Figures

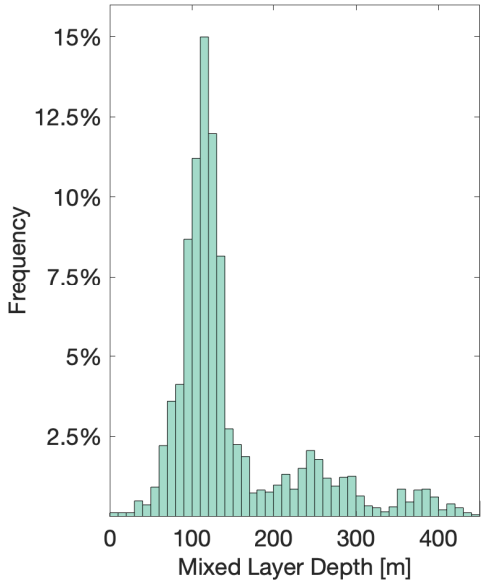


Figure 4.5: Histogram of mixed layer depths from glider data, using the criterion of $\Delta\sigma_0 = 0.125$ kg m$^{-3}$ from the surface (Monterey and Levitus, 1997). The trimodal distribution represents, from smallest to largest, mixed layers south of the PF, mixed layers at the PF during the June transect, and mixed layers at the PF during the July transect.

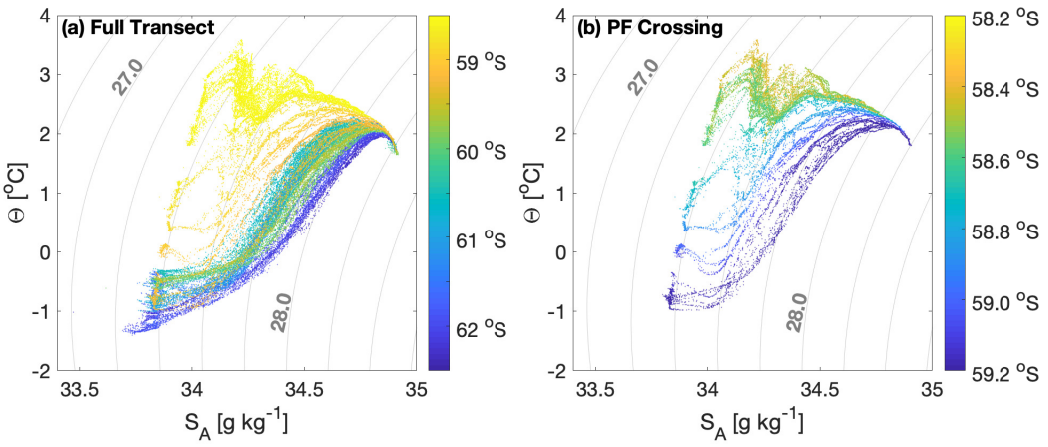


Figure 4.6: Temperature-Salinity diagrams for the June northward transect by the second Seaglider. Points are colored by the latitude at which they were collected. (a) shows data for the entire transect; (b) shows data only in the region immediately surrounding the PF (approximately 1 degree of latitude). The core of the PF was located at approximately 58.5°S.

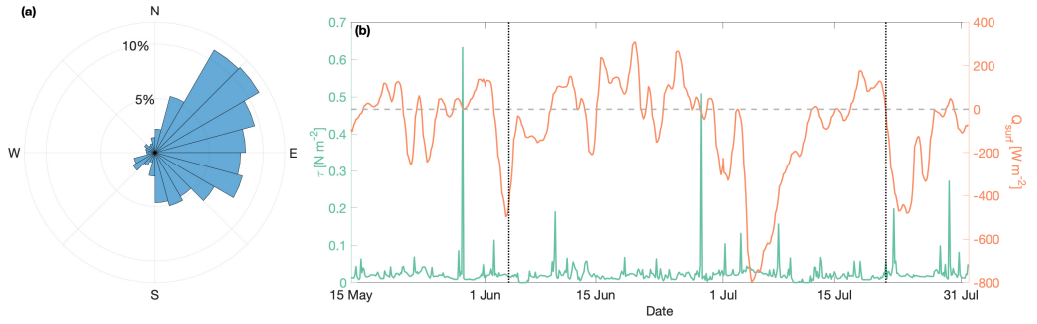


Figure 4.7: Surface forcing over Drake Passage over the deployment, from ECMWF Era-Interim reanalysis. Drake Passage is taken as the box bounded by 62 °S, 68 °S and 62 °W, 66 °W. (a) Histogram of wind directions. The winds are primarily westerly and south-westerly , as is typical of Drake Passage. (b) Wind stress (teal) and surface heat flux (orange), with the diurnal cycle removed. The dashed gray line denotes zero surface heat flux. Dotted lines indicate crossings of the PF.

*Chapter 5*

# CONCLUSIONS AND FUTURE RESEARCH DIRECTIONS

Despite its importance in controlling global climate, the Southern Ocean remains an under-studied region of the world's ocean. This dearth of observational data is felt even more strongly at the meso- and submesoscale, which are not resolved by most traditional ship-based observational oceanographic programs. This thesis comprises three studies that aim to highlight the importance of resolving motions at these scales and to begin to fill in the gaps in our knowledge of this vital region.

Beginning at the mesoscale, Chapter 2 uses eddy-permitting model output to examine outcropping into the Southern Ocean mixed layer and mixed layer residence times. That work found a strong dependence of mixed layer outcropping on abrupt changes in bottom bathymetry. It also identified the tendency of watermasses to re-outcrop seasonally, rather than remaining in the mixed layer year-round, leading to further questions about the air-sea equilibration time of waters in Southern Ocean mixed layers. Chapter 3 uses data from an observational field campaign to compare differences in submesoscale activity in a small region separated by a large bathymetric feature; that work found a propensity towards submesoscale activity during summer months that had previously been little-observed. It also highlighted the need for a more nuanced understanding of where and when submesoscales can play a role in setting upper-ocean stratification. Chapter 4 uses data from a second high-resolution field campaign to diagnose changes in mixed layer depth and thermocline ventilation on sub-seasonal timescales. It showed that ventilation in Drake Passage is both spatially localized and time-variant. This result may help provide physical insight into the recent study by Gray et al. (2018) that found a large discrepancy between traditional estimates of $CO_2$ outgassing in the Southern Ocean and new, float-based estimates.

The dataset produced as part of the ChinStrAP2 field campaign is unique not just in the time of year and location in which it was collected, but in the possibilities that parallel glider sections provide for calculating spatial gradients. Future work with this dataset could involve the calculation of a full, 3-dimensional Ertel potential vorticity, as well as a comparison between the full PV field and the "traditional" observational PV that has been used for data from a single glider.

This thesis was motivated in part by a desire to better understand the physical controls of the Southern Ocean on its ability to take up anthropogenic carbon dioxide. Further research would build on this thesis by beginning to couple the physical and chemical controls on air-sea exchange in the mixed layer itself. One method to do this would be to use virtual Lagrangian particles, as in Chapter 2, with some sort of equilibration parameter that could help elucidate the true effects of the subduction and re-outcropping behavior found in that work on the extent to which the atmosphere can equilibrate with the mixed layer.

The majority of this work has focused on observations at the meso- and submesoscale in Drake Passage, representing a very small slice of the Southern Ocean. Properties measured and phenomena observed in Drake Passage are often extrapolated circumpolarly; this may lead to incorrect estimates of transit times, air-sea exchange of carbon dioxide, and subduction rates. This thesis highlights the need for more nuanced analyses in a zonal sense: submesoscale activity can change drastically over relatively small spatial scales, as demonstrated in Chapter 3. Recent modeling work, such as that of Balwada et al. (2018), has corroborated the findings of the influence of bathymetry on submesoscales in the Southern Ocean and begun to investigate the subsequent impact on vertical tracer fluxes. Further investigations could focus on areas of the Southern Ocean where similar abrupt changes in bathymetry could cause large changes in submesoscale activity over short spatial scales. Future work should also focus on the implementation of these new insights into global climate models, as submesoscales remain unresolved in such large-scale models.

# BIBLIOGRAPHY

Abernathey, R. and P. Cessi (2014). "Topographic Enhancement of Eddy Efficiency in Baroclinic Equilibration". In: *J. Phys. Oceanogr.* 44.8, pp. 2107–2126.

Abernathey, R. et al. (2016). "Water-mass transformation by sea ice in the upper branch of the Southern Ocean overturning". In: *Nat. Geosci.* 9.8, pp. 596–601.

Adams, K. A. et al. (2017). "Frontal circulation and submesoscale variability during the formation of a Southern Ocean mesoscale eddy". In: *J. Phys. Oceanogr.* 47.7, pp. 1737–1753.

Adcroft, A. et al. (1997). "Representation of Topography by Shaved Cells in a Height Coordinate Ocean Model". In: *Mon. Wea. Rev.* 125, pp. 2293–2315.

Bachman, S. D. et al. (2017a). "Mesoscale and Submesoscale Effects on Mixed Layer Depth in the Southern Ocean". In: *J. Phys. Oceanogr.* 47.9, pp. 2173–2188.

Bachman, S. D. et al. (2017b). "Parameterization of Frontal Symmetric Instabilities. I: Theory for Resolved Fronts". In: *Ocean Modelling* 109, pp. 72–95.

Bakker, D. C. E. et al. (2016). "A multi-decade record of high-quality $fCO_2$ data in version 3 of the Surface Ocean $CO_2$ Atlas (SOCAT)". In: *Earth System Science Data* 8.2, pp. 383–413.

Balwada, D. et al. (2018). "Submesoscale Vertical Velocities Enhance Tracer Subduction in an Idealized Antarctic Circumpolar Current". In: *Geophys. Res. Lett.* 45.18, pp. 9790–9802.

Barré, N. et al. (2008). "Circulation in the Ona Basin, southern Drake Passage". In: *J. Geophys. Res.-Oceans* 113.C4.

Belcher, S. E. et al. (2012). "A global perspective on Langmuir turbulence in the ocean surface boundary layer". In: *Geophys. Res. Lett.* 39.18.

Bishop, S. P. et al. (2016). "Southern Ocean overturning compensation in an eddy-resolving climate simulation". In: *J. Phys. Oceanogr.* 46.5, pp. 1575–1592.

Boccaletti, G. et al. (2007). "Mixed layer instabilities and restratification". In: *J. Phys. Oceanogr.* 37.9, pp. 2228–2250.

Bopp, L. et al. (2015). "Pathways of anthropogenic carbon subduction in the global ocean". In: *Geophys. Res. Lett.* 42.15, pp. 6416–6423.

Boyer Montégut, C. de et al. (2004). "Mixed layer depth over the global ocean: An examination of profile data and a profile-based climatology". In: *J. Geophys. Res.* 109.

Broecker, W. S. et al. (1998). "How much deep water is formed in the Southern Ocean?" In: *J. Geophys. Res.* 103 (C8), pp. 15833–15843.

Buckingham, C. E. et al. (2016). “Seasonality of submesoscale flows in the ocean surface boundary layer”. In: *Geophys. Res. Lett.* 43.5, pp. 2118–2126.

Bullister, J. L. (1989). “Chlorofluorocarbons as time dependent tracers in the ocean”. In: *Oceanography* 2.2, pp. 12–17.

Callies, J. et al. (2015). “Seasonality in submesoscale turbulence”. In: *Nat. Comm.* 6, p. 6862.

Capet, X. et al. (2008). “Mesoscale to submesoscale transition in the California Current System. Part I: Flow structure, eddy flux, and observational tests”. In: *J. Phys. Oceanogr.* 38.1, pp. 29–43.

Cerovečki, I. et al. (2011). “A Comparison of Southern Ocean Air-Sea Buoyancy Fluxes from an Ocean State Estimate with Five Other Products”. In: *J. Climate* 24, pp. 6283–6306.

Chao, Y. et al. (2009). “Blended sea surface temperatures from multiple satellites and in-situ observations for coastal oceans”. In: *J. Atmos. Oceanic Technol.* 26.7, pp. 1435–1446.

Close, S. E. et al. (2013). “Control of mode and intermediate water mass properties in Drake Passage by the Amundsen Sea Low”. In: *J. Climate* 26.14, pp. 5102–5123.

Daru, V. and C. Tenaud (2004). “High order one-step monotonicity-preserving schemes for unsteady compressible flow calculations”. In: *J. Comput. Phys.* 193, pp. 563–594.

D’Asaro, E. et al. (2011). “Enhanced turbulence and energy dissipation at ocean fronts”. In: *Science* 332.6027, pp. 318–322.

Davis, R. E., P. Niiler, et al. (1981). “Variability in the upper ocean during MILE. Part II: Modeling the mixed layer response”. In: *Deep Sea Res.* 28.12, pp. 1453–1475.

Davis, R. E. et al. (1996). “Comparison of Autonomous Lagrangian Circulation Explorer and fine resolution Antarctic model results in the South Atlantic”. In: *J. Geophys. Res.* 101, pp. 855–884.

Dee, D. P. et al. (2011). “The ERA-Interim reanalysis: configuration and performance of the data assimilation system”. In: *Q. J. Roy. Meteor. Soc.* 137.656, pp. 553–597.

Dong, S. et al. (2008). “Southern Ocean mixed-layer depth from Argo float profiles”. In: *J. Geophys. Res.* 113.

Donners, J. et al. (2005). “Water Mass Transformation and Subduction in the South Atlantic”. In: *J. Phys. Oceanogr.* 35, pp. 1841–1860.

Drake, H. F. et al. (2018). “Lagrangian timescales of Southern Ocean upwelling in a hierarchy of model resolutions”. In: *Geophys. Res. Lett.* 45, pp. 891–898.

du Plessis, M. et al. (2017). "Submesoscale processes promote seasonal restratification in the Subantarctic Ocean". In: *J. Geophys. Res.-Oceans* 122.4, pp. 2960–2975.

Dufour, C. O. et al. (2015). "Role of mesoscale eddies in cross-frontal transport of heat and biogeochemical tracers in the Southern Ocean". In: *J. Phys. Oceanogr.* 45.12, pp. 3057–3081.

Erickson, Z. K. et al. (2016). "An advective mechanism for deep chlorophyll maxima formation in southern Drake Passage". In: *Geophys. Res. Lett.* 43.20.

Ferrari, R. and M. Nikurashin (2010). "Suppression of eddy diffusivity across jets in the Southern Ocean". In: *J. Phys. Oceanogr.* 40.7, pp. 1501–1519.

Ferrari, R. et al. (2014). "Antarctic sea ice control on ocean circulation in present and glacial climates". In: *Proc. Natl. Acad. Sci. (USA)* 111.24, pp. 8753–8758.

Fine, R. A. (1993). "Circulation of Antarctic Intermediate Water in the South Indian Ocean". In: *Deep-Sea Res. Pt. I* 40.10, pp. 2021–2042.

Flexas, M. M. et al. (2015). "Role of tides on the formation of the Antarctic Slope Front at the Weddell-Scotia Confluence". In: *J. Geophys. Res.-Oceans* 120, pp. 3658–3680.

Fox-Kemper, B. and D. Menemenlis (2008). "Can large eddy simulation techniques improve mesoscale rich ocean models?" In: *Ocean Modeling in an Eddying Regime*. Ed. by M. Hecht and H. Hasumi. Amer. Geophys. Union, pp. 319–338.

Fox-Kemper, B. et al. (2008). "Parameterization of Mixed Layer Eddies. Part I: Theory and Diagnosis". In: *J. Phys. Oceanogr.* 38.6, pp. 1145–1165.

Fox-Kemper, B. et al. (2011). "Parameterization of mixed layer eddies. III: Implementation and impact in global ocean climate simulations". In: *Ocean Modelling* 39.1-2, pp. 61–78.

Friocourt, Y. et al. (2005). "Water Mass Export from Drake Passage to the Atlantic, Indian, and Pacific Oceans: A Lagrangian Model Analysis". In: *J. Phys. Oceanogr.* 35, pp. 1206–1222.

Gary, S. F. et al. (2012). "Reconciling tracer and float observations of the export pathways of Labrador Sea Water". In: *Geophys. Res. Lett.* 39.44.

Gebbie, G. and P. Huybers (2011). "How is the ocean filled?" In: *Geophys. Res. Lett.* 38.

Gill, A. E. (1973). "Circulation and bottom water production in the Weddell Sea". In: *Deep-Sea Res.* 20, pp. 111–140.

Gille, S. T. et al. (2009). "Anomalous spiking in spectra of XCTD temperature profiles". In: *J. Atmos. Oceanic Technol.* 26.6, pp. 1157–1164.

Gray, A. R. et al. (2018). "Autonomous biogeochemical floats detect significant carbon dioxide outgassing in the high-latitude Southern Ocean". In: *Geophys. Res. Lett.* 45.17, pp. 9049–9057.

Hägeli, P. et al. (2000). “Spatial and temporal variability of mixed-layer depth and entrainment zone thickness”. In: *Bound.-Lay. Meteorol.* 97, pp. 47–71.

Haine, T. W. N. and J. A. Marshall (1998). “Gravitational, symmetric, and baroclinic instability of the ocean mixed layer”. In: *J. Phys. Oceanogr.* 28.4, pp. 634–658.

Heywood, K. J. et al. (2004). “On the fate of the Antarctic Slope Front and the origin of the Weddell Front”. In: *J. Geophys. Res.-Oceans* 109.C6.

Hill, C. et al. (2007). “Investigating solution convergence in a global ocean model using a 2048-processor cluster of distributed shared memory machines”. In: *Scientific Programming* 15, pp. 107–115.

Hines, S. K. V. et al. (2019). “The role of the Southern Ocean in abrupt transitions and hysteresis in glacial ocean circulation”. In: *Paleoceanography and Paleoclimatology* 34.

Hosegood, P. J. et al. (2013). “Wind-driven submesoscale subduction at the north Pacific subtropical front”. In: *J. Geophys. Res.-Oceans* 118.10, pp. 5333–5352.

Itoh, S. and D. L. Rudnick (2017). “Fine-scale variability of isopycnal salinity in the California Current System”. In: *J. Geophys. Res.-Oceans* 122.9, pp. 7066–7081.

Iudicone, D. et al. (2008). “Water-mass transformations in a neutral density framework and the key role of light penetration”. In: *J. Phys. Oceanogr.* 38.7, pp. 1357–1376.

Jacobs, S. S. (1991). “On the nature and significance of the Antarctic Slope Front”. In: *Mar. Chem.* 35, pp. 9–24.

Jones, C. S. and P. Cessi (2016). “Interbasin transport of the meridional overturning circulation”. In: *J. Phys. Oceanogr.* 46.4, pp. 1157–1169.

Jones, D. C. et al. (2014). “Spatial and seasonal variability of the air-sea equilibration timescale of carbon dioxide”. In: *Global Biogeochem. Cy.* 28.11, pp. 1163–1178.

Kim, Y. S. and A. H. Orsi (2014). “On the variability of Antarctic Circumpolar Current fronts inferred from 1992–2011 altimetry”. In: *J. Phys. Oceanogr.* 44.12, pp. 3054–3071.

Klein, P. and G. Lapeyre (2009). “The oceanic vertical pump induced by mesoscale and submesoscale turbulence”. In: *Annu. Rev. Mar. Sci.* 1, pp. 351–375.

Klocker, A. et al. (2012). “Estimating suppression of eddy mixing by mean flows”. In: *J. Phys. Oceanogr.* 42.9, pp. 1566–1576.

Kwon, Y. O. et al. (2015). “Year-to-Year Reoutcropping of Eighteen Degree Water in an Eddy-Resolving Ocean Simulation”. In: *J. Phys. Oceanogr.* 45, pp. 1189–1204.

LaCasce, J. H. et al. (2014). “Float-Derived Isopycnal Diffusivities in the DIMES Experiment”. In: *J. Phys. Oceanogr.* 44, pp. 764–780.

Large, W. G. et al. (1994). “Oceanic vertical mixing: a review and a model with a nonlocal boundary layer parameterization”. In: *Rev. Geophys.* 32, pp. 363–403.

Le Quéré, C. et al. (2009). “Trends in the sources and sinks of carbon dioxide”. In: *Nat. Geosci.* 2.12, pp. 831–836.

Lenn, Y.-D. and T. K. Chereskin (2009). “Observations of Ekman Currents in the Southern Ocean”. In: *J. Phys. Oceanogr.* 39.3, pp. 768–779.

Lévy, M. et al. (2010). “Modifications of gyre circulation by sub-mesoscale physics”. In: *Ocean Modelling* 34.1-2, pp. 1–15.

Lévy, M. et al. (2013). “Physical pathways for carbon transfers between the surface mixed layer and the ocean interior”. In: *Global Biogeochem. Cy.* 27.4, pp. 1001–1012.

Lévy, M. et al. (2018). “The role of submesoscale currents in structuring marine ecosystems”. In: *Nat. Comm.* 9.1, p. 4758.

Losch, M. et al. (2010). “On the formulation of sea-ice models. Part 1: Effects of different solver implementations and parameterizations”. In: *Ocean Modell.* 33, pp. 129–144.

Mahadevan, A. (2016). “The impact of submesoscale physics on primary productivity of plankton”. In: *Annu. Rev. Mar. Sci.* 8, pp. 161–184.

Mahadevan, A. and A. Tandon (2006). “An analysis of mechanisms for submesoscale vertical motion at ocean fronts”. In: *Ocean Modelling* 14.3, pp. 241–256.

Mahadevan, A. et al. (2010). “Rapid changes in mixed layer stratification driven by submesoscale instabilities and winds”. In: *J. Geophys. Res.-Oceans* 115.C3.

Mahadevan, A. et al. (2012). “Eddy-driven stratification initiates North Atlantic spring phytoplankton blooms”. In: *Science* 337.6090, pp. 54–58.

Marshall, D. (1995). “Topographic steering of the Antarctic Circumpolar Current”. In: *J. Phys. Oceanogr.* 25.7, pp. 1636–1650.

– (1997). “Subduction of water masses in an eddying ocean”. In: *J. Mar. Res.* 55.2, pp. 201–222.

Marshall, J. A. and T. Radko (2003). “Residual-Mean Solutions for the Antarctic Circumpolar Current and its Associated Overturning Circulation”. In: *J. Phys. Oceanogr.* 33, pp. 2341–2354.

Marshall, J. A. and K. Speer (2012). “Closure of the meridional overturning circulation through Southern Ocean upwelling”. In: *Nat. Geosci.* 5, pp. 171–180.

Marshall, J. A. et al. (1997). “A finite-volume, incompressible Navier-Stokes model for studies of the ocean on parallel computers”. In: *J. Geophys. Res.* 102, pp. 5753–5766.

Masumoto, Y. et al. (2004). “A fifty-year eddy-resolving simulation of the world ocean: Preliminary outcomes of OFES (OGCM for the Earth Simulator)”. In: *J. Earth Simulator* 1, pp. 35–56.

Matear, R. (2001). “Effects of numerical advection schemes and eddy parameterizations on ocean ventilation and oceanic anthropogenic $CO_2$ uptake”. In: *Ocean Modelling* 3, pp. 217–248.

McDougall, T. J. and P. M. Barker (2011). “Getting started with TEOS-10 and the Gibbs Seawater (GSW) oceanographic toolbox”. In: *SCOR/IAPSO WG* 127, pp. 1–28.

McPhee, M. G. and D. G. Martinson (1994). “Turbulent Mixing Under Drifting Pack Ice in the Weddell Sea”. In: *Science* 263.5144, pp. 218–221.

McWilliams, J. C. (2016). “Submesoscale currents in the ocean”. In: *P. Roy. Soc. Lond. A. Mat.* 472.2189.

Menemenlis, D. et al. (2005). “Using Green’s Functions to Calibrate an Ocean General Circulation Model”. In: *Mon. Wea. Rev.* 133, pp. 1224–1240.

Menemenlis, D. et al. (2008). “ECCO2: High resolution global ocean and sea ice data synthesis”. In: *Mercator Ocean Quarterly Newsletter* 31, pp. 13–21.

Meredith, M. P. et al. (2011). “Sustained monitoring of the Southern Ocean at Drake Passage: Past achievements and future priorities”. In: *Rev. Geophys.* 49.4.

Monterey, G. I. and S. Levitus (1997). *Seasonal variability of mixed layer depth for the world ocean*. US Department of Commerce, National Oceanic, Atmospheric Administration, National Environmental Satellite, Data, and Information Service.

Naveira Garabato, A. C. et al. (2001). “Mesoscale subduction at the Antarctic Polar Front driven by baroclinic instability”. In: *J. Phys. Oceanogr.* 31.8, pp. 2087–2107.

Naveira Garabato, A. C. et al. (2004). “Widespread Intense Turbulent Mixing in the Southern Ocean”. In: *Science* 303, pp. 210–213.

Naveira Garabato, A. C. et al. (2009). “Variability of Subantarctic Mode Water and Antarctic Intermediate Water in the Drake Passage during the late-twentieth and early-twenty-first centuries”. In: *J. Climate* 22.13, pp. 3661–3688.

Naveira Garabato, A. C. et al. (2011). “Eddy stirring in the Southern Ocean”. In: *J. Geophys. Res.-Oceans* 116.C9.

Naveira Garabato, A. C. et al. (2016). “A Microscale View of Mixing and Overturning across the Antarctic Circumpolar Current”. In: *J. Phys. Oceanogr.* 46 (1), pp. 233–254.

Newsom, E. R. et al. (2016). “Southern Ocean deep circulation and heat uptake in a high-resolution climate model”. In: *J. Climate* 29.7, pp. 2597–2619.

Omand, M. M. et al. (2015). “Eddy-driven subduction exports particulate organic carbon from the spring bloom”. In: *Science* 348.6231, pp. 222–225.

Orsi, A. H. et al. (1995). “On the meridional extent and fronts of the Antarctic Circumpolar Current”. In: *Deep-Sea Res. Pt. I* 42.5, pp. 641–673.

Palmer, M. et al. (2012). “Water mass pathways and transports over the South Scotia Ridge west of 50 W”. In: *Deep-Sea Res. Pt. I* 59, pp. 8–24.

Patterson, S. L. and H. A. Sievers (1980). “The Weddell-Scotia Confluence”. In: *J. Phys. Oceanogr.* 10.10, pp. 1584–1610.

Paulson, C. A. and J. J. Simpson (1977). “Irradiance Measurements in the Upper Ocean”. In: *J. Phys. Oceanogr.* 7.6, pp. 952–956.

Peacock, S. and M. Maltrud (2006). “Transit-Time Distributions in a Global Ocean Model”. In: *J. Phys. Oceanogr.* 36, pp. 474–495.

Pellichero, V. et al. (2017). “The ocean mixed layer under Southern Ocean sea-ice: Seasonal cycle and forcing”. In: *J. Geophys. Res.-Oceans* 122.2, pp. 1608–1633.

Pellichero, V. et al. (2018). “The southern ocean meridional overturning in the sea-ice sector is driven by freshwater fluxes”. In: *Nat. Comm.* 9.1, p. 1789.

Piñones, A. et al. (2011). “Lagrangian simulation of transport pathways and residence times along the western Antarctic Peninsula”. In: *Deep-Sea Res. Pt. II* 58.13-16, pp. 1524–1539.

Prandtl, Ludwig (1925). “7. Bericht über Untersuchungen zur ausgebildeten Turbulenz”. In: *Z. Angew. Math. Mech.* 5.2, pp. 136–139.

Price, P. F. et al. (1986). “Diurnal cycling: Observations and models of the upper ocean response to diurnal heating, cooling, and wind mixing”. In: *J. Geophys. Res.-Oceans* 91.C7, pp. 8411–8427.

Rintoul, S. R. (2013). “Large-Scale Ocean Circulation: Deep Circulation and Meridional Overturning”. In: *Earth System Monitoring*. Springer, pp. 199–232.

Rocha, C. B. et al. (2016). “Mesoscale to Submesoscale Wavenumber Spectra in Drake Passage”. In: *J. Phys. Oceanogr.* 46.2, pp. 601–620.

Rosso, I. et al. (2014). “Vertical transport in the ocean due to sub-mesoscale structures: Impacts in the Kerguelen region”. In: *Ocean Modelling* 80, pp. 10–23.

Ruan, X. et al. (2017). “Contribution of topographically generated submesoscale turbulence to Southern Ocean overturning”. In: *Nat. Geosci.* 10, pp. 840–845.

Rudnick, Daniel L et al. (2004). “Underwater gliders for ocean research”. In: *Mar. Technol. Soc. J.* 38.2, pp. 73–84.

Sallée, J.-B. et al. (2010). “Zonally asymmetric response of the Southern Ocean mixed-layer depth to the Southern Annular Mode”. In: *Nat. Geosci.* 3.4, p. 273.

Sallée, J.-B. et al. (2012). "Localized subduction of anthropogenic carbon dioxide in the Southern Hemisphere oceans". In: *Nat. Geosci.* 26.1, pp. 80–97.

Sallée, J.-B. et al. (2013). "Assessment of Southern Ocean mixed-layer depths in CMIP5 models: Historical bias and forcing response". In: *J. Geophys. Res.-Oceans* 118.4, pp. 1845–1862.

Sarmiento, J. L. et al. (1992). "A perturbation simulation of $CO_2$ uptake in an Ocean General Circulation Model". In: *J. Geophys. Res.* 97, pp. 3621–3645.

Sasaki, H. et al. (2014). "Impact of oceanic-scale interactions on the seasonal modulation of ocean dynamics by the atmosphere". In: *Nat. Comm.* 5, p. 5636.

Sebille, E. van et al. (2009). "Lagrangian validation of numerical drifter trajectories using drifting buoys: Application to the Agulhas system". In: *Ocean Modelling* 29.4, pp. 269–276.

Sebille, E. van et al. (2012). "Tasman leakage in a fine-resolution ocean model". In: *Geophys. Res. Lett.* 39.6.

Sebille, E. van et al. (2013). "Abyssal connections of Antarctic Bottom Water in a Southern Ocean state estimate". In: *Geophys. Res. Lett.* 40.10, pp. 2177–2182.

Shcherbina, A. Y. et al. (2013). "Statistics of vertical vorticity, divergence, and strain in a developed submesoscale turbulence field". In: *Geophys. Res. Lett.* 40.17, pp. 4706–4711.

Sheen, K. L. et al. (2013). "Rates and mechanisms of turbulent dissipation and mixing in the Southern Ocean: Results from the Diapycnal and Isopycnal Mixing Experiment in the Southern Ocean (DIMES)". In: *J. Geophys. Res.* 118.6, pp. 2774–2792.

Shinoda, T. and H. H. Hendon (1998). "Mixed layer modeling of intraseasonal variability in the tropical western Pacific and Indian Oceans". In: *J. Climate* 11.10, pp. 2668–2685.

Smethie Jr., W. M. and R. A. Fine (2001). "Rates of North Atlantic Deep Water formation calculated from chlorofluorocarbon inventories". In: *Deep-Sea Res. Pt. I* 48 (1), pp. 189–215.

Smith, W. H. F. and D. T. Sandwell (1997). "Global seafloor topography from satellite altimetry and ship depth soundings". In: *Science* 277, pp. 1957–1962.

Speer, K. et al. (2000). "The diabatic Deacon cell". In: *J. Phys. Oceanogr.* 30.12, pp. 3212–3222.

Sprintall, J. (2003). "Seasonal to interannual upper-ocean variability in the Drake Passage". In: *J. Mar. Res.* 61.1, pp. 27–57.

Sprintall, J. et al. (2012). "High-resolution underway upper ocean and surface atmospheric observations in Drake Passage: Synergistic measurements for climate science". In: *Oceanography* 25.3, pp. 70–81.

Su, Z. et al. (2018). “Ocean submesoscales as a key component of the global heat budget”. In: *Nat. Comm.* 9.1, p. 775.

Takahashi, T. et al. (2009). “Climatological mean and decadal change in surface ocean pCO 2, and net sea-air CO 2 flux over the global oceans”. In: *Deep-Sea Res. Pt. II* 56.8, pp. 554–577.

Takahashi, T. et al. (2012). “The changing carbon cycle in the Southern Ocean”. In: *Oceanography* 25.3, pp. 26–37.

Talley, L. D. (2013). “Closure of the global overturning circulation through the Indian, Pacific, and Southern Oceans: Schematics and transports”. In: *Oceanography* 34.

Tamsitt, V. et al. (2016). “Zonal variations in the Southern Ocean heat budget”. In: *J. Climate* 29.18, pp. 6563–6579.

Tamsitt, V. et al. (2017). “Spiraling pathways of global deep waters to the surface of the Southern Ocean”. In: *Nat. Comm.* 8.1, p. 172.

Taylor, J. R. and R. Ferrari (2010). “Buoyancy and Wind-Driven Convection at Mixed Layer Density Fronts”. In: *J. Phys. Oceanogr.* 40, pp. 1222–1242.

Thomas, L. N. (2005). “Destruction of Potential Vorticity by Winds”. In: *J. Phys. Oceanogr.* 35.12, pp. 2457–2466.

Thomas, L. N. and R. Ferrari (2008). “Friction, frontogenesis, and the stratification of the surface mixed layer”. In: *J. Phys. Oceanogr.* 38.11, pp. 2501–2518.

Thomas, L. N. et al. (2013). “Symmetric instability in the Gulf Stream”. In: *Deep-Sea Res. Pt. II* 91, pp. 96–110.

Thomas, L. N. et al. (2016). “Symmetric instability, inertial oscillations, and turbulence at the Gulf Stream front”. In: *J. Phys. Oceanogr.* 46.1, pp. 197–217.

Thompson, A. F. and A. C. Naveira Garabato (2014). “Equilibration of the Antarctic Circumpolar Current by standing meanders”. In: *J. Phys. Oceanogr.* 44.7, pp. 1811–1828.

Thompson, A. F. and K. J. Richards (2011). “Low frequency variability of Southern Ocean jets”. In: *J. Geophys. Res.* 116.

Thompson, A. F. and J.-B. Sallée (2012). “Jets and Topography: Jet Transitions and the Impact on Transport into the Antarctic Circumpolar Current”. In: *J. Phys. Oceanogr.* 42, pp. 956–972.

Thompson, A. F. and M. K. Youngs (2013). “Surface exchange between the Weddell and Scotia Seas”. In: *Geophys. Res. Lett.* 40.22, pp. 5920–5925.

Thompson, A. F. et al. (2009). “Surface Circulation at the Tip of the Antarctic Peninsula from Drifters”. In: *J. Phys. Oceanogr.* 39.1, pp. 3–26.

Thompson, A. F. et al. (2014). “Eddy transport as a key component of the Antarctic overturning circulation”. In: *Nat. Geosci.* 7, pp. 879–884.

Thompson, A. F. et al. (2016a). “A multibasin residual-mean model for the global overturning circulation”. In: *J. Phys. Oceanogr.* 46.9, pp. 2583–2604.

Thompson, A. F. et al. (2016b). “Open-Ocean Submesoscale Motions: A Full Seasonal Cycle of Mixed Layer Instabilities from Gliders”. In: *J. Phys. Oceanogr.* 46.4, pp. 1285–1307.

Todd, R. E. et al. (2016). “Potential vorticity structure in the North Atlantic western boundary current from underwater glider observations”. In: *J. Phys. Oceanogr.* 46.1, pp. 327–348.

Viglione, G. A. and A. F. Thompson (2016). “Lagrangian pathways of upwelling in the Southern Ocean”. In: *J. Geophys. Res.-Oceans* 121.8, pp. 6295–6309. DOI: 10.1002/2016JC011773.

Viglione, G. A. et al. (2018). “Abrupt transitions in submesoscale structure in Southern Drake Passage: Glider observations and model results”. In: *J. Phys. Oceanogr.* 48.9, pp. 2011–2027. DOI: 10.1175/JPO-D-17-0192.1.

Warner, M. J. et al. (1996). “Basin-wide distributions of chlorofluorocarbons CFC-11 and CFC-12 in the North Pacific: 1985–1989”. In: *J. Geophys. Res.* 101.C9, pp. 20523–20542.

Waugh, D. W. et al. (2006). “Anthropogenic $CO_2$ in the oceans estimated using transit time distributions”. In: *Tellus B* 58.5, pp. 376–389.

Weijer, W. et al. (2002). “Response of the Atlantic overturning circulation to South Atlantic sources of buoyancy”. In: *Global Planet. Change* 34, pp. 293–311.

Whitworth, T. et al. (1994). “Weddell Sea shelf water in the Bransfield Strait and Weddell-Scotia confluence”. In: *Deep-Sea Res. Pt. I* 41.4, pp. 629–641.

Whitworth, T. et al. (1998). “Water masses and mixing near the Antarctic Slope Front”. In: *Ice, and Atmosphere: Interactions at the Antarctic Continental Margin*. Ed. by S. S. Jacobs and R. F. Weiss. Vol. 75. Antarctic Research Series. Amer. Geophys. Union, pp. 1–27.

# APPENDIX A: GLIDER RECOVERY — THE MUSICAL

*This skit was co-written with Zach Erickson, Janet Sprintall, Adele Morrison, and Jamie Yin. It was first performed at Palmer Station on 06 May, 2015, during an open mic night, with Adele Morrison as the Narrator, Jamie Yin as the glider, Zach Erickson as Robert (third mate), Giuliana Viglione and Matt Louis as themselves, and Janet Sprintall as a chorus member.*

**Narrator:** This is the story of a group of scientists studying Changes in Stratification at the Antarctic Peninsula – a group known as ChinStrAP [all else turn around, point to t-shirt]. One of their Seagliders has run out of battery power and is slowly drifting northwards into the middle of Drake Passage. We join our intrepid team of young scientists on the good ship Laurence M. Gould as they pursue the glider.
**All:** Hi ho, hi ho, it's across the Drake we go / We're looking for our Seaglider, hi ho, hi ho / Hi ho, hi ho, halfway to Punta we will go / For science, we will go all night, hi ho, hi ho, hi ho, hi ho. (to the tune of "Heigh Ho")
**Narrator:** The sun rises on the morning of recovery.
**Matt:** [Goofy voice] Its a beautiful day in Antarctica! (from Mr. Rogers)
**Narrator:** There is no wind and conditions are ideal. The science team is up on the bridge and all are feeling confident about recovering the glider.
**Narrator:** Young Master Robert, the third mate, spots the glider bobbing up and down in the water [glider bobs up and down]. The glider recovery team mobilizes the zodiac. They are three: Matt, the MT with the Mostest, Giuliana, the Caltech science girl, and ...
**All:** I met him at the Palmer Store / He turned around and smiled at me / You get the picture?
**Audience:** Yes, we see!
**All:** That's when I fell for, Zodiac Jack, vroom, vroom! ("Leader of the Pack")
**Narrator:** Young Master Robert goes down to breakfast, and as he leaves, he implores:
**Robert:** The Antenna!
**All:** Do not let it go!
**Glider:** Let me go!
**Robert:** The Antenna!

**All:** Do not let it go!

**Glider:** Let me go!

**All:** Do not let it go!

**Glider:** Let me go!

**All:** Do not let it go! There it goes, goes, goes, goes, goes, goes, goes, goes, goes! ("Bohemian Rhapsody")

**Narrator:** The bridge radios down to the zodiac team. The glider is lost! The bridge crew resumes their search as the skies begin to darken. A storm is brewing!

**All:** The weather started getting rough, the LM Gould was tossed, if not for the effort of the fearless crew, the glider would be lost, the glider would be lost ("Gilligan's Island")

**Narrator:** All hands join the search, but in vain. Without other options, we must call upon Young Master Robert once more.

**Giuliana:** Save us, Young Master Robert! You're our only hope!

**Narrator:** Once again he locates the antenna of the glider with his young eagle eyes. The bridge radios down to put the zodiac in the water. When Matt tries to start the engine, the batteries begin smoking!

**All:** The boat, the boat, the boat is on fire! / We don't need no water, let the mother***er burn! ("The Roof is on Fire")

**Matt:** Actually, we do kind of need the boat ...

**Narrator:** The zodiac comes back aboard, the batteries are replaced, and the boat is relaunched. The recovery team drives out in a tempest of blinding snow and howling winds.

**All:** Say it ain't so / Can't see through the snow / Winds're picking up / Man, does this blow! Na, na, na, na, na, na, na, na, na, na, na, na, na, na, na, na, na, na, na ("All the small things")

[Matt/Giuliana lassos Glider and brings her on board]

**Narrator:** Zodiac Jack hoists the glider into the boat and the team secures it and returns to the ship. All is well ... but wait! Catastrophe strikes the glider team. While climbing from the zodiac, Giuliana is plunged into the icy waters of Drake Passage!

**All:** Mamma mia! There she goes again! My my!

**Matt:** Just jump when I tell you!

**Giuliana:** Mamma mia! Here I go again! Sorry guys, swear I didn't mean to! ("Mamma Mia!")

**Narrator:** Both Giuliana and the glider are successfully brought aboard.

**All:** Sweet glider of mine, woah, woah, woah / Good times never seemed so good! [so good, so good, so good] / Science is sublime, woah, woah, woah / Who'd believe we ever would see you again. ("Sweet Caroline")

**Narrator:** And they all lived happily ever after!

**All:** [form a kickline] Start spreading the news, the glider's okay / Hope you enjoyed our show of it, ChinStrAP, ChinStrAP / Let's get underway, we'll get drunk in PA / Glad that you were a part of it, Boat Trash, Boat Trash / If we can get back here, We'll see you all next year / It's been a blast, ChinStrAP, ChinStrAP ("New York, New York")

# APPENDIX B: MOBYHIAN CRICKSODY

*This song was co-written with several scientists on the US GO-SHIP I06S 2019 cruise as a parody of "Bohemian Rhapsody" and in honor of our beloved pet, Moby Crick. It was performed on board the R/V Thomas G. Thompson on 15 April, 2019 as part of the group's Antarctic Circle crossing ceremony by Giuliana Viglione, Max Kotz, Zac Anderson, Ben Musci, Kay McMonigal, Daniela Faggiani Dias, Wiley Wolfe, Mike Kovatch, and Garrett Walsh, and accompanied by Max Kotz and Zac Anderson on guitar.*

**Giuliana:** Is this the real life? / Is this just fantasy? / Caught in a maelstrom / No escape from these heaving seas / Open your eyes / Look out to the skies and sea / I'm just a student, I watch the CTD / Because I'm easy come, easy go / Little high, little low / Any way the waves go, doesn't really matter to me / To me...
**Kay:** [Stomping on cricket] Mama, just killed a cricket
**All:** Put a shoe against his head / Curb stomped him, now he's dead / Mama, life had just begun / But now he is squished against the floor / Mama!
**Max:** [Whale noises] Oooooooo!
**All:** Didn't mean to make you cry / If I'm not on the ship this time tomorrow / Carry on, carry on, as if nothing really matters...

[Musical interlude]

**All:** Too late, my time has come / His chirps they haunt my mind / Body's aching all the time / Goodbye, everybody, I've got to go / Gotta leave you all behind and jump the ship / Mama!
**Max:** [Whale noises] Oooooooo!
**All:** I don't wanna die / I wish I'd never killed that crick at all

[Musical interlude]

**All:** I see a little silhouetto of a crick / Moby Crick! Moby Crick! Will you do the fandango? / Isa, Alejandro very very frightening me!

**Men, high:** Little cricket!
**Women, low:** Little cricket!
**Men, high:** Little cricket!
**Women, low:** Little cricket!
**All:** Little cricket, Figaro!
**Max:** Magnificooooooooooo!
**Kay:** I'm just a sea cow, nobody loves me
**All:** He's just a sea cow from a cow family / Spare him his life from this moo-strosity

[Musical interlude]

**All:** Easy come, easy go will you let me go / Al-e-jan-dro, we will not let you go (let me go!) / Is-bell-a, we will not let you go (let me go!) / Po-sei-don, we will not let you go (let me go!) / Will not let you go (let me go!) / Will not let you go
**Kay:** Let me gooooooooooo
**All:** No no no no no no no / Oh mamma mia, mamma mia, mamma mia let me go / Davy Jones has a devil put aside for me, for me, FOR MEEEEEEEEEEE

[Musical interlude]

**Daniela:** So you think you can stomp me and squi-ish my eye? / So you think you can stomp me and leave me to die?
**All:** Oh baby, can't do this to me baby / Just gotta off, just gotta get right off this ship

[Musical interlude]

**All:** Ooh ooh oh yeah, oh yeah / Nothing really matters / When you're out at sea / Nothing really matters / But the cricket really matters... to me